Numerical simulation of electromagnetic wave scattering from very rough, Gaussian, surfaces.

Submitted by

ROBERT H. DEVAYYA

for the degree of Ph. D. of the University of London.

1992

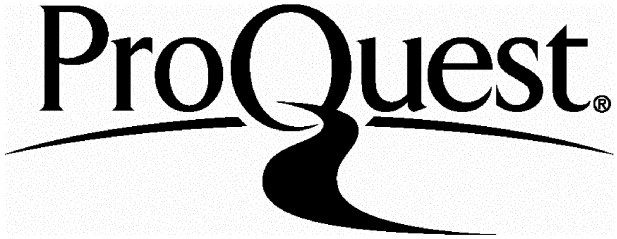

Acknowledgement.

I would like to thank my supervisor Dr. Duncan Wingham for his guidance, and his critical assessment of my work during the three years. I would also like to thank Dr. Andrew Stoddart of Kings College London for some useful discussions. With regard to the use of the computer facilities at UCL, my thanks go to Mr. Mark Abbott and Mr. Mark Morrissey. I am also grateful for the financial support for this project provided by the SERC, and the Royal Aerospace Establishment.

On a personal note, I would like to thank my parents and my friends. Special thanks go to Amanda Stewart without whom this thesis would have been finished sooner.

Abstract

A numerical investigation into electromagnetic wave scattering from perfectly-conducting, two-dimensional, Gaussian, rough surfaces is conducted. The rough surfaces considered have a root-mean-square surface height and a correlation-length of the same order, and of the order of the incident wavelength. These surfaces are beyond the range of application of existing scattering theories.

The scattering problem is solved by determining the solution of the magnetic-field-integral-equation. The convergence and the rate of convergence of two iterative methods applied to the numerical solution of the magnetic-field-integral-equation are investigated; the Neumann expansion, which has been used to formally represent the solution of the rough surface scattering problem; and the conjugate-gradient method, an iterative method of solving matrix equations whose convergence is in theory sure. However, applied to the solution of scattering from very rough surfaces, both methods have been found to diverge. Presented in this thesis is a step-by-step procedure for identifying divergent Neumann expansions, and a numerically robust conjugate-gradient method that has been successfully applied to the solution of the scattering problem.

This study provides a comparative investigation of vertical and horizontal polarization wave scattering. Results are presented for both the field in the vicinity of the surface boundary, and the average value of the power scattered from an ensemble of rough surface realizations.

A procedure is presented for obtaining from the solution of the magnetic-field-integral-equation, two explicit corrections to the Kirchhoff method. In the high-frequency limit one of the corrections accounts for shadowing, and the other accounts for multiple-reflections at the randomly rough, surface boundary. The significance of the two corrections at lower frequencies is investiagted. It is concluded that at lower frequencies the

former correction accounts for the partial-shadowing and diffraction of the incident and scattered waves, and the latter correction accounts for the illumination of the surface by waves scattered from other parts of the surface.

Table of contents

1
Introduction.

A plane wave incident upon an infinite plane interface between two media is scattered according to the Fresnel laws of reflection and transmission. However, when the boundary is not plane but rough the precise manner in which the wave is scattered is in many cases unclear. The most observable difference between the behaviour of a plane and a rough surface, is that a plane surface will reflect the wave in the specular direction. A rough surface on the other hand, scatters the wave in all directions, albeit that the scattered power is greater in some directions than in others.

A quantitative description of the scattering of electromagnetic waves from rough surfaces is required in many areas of science and technology, (Marcuse, 1982), (Ulaby *et al*, 1982). The scattering problem is formally solved once the electromagnetic field at the surface boundary is known (Stratton and Chu, 1939). The field at the surface boundary is the solution of the field-integral-equations (Poggio and Miller, 1973). However, exact solutions to these equations are only available for simple geometries (Poggio and Miller, 1973). This study is concerned with the scattering of an electromagnetic wave from a perfectly-conducting, Gaussian rough surface. In § 1·1, we discuss the analytic methods that have been used to describe this scattering problem. Particular attention is paid to the geometric range where each theory is available. In § 1·2 we provide an overview of the work presented in Chapters 2 to 7.

1·1 The rough surface scattering problem.

The two principal analytic tools for describing rough surface

scattering are the Kirchhoff approximation (Beckmann and Spizzichino, 1963) and the field-perturbation method (Valenzuela, 1967). For a perfect-conductor the central assumption of the Kirchhoff approximation is that the scattered magnetic field in the plane tangent to the surface boundary is equal to the incident magnetic field. This is a high frequency assumption, which also requires small shadowing by the surface of the incoming and outgoing waves. The geometric range of the Kirchhoff approximation has recently been examined at lower frequencies. Thorsos (1988) compared the expected scattered power obtained with the Kirchhoff approximation with numerical simulations of the scattering of an acoustic wave from a two-dimensional (corrugated), Gaussian rough surface with a Dirichlet boundary condition. In the context of this study, this scattering problem is analogous to the scattering of a horizontally polarized electromagnetic wave from a perfectly-conducting, two-dimensional, Gaussian rough surface. The shaded region "KA" in fig. 1·1 is where the Kirchhoff approximation is successful for incident and scattered grazing angles larger than twice the root-mean-square (RMS) surface slope. Furthermore, in this region the Kirchhoff approximation plus a geometric shadowing correction (Wagner, 1967) is successful at large backward scattering angles too.

There has been considerable effort devoted to finding analytic approaches that lift the central assumption of the Kirchhoff approximation. The field-perturbation method (Valenzuela, 1967) provides a method for small surface height and slope. Numerical simulations of the acoustic scattering problem described above have been compared with the field-perturbation solutions to the scattering problem (Thorsos and Jackson, 1989). The geometric range of the first two terms of the perturbation series is illustrated by the shaded region "FP" in fig. 1·1. It is no surprise that surface height should restrict the methods range of application; the surface height is the small parameter in the perturbation expansion. However, the fact that the surface correlation-length must be small too, is less obvious.

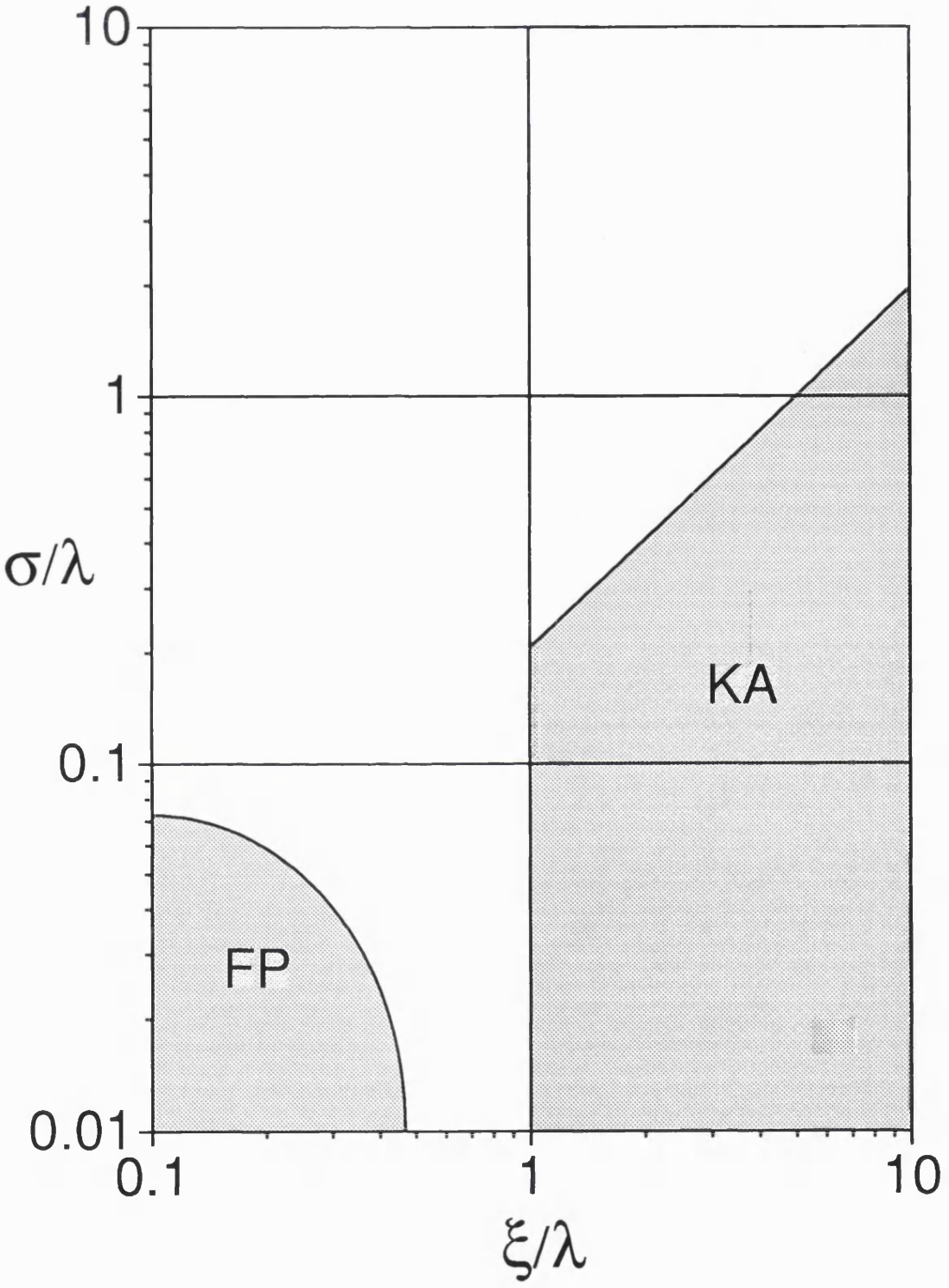

Fig. 1·1. The range of validity of the Kirchhoff approximation (KA) (Thorsos, 1988) and the field-perturbation method (FP) (Thorsos and Jackson, 1989) for a perfectly-conducting, two-dimensional, Gaussian rough surface. In the figure σ is the RMS surface height, ξ is the surface correlation-length and λ is the incident wavelength.

The influence of the surface correlation-length on the range of validity of the field-perturbation method is discussed in (Thorsos and Jackson, 1989).

The results of Thorsos (1988) and Thorsos and Jackson (1989) demonstrate that the Kirchhoff approximation and the field-perturbation method operate in separate regions of the parameter space. Up-until 1985 the issue of a common region of application was a matter of controversy. The controversy was resolved by Holliday (1985), who by using the first two terms of the Neumann series expansion (Kreysig, 1978) of the magnetic-field-integral-equation (MFIE) (Poggio and Miller 1973), showed that with the Kirchhoff approximation as the first term in the expansion, the second term was required to derive the first-order field-perturbation result for a rough surface surface with small heights and slopes.

Up until the late 1970's the Kirchhoff approximation and the field-perturbation method were the only analytic tools for describing rough surface scattering. The situation today is very different; the last decade has spawned phase-perturbation expansions (Shen and Marududin,1980), (Winebrenner and Ishimaru, 1985 a, b), momentum-transfer expansions (Rodriguez, 1989), unified-perturbation expansions (Rodriguez and Y. K. Kim, submitted in 1990), full wave theories (Bahar, 1981) and magnetic-field-integral iterations (Brown, 1982), (Holliday *et al*, 1987), (Fung and Pan, 1987). However, in spite of the host of approximate theories to choose from the accuracy of each theory is uncertain. We have found it very difficult to locate most of these methods within the parameter space of fig. 1·1. The phase-perturbation-method, however, has been compared with numerical simulations of the acoustic scattering problem described above (Broschat *et al*, 1989), and its range of validity is the shaded region "PP" in fig. 1·2. We suspect that the region "PP" is representative of the progress made by the analytic methods of the last decade. To the best of our knowledge, the methods referred to above are unproven or else fail for

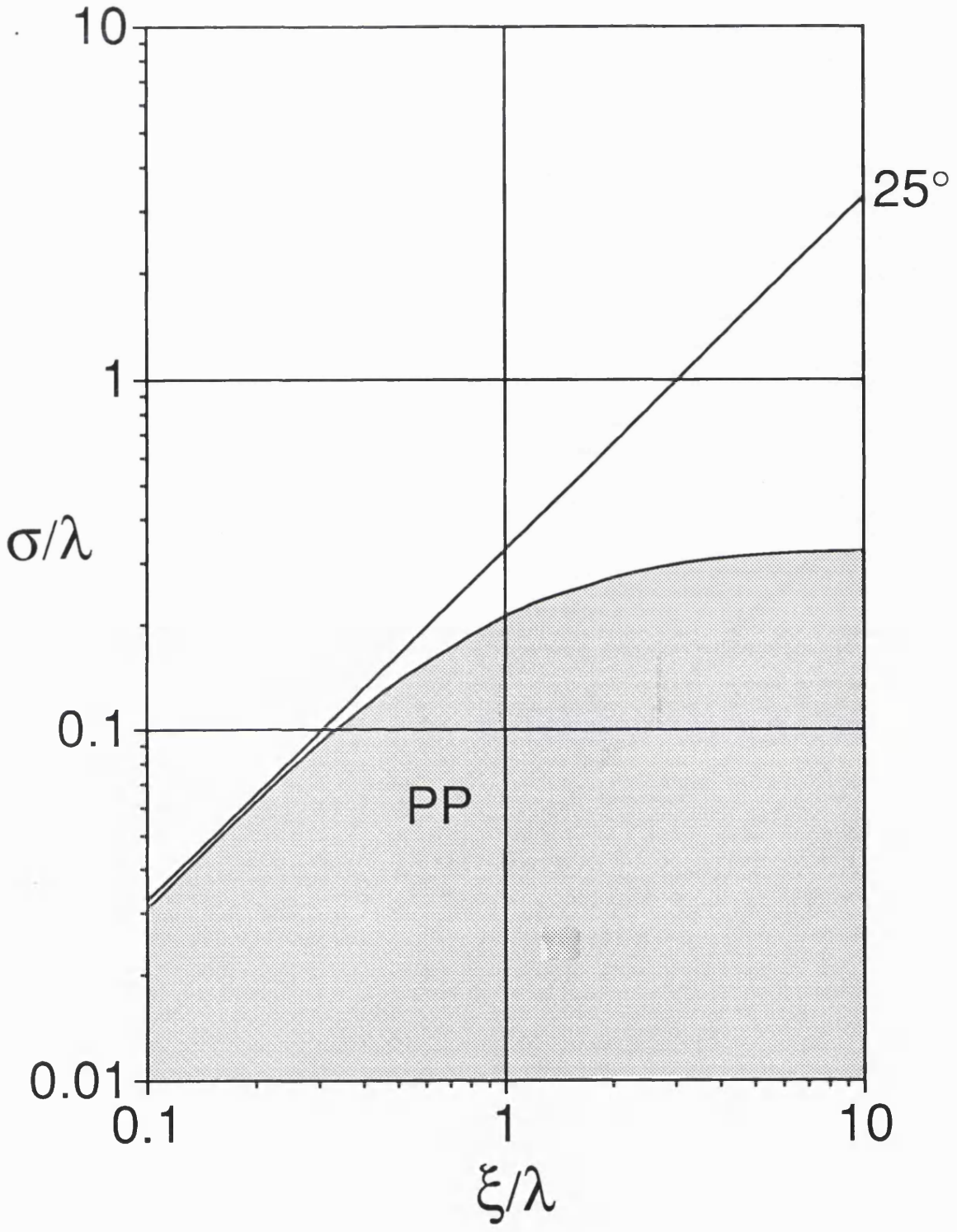

Fig. 1-2. The range of validity of the phase-perturbation method (PP) for a perfectly-conducting, two-dimensional, Gaussian rough surface. The illustration is taken from (Ishimaru and Chen, 1990 b). In the figure σ is the RMS surface height, ξ is the surface correlation-length and λ is the incident wavelength. The RMS slope is given by arctan ($\sqrt{2}\sigma/\xi$) and the surfaces below the diagonal line have a RMS slope of less than 25°.

a Gaussian rough surface with a correlation-length of the same order as the electromagnetic wavelength and a RMS slope as large as 25°.

An understanding of wave scattering from rough surfaces with large slopes is of considerable theoretical interest, and is required in optics applications. Much of the recent interest in wave scattering from very rough surfaces was stimulated by the experiments of O'Donnell and Mendez (1987). These authors observed that the average value of the power scattered from very rough, Gaussian, surfaces was largest in the backscattering direction. Furthermore, they noted that the angular width of the backward scattered power was relatively narrow. This phenomenon is called enhanced backscattering and prior to their observations had only been seen in volume scattering materials.

The oval "EB" in fig. 1·3 is the region of the parameter space where enhanced backscattering has been experimentally observed (O' Donnell and Mendez, 1987), (M. J. Kim *et al*, 1990), or numerically simulated (Nieto-Vesperinas and Soto-Crespo, 1987), (Soto-Crespo and Nieto-Vesperinas, 1989), (Saillard and Maystre, 1990), (Ishimaru and Chen, 1990 a). The ray picture of scattering has provided an intuitive explanation of enhanced backscattering. The following explanation is due to O'Donnell and Mendez (1987). In fig. 1·4 we illustrate a scattering path that may occur in the valley of a rough surface. In the figure the incoming ray is reflected from point B onto point C, where it escapes from the surface in the direction of the scattering angle θ^s. If Δr is the vector from point C to point D, then for a rough surface with substantially varying Δr the phase difference between all such double-scatter paths will wash out any mutual interference terms. Consequently, the field from each double-scatter path will contribute on an intensity basis to the mean intensity. However, some of the incoming rays will follow the reversed path DCBA, and also contribute to the scattered field in the direction of θ^s. The amplitude of the fields from paired double-scatter paths, ABCD and DCBA, for example, will add constructively,

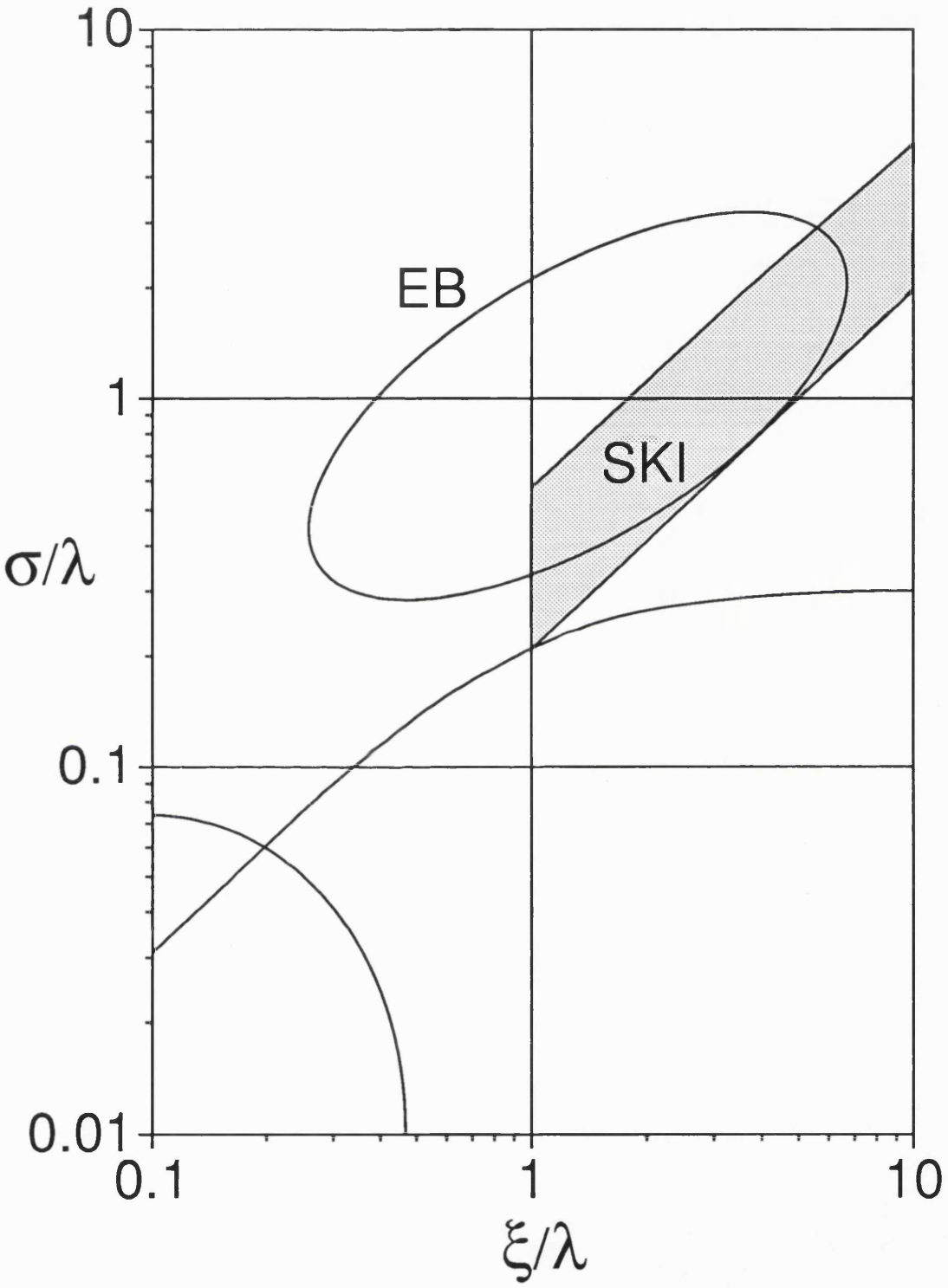

Fig. 1-3. The enhanced backscattering region (EB) and the region where the modified second-order Kirchhoff iteration (SKI) has described wave scattering from a Gaussian rough surface. In the figure σ is the RMS surface height, ξ is the surface correlation-length and λ is the incident wavelength.

thereby providing a strong contribution to the mean intensity. It is in this manner that the mean backscattered intensity is enhanced.

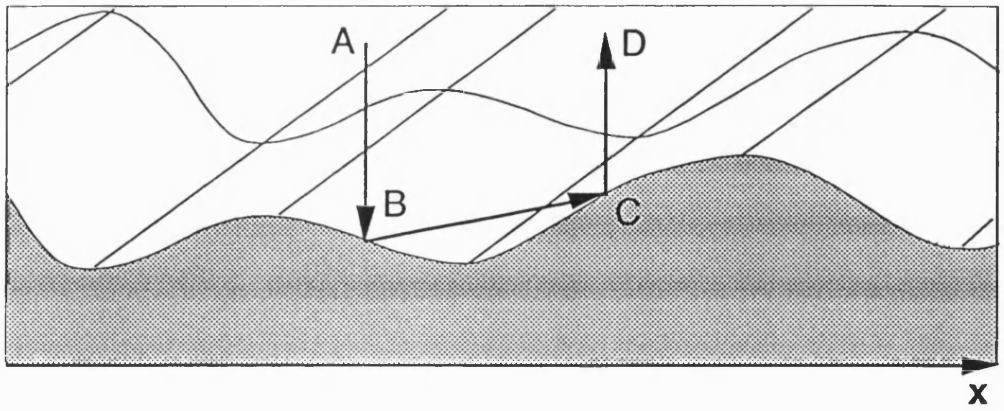

Fig. 1-4. A possible double-scattering path.

In the high-frequency limit, single and multiple-scattering does have a geometric interpretation, which allows these scattering contributions to be considered separately. It is not clear to us that the high-frequency, ray picture of scattering can be extended to lower frequencies. Nevertheless, key in the development of models for very rough, random surfaces is the separation of the scattered field into a "single-scattering" and "multiple-scattering" contributions (Liszka and McCoy, 1982), (Stoddart, 1992). The single-scattering contribution is obtained with the Kirchhoff method. Each higher-order scattering contribution corresponds to a term in an iterative expansion of a field-integral-equation. Ishimaru and Chen (1990 a, b), (1991), for example, have used the first two terms of a Kirchhoff iteration to describe some aspects of wave scattering in the region "SKI" of fig. 1-4. In particular these authors have found that the second-iteration is required to account for enhanced backscattering.

To obtain a description of wave scattering from rough surfaces with large slopes and a roughness structure of the same order as the incident wavelength, there seems little alternative at present but to solve the

scattering problem numerically. Numerical studies of rough surface scattering have been done by, among others, Chan and Fung (1978), Axline and Fung (1978), Nieto-Vesperinas and Soto-Crespo (1987), Macaskill and Kachoyan (1987), Thorsos (1988), Thorsos and Jackson (1989), Broschat *et al* (1989), Ishimaru and Chen (1990 a), and Saillard and Maystre (1990). It is important to recognize that the solutions obtained by solving the field-integral-equations numerically are not exact. However, the results obtained by these authors suggest that good solutions to the scattering problem can be obtained numerically, and for a wide range of rough surface geometries.

1·2 The present work.

This study is an investigation into wave scattering from perfectly-conducting, two-dimensional (corrugated), Gaussian rough surfaces where the RMS height and correlation-length are of the same order, and of the same order as the electromagnetic wavelength. The surfaces we will consider occupy the darker of the shaded regions in fig. 1·5. Wave scattering from the surfaces in the lighter shaded regions of the figure is described with varying success by the scattering theories reviewed in § 1·1.

The rough surface scattering problem is formally solved once the electromagnetic field at the surface boundary is known. In the case of a perfectly-conducting surface, only the component of the magnetic-field in the plane tangent to the surface boundary is required (Poggio and Miller, 1973). The magnetic field in the plane tangent to the surface boundary is the surface current density J, and a suitable equation to solve for J is the magnetic-field-integral-equation (MFIE) (Poggio and Miller, 1973). The MFIE for a time-harmonic $e^{i\omega t}$ wave incident on a two-dimensional surface is

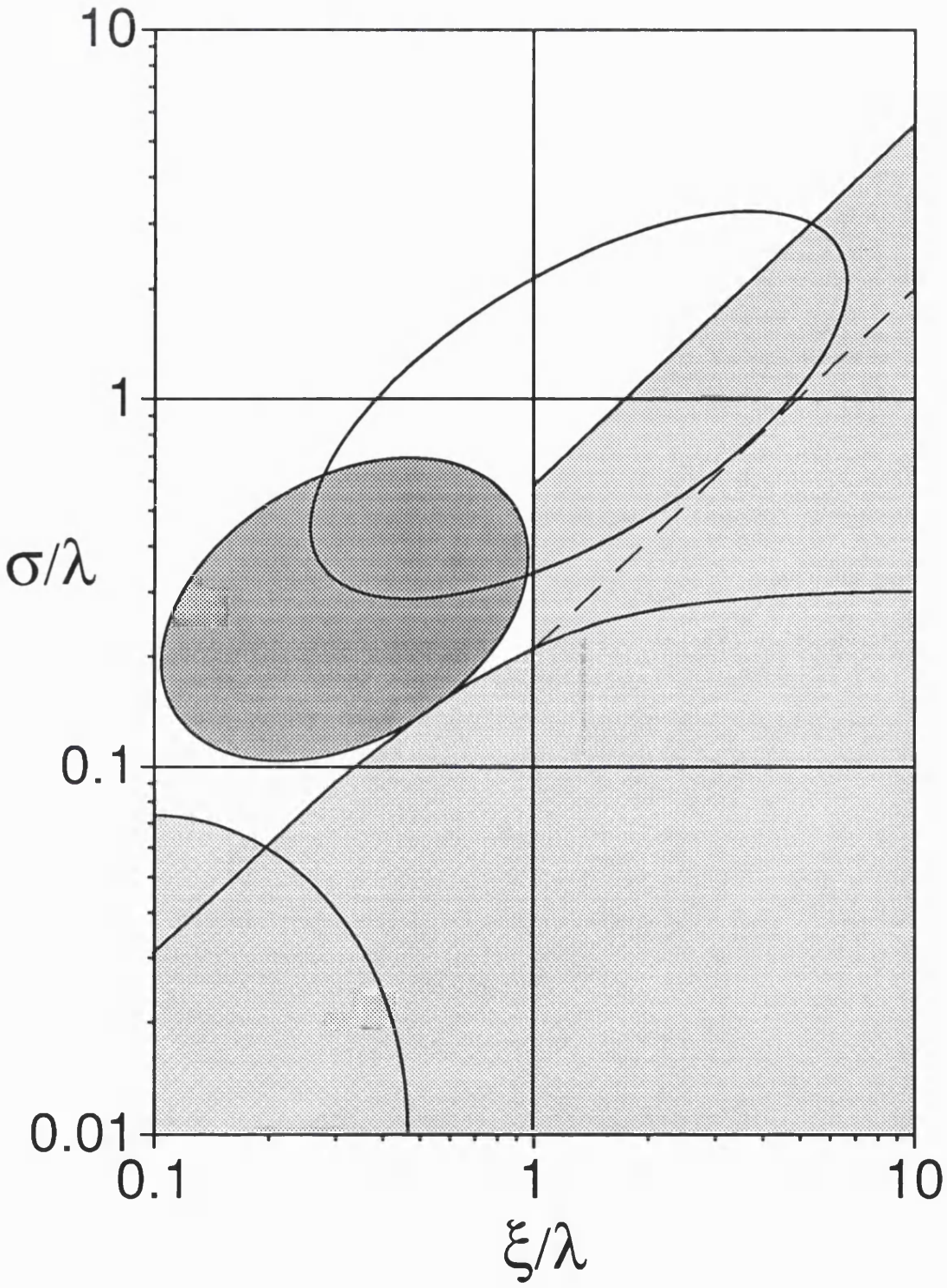

Fig. 1-5. The region of the parameter space that we will consider is the darker shaded region of the figure. Wave scattering from geometries in the lighter shaded area of the figure is described with varying success by existing scattering theories.

$$J(x) = 2\hat{n}(x) \times H^i(x) + \frac{1}{2\pi} \hat{n}(x) \times \int_{-\infty}^{\infty} J(x') \times \nabla\Phi(r, r') \left| \hat{z} + \hat{x} \frac{dz'}{dx} \right| dx' \qquad (1\cdot1)$$

Here, J is the surface current density, H^i is the incident magnetic field at the surface, Φ is the Greens' function for the scattering problem, **r** and **r'** are position vectors of the surface at x and x', and $\hat{n}$ is the unit vector normal to the surface boundary. The first term on the right-hand-side (RHS) of (1·1) is the Kirchhoff approximation. The integral in (1·1) gives the contribution to J from the rest of the surface. This contribution provides the multiple-scattering correction to the Kirchhoff approximation, and the term "multiple-scattering" will be used by us to indicate this fact.

The integral-equations that we solve are simpler than the one in (1·1). For a two-dimensional surface the surface current vectors for vertical and horizontal polarization are perpendicular to each another. This permits the MFIE (1·1) to be replaced by two uncoupled, scalar integral-equations. In Chapter 2 we present the scalar MFIEs for the two-dimensional scattering problem. We then proceed to how we generated the Gaussian rough surfaces used in our numerical simulations, and the procedures used to validate the height distribution and the autocorrelation function of the generated surfaces.

The starting-point for the numerical solution of the MFIE, is the approximation of the continuous equation by a discrete equation of the form

$$2H^i(x_n) = J(x_n) + \sum_{m=0}^{N-1} K(x_n, x_m) J(x_m). \qquad (1\cdot2)$$

Here, $K(x_n, x_m)$ is the weighted value of the kernel of (1·1), J is the surface current density , and H^i is the first term on the RHS of the MFIE at the

sample points x_n n = 0, ..., N-1. A preferred method of solving non-singular, complex matrix-equations is LU decomposition (Wilkinson and Rheinsch, 1971). We have found that the solution obtained by factorizing (1·2) into its LU form solves the discrete equation to within the numerical accuracy of the double-precision, floating-point arithmetic used in its computation. Although we have found that we can solve (1·2) exactly, there is no guarantee that the numerical solution for J will be a good solution to the MFIE, even at the sample points. Moreover, increasing the density of the sample points does not guarantee that the numerical solution will be closer to the true solution of the MFIE (Sarkar, 1983), (Reddy, 1986). It seems to us a very difficult matter to determine the error in the surface current density directly, so we have not attempted to do this. We take the view that the degree to which we can zero the total field beneath the perfect-conductor is the best way of determining both the quality of the numerical solution for the surface current density, and the scattered field. We have found that the scattered field beneath the perfect-conductor computed with our numerical solution for the surface current density closely equals minus the incident field. We will illustrate this in Chapter 2 with contour-plots of the modulus of the total field in the vicinity of the surface boundary.

The principal problem that emerges in the numerical solution of the MFIE is that very large matrices are generated, even for moderately sized two-dimensional surfaces. Direct methods of solving these matrix-equations can consume substantial computer resources. For this reason, there is considerable interest in solving these matrix-equations by iterative methods that one hopes will give a good estimate of the solution in relatively few iterations, thereby reducing the computational requirement. In Chapter 3 we examine the convergence and the rate of convergence of two iterative methods of solving the discrete approximation of the MFIE; the Neumann expansion (Kreysig, 1978), which has been used to formally

represent the solution of the continuous MFIE (Brown, 1982); and the conjugate-gradient method (Hestenes, 1980), an iterative method of solving matrix-equations whose convergence is in theory sure.

The Neumann expansion used by Holliday (1985) and Holliday *et al* (1987) is a natural candidate for an iterative solution of (1·2). However, although the expansion has been used to formally represent the solution of the MFIE (Brown, 1982), there is no proof that the expansion either of the continuous equation or its discrete representation converges. We have found that the expansion may provide a rapid numerical solution for small values of surface height and slope. However, when the roughness structure is of the same order as the electromagnetic wavelength the series diverges rapidly. We present in Chapter 3, step-by-step methods of identifying divergent Neumann expansions. This has allowed us to recognize divergent expansions within a few iterations. Furthermore, to the extent that our numerical simulation is a good one, we consider that the results presented in Chapter 3 provide strong evidence that the Neumann expansion cannot be used without qualification to provide a formal solution to the rough surface MFIE (Wingham and Devayya, 1992).

The conjugate-gradient methods (Hestenes, 1980) are iterative methods of solving matrix-equations whose convergence are in theory sure. A conjugate-gradient method suitable for electromagnetic scattering problems is given by Hestenes (1980; eqn. 12·7(a) - (d), p. 297). We refer to this method as the least-square, conjugate-gradient (LSCG) method. In spite of the theoretical assurance of convergence, it is not uncommon to find references in the literature to the iteration diverging (Sarkar *et al*, 1988), (Peterson and Mittra, 1985). We have ourselves found that applied to the large matrix-equations generated in the discretization of the rough surface MFIE, convergence is not sure. The LSCG method proceeds by generating at each iteration a conjugate-vector that has some orthogonality properties in

theory. Convergence is sure by virtue of these properties. However, due to rounding errors the conjugate-vectors may fail to satisfy the theoretical orthogonality properties. We present in Chapter 3 a numerically robust form of the LSCG method that uses Gram-Schmidt orthogonalization to correct for rounding errors at each iteration. For obvious reasons we call this algorithm the Gram-Schmidt, least-square, conjugate-gradient (GS-LSCG) method (Devayya and Wingham, submitted 1992). In all the cases that we have applied the GS-LSCG method to, we have never experienced a problem with its convergence.

We examine in Chapter 3 the rate of convergence of the GS-LSCG method for various values of RMS surface height, surface correlation-length and incidence angle. We have found that the rate of convergence depends less upon particular values of RMS surface height and surface correlation-length, but more upon there ratio. This ratio is proportional to the RMS surface slope. We have found that the rate of convergence is largely unaffected by the angle of incidence of the incident wave, or its polarization. We have also found that the size of the surface, which determines the matrix size N, does not effect the rate of convergence of the GS-LSCG method. This last point is important, because the advantages of the GS-LSCG method then grow with N.

The potential advantage of an iterative method is that the iteration can be stopped once a good estimate to the solution of the discrete equation has been found. To establish the point at which to stop the iteration we have compared the scattered far-field power computed with the iterated solution for the surface current density, and the scattered far-field power computed with the exact solution of (1·2). For the cases we have considered, we have found that when normalized error between the iterated and exact solutions is less than 0·01 there is small difference between the scattered powers. We have found this to be true, even when the dynamic range of the scattered power is as large as 50dB. We have found that when the size of the matrix

is very large, or when the surface slope is small, the GS-LSCG method obtains a good solution to the discrete equation with an order of magnitude reduction in the computation required by LU decomposition (Devayya and Wingham, 1992).

The disadvantage of the conjugate-gradient method is that it is implemented for one incident field at a time. LU decomposition on the other hand, is a method that allows solutions for any incident field to be directly obtained. In Chapter 3, we present a numerically robust conjugate-gradient method for electromagnetic scattering problems that require solutions for several incident fields. The method uses the information obtained in previous implementations to determine an initial-guess at the solution of the matrix-equation for additional incident fields. However, for the cases we have considered, the surface currents for different incident fields prove too distinct for the method to provide any significant computational advantage over LU decomposition. This disappointing result concludes Chapter 3.

We neglected to mention that to solve the MFIE numerically the integral in (1·1) must be truncated at some point. The scattering problem described by the truncated integral-equation is that of a wave scattered from a patch of surface. To guard against scattering from the patch edges the amplitude of the incident wave is chosen to fall off smoothly to negligible levels at the ends of the patch. In this study, we obtain an estimate of the expected scattered power for a random rough surface by solving the MFIEs for a number of uncorrelated, rough surface patches and then averaging the power scattered from each patch. From a computational standpoint a small patch size is preferable. However, since it is hoped that the normalized incoherent scattered power computed from an ensemble of rough surface patches will apply to the infinite surface, the patch size must be large enough to accommodate the average scattering properties of the infinite surface. In Chapter 4, we investigate the influence

of the patch size on the value of the incoherent scattered power. We have found that a relatively small patch size can accurately represent the second-order scattering properties of the infinite surface. In fact, for the surfaces we have considered the limit on the patch size depends more upon the method used to guard against edge effects. The tapered incident wave used in our numerical simulation, for example, becomes less consistent with the wave equation as the tapering on the incident wave is increased.

Chapter 5 starts with a discussion on the Kirchhoff approximation. The Kirchhoff approximation is used to test the computations in the calculation of the scattered far-field, and also provides a framework for some of the discussions in Chapters 5 and 6. The scattered far-field obtained with the Kirchhoff approximation is referred to as the Kirchhoff-field. It can be recognized from the MFIE (1·1), that the scattered far-field is the Kirchhoff-field plus the far-field obtained with the surface current due to the integral in (1·1), which we refer to as the integral-field. We present a procedure in Chapter 5 for determining from the solution of the MFIE, two corrections to the expected scattered power obtained with the Kirchhoff approximation. The corrections are discussed with a view to scattering in the high frequency limit. In this limit wave scattering is not complicated by diffraction, and the roles of the Kirchhoff and integral-fields are intuitively understood. A correction to the Kirchhoff method for shadowing, is determined from the linear-mean square estimate of the integral-field in terms of the Kirchhoff-field. We will show that the error in the estimate, which provides the second correction to the Kirchhoff method, then satisfies the coherence properties of the scattered field due to multiple-reflections. The significance of these two corrections at lower frequencies is investigated in Chapter 6.

In Chapter 6 we present the bistatic average scattered powers computed

from our numerical simulations of rough surface scattering. Results are presented for Gaussian rough surfaces with moderate to large slopes and a correlation-length of the same order as the electromagnetic wavelength. We have compared our numerical results for the average scattered power with the expected scattered power obtained with the Kirchhoff method. The results presented in Chapter 6 provide strong evidence that the degree of shadowing at the surface boundary is greater for horizontal polarization than for vertical polarization. This point is illustrated in the near-field of the surface with contour-plots of the electromagnetic field in the vicinity of the surface boundary. In the far-field, we have found that the Kirchhoff method can provide a qualitative description of the average scattered power, even when the surface correlation-length is comparable to the electromagnetic wavelength. In the horizontal polarization case, this description is obtained by using the Kirchhoff approximation with the correction for shadowing derived in (Wagner, 1967). In the vertical polarization case on the other hand, the Kirchhoff method often gives a better estimate to the backward scattered power when the shadowing correction is not used.

The results for Gaussian rough surfaces with very large slopes illustrate the enhanced backscattering reported in the literature (O'Donnell and Mendez, 1987). The results for these surfaces also show how the correction for shadowing presented in Chapter 5 is close to the correction for shadowing derived in (Wagner, 1967). Whereas the correction presented in Chapter 5 for multiple-reflections, at lower frequencies describes the angular distribution of the enhanced backward scattered power.

In the concluding chapter, Chapter 7, the main results of this study are presented, the previous literature is reviewed in the light of the present findings, and the thesis concluded with a general discussion of the work.

2
Numerical simulation of rough surface scattering.

In this chapter we present the magnetic-field-integral-equations (MFIEs) for a two-dimensional surface. This is followed by a discussion of the method of generating the Gaussian rough surfaces used in our numerical simulations of rough surface scattering, and the procedures used to validate the height distribution and autocorrelation function of the generated surfaces. The starting-point for the numerical solution of the MFIE is the approximation of the continuous equation by a matrix-equation. We use the extinction theorem to verify that our discrete approximation of the MFIE is a good one. Contour-plots of the total electromagnetic field in the vicinity of the surface boundary show how our numerical solution for the scattered field beneath the perfect conductor closely equals minus the incident field, a property of the exact solution of the MFIE.

2·1 The magnetic-field-integral-equations for a two-dimensional surface.

Two forms of the two-dimensional, magnetic-field-integral-equation (MFIE) are used in this study. One of them, equation (2·1), is appropriate when the incident wave is vertically polarized (Poggio and Miller, 1973; pp. 173 - 176);

$$J(x) = 2H^{i}(x) - \frac{ik}{2}\int_{-\infty}^{\infty} J(x') \frac{H_1^{(2)}[k|r - r'|]}{|r - r'|} ((z - z') - (x - x')\, dz'/dx)\, dx' , \quad (2\cdot1)$$

and the other, equation (2·2), is appropriate when the incident wave is horizontally polarized;

$$J(x) = 2H^i(x)\frac{(\sin\theta^i - \cos\theta^i\, dz/dx)}{\sqrt{1+(dz/dx)^2}} -$$

$$-\frac{ik}{2}\int_{-\infty}^{\infty} J(x')\,\frac{H_1^{(2)}[k|r-r'|]}{|r-r'|}\,((z-z')-(x-x')\,dz/dx)\sqrt{\frac{1+(dz'/dx)^2}{1+(dz/dx)^2}}\,dx'. \qquad (2\cdot2)$$

Here, z and dz/dx are the height and slope of the surface at x, **r** and **r′** are position vectors of the surface at x and x′, H^i is the incident magnetic field at the surface, $H_1^{(2)}$ is the first-order Hankel function of the second-kind (Abramowitz and Stegun, 1970), k is the electromagnetic wavenumber for the medium above the surface boundary, θ^i is the angle of incidence of the incident wave and J is the surface current density.

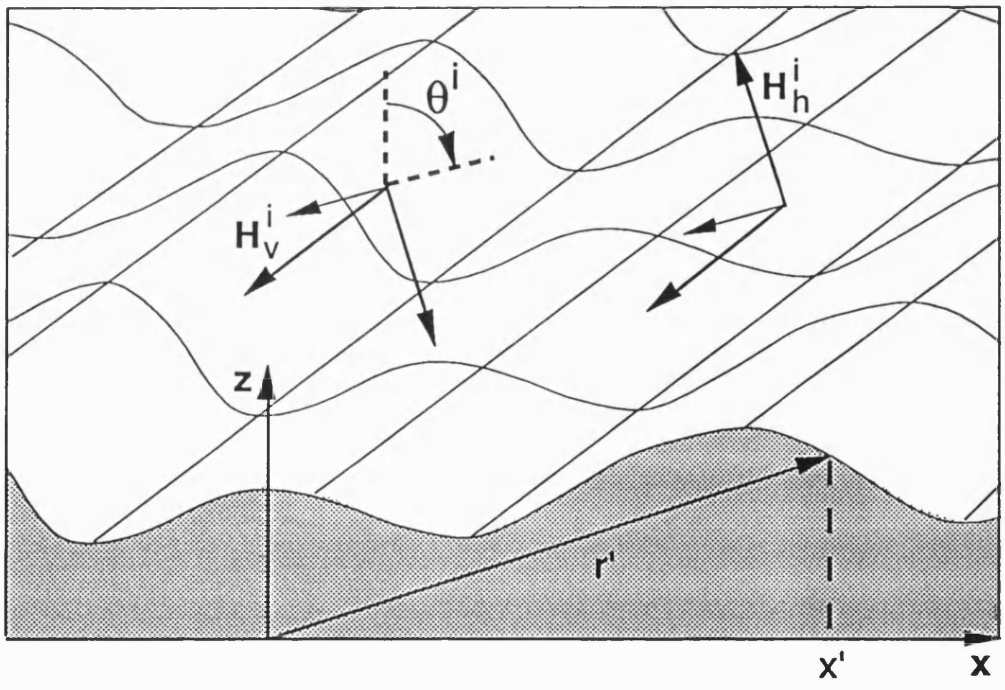

Fig. 2·1. The geometry of the rough surface scattering problem.

The geometry of the problem is illustrated in fig. 2·1. In the figure the subscripts "v" and "h" denote vertical and horizontal polarization.

The first term on the right-hand-side (RHS) of (2·1) and (2·2) is the Kirchhoff approximation. Only the component of the magnetic field in the plane tangent to the surface contributes to J, and this is why in (2·2) the Kirchhoff approximation is a function of the surface slope. The second term on the RHS of the MFIE describes the contribution to the surface current from the rest of the surface. When the curvature at every point on the surface boundary is very small, the geometric term in the integrand of the MFIE makes this contribution to J of second-order importance (Poggio and Miller, 1973). For the surfaces we have considered this contribution is not of second-order importance and the MFIE must be solved.

We cannot numerically solve the MFIE for an infinite length of surface; the integral in (1·1) must be truncated at some point. The solution of the truncated integral-equation is the surface current induced on a isolated, patch of surface. To guard against scattering from the patch edges the amplitude of the incident wave is chosen to fall off smoothly to negligible levels at the ends of the patch. In our simulations the incident wave is tapered according to (Thorsos, 1988)

$$H^i(x, z) = H_0\, e^{-w(x, z)}\, e^{ik(x\sin\theta^i + z\cos\theta^i).(1 - \alpha)},$$

where,

$$w(x, z) = \frac{(x - z\tan\theta^i)^2}{\gamma^2},$$

$$\alpha = \frac{2w(x, z) - 1}{(k\gamma\cos\theta^i)^2} \qquad (2\cdot3)$$

The taper is a Gaussian with a decay determined by the parameter γ. The phase term α introduces a curvature to the phase-front of the incident

wave, which ensures that to order $1/(k\gamma\cos\theta^i)^2$ the incident wave is consistent with the Helmholtz wave equation (Thorsos, 1988). In our simulations, the integral is truncated at $\pm L = \pm 25\lambda$ and a $\gamma = 12\lambda$ is used. For this value of γ the wave equation is satisfied to order 10^{-3} when $\theta^i = 70°$.

2·2 Generating a Gaussian rough surface.

In this study "Gaussian rough surface" refers to a statistically stationary, random surface with a Gaussian spectrum and surface heights normally distributed about zero. To generate a Gaussian rough surface with a known correlation-length and height distribution at the sample points, we generated a white, Gaussian, series and filtered it to obtain a regularly sampled surface with the correct correlation-length ξ and RMS height σ (Axline and Fung, 1978). A Gaussian rough surface with a RMS height of $0{\cdot}2\lambda$ and a correlation-length of $0{\cdot}4\lambda$ was generated by filtering approximately 10,000 noise samples to acquire the height of the surface at each sample point. Rough surfaces with a RMS height and a correlation-length different from this one, were obtained by scaling the vertical and horizontal dimensions of the generated surface.

In fig. 2·2, we present the height distribution (Papoulis, 1984) of a 3000 correlation-length long section of rough surface generated by this procedure for a RMS height of $0{\cdot}2\lambda$ and a correlation-length of $0{\cdot}4\lambda$. In the figure, the curve is the distribution function of a Gaussian rough surface, and the dots are the height distribution computed from a 3000 correlation-length long section of the generated surface. A quantitative measure of the error in the height distribution of the generated surface, was obtained using the Chi-squared goodness of fit test (Bendat and Piersol, 1986). The height distribution of the rough surfaces used in our numerical simulations of rough surface scattering are consistent at the 5% significance level (Bendat

and Piersol, 1986), (Priestley, 1987) with the height distribution of a Gaussian rough surface .

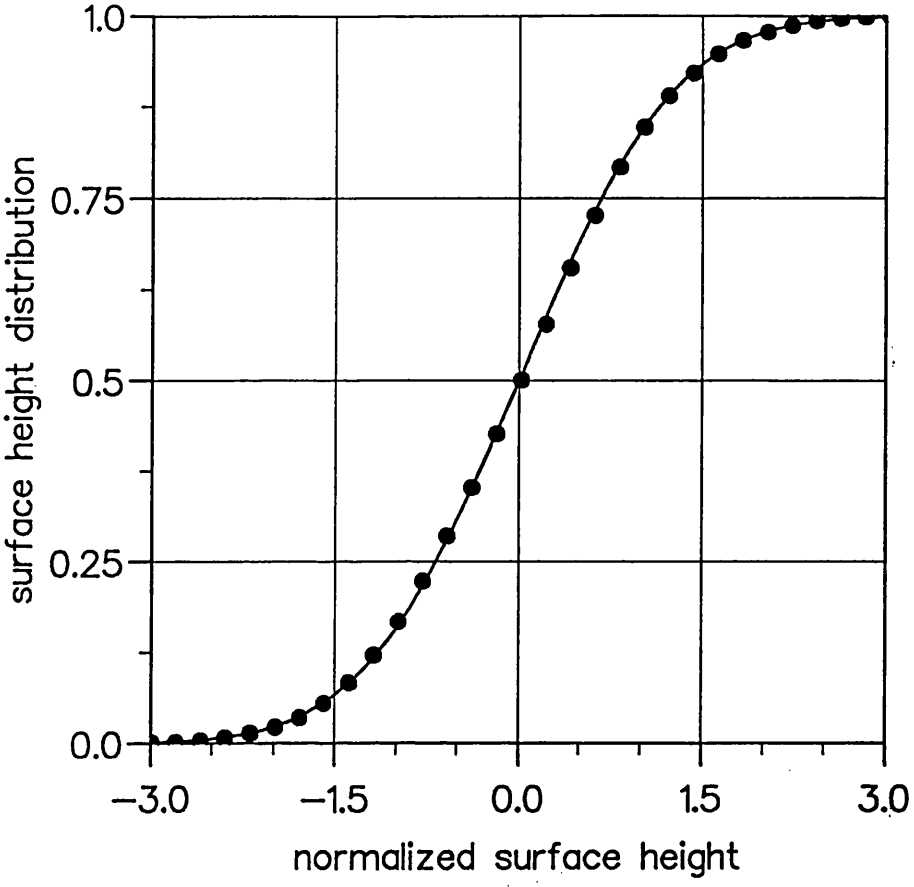

Fig. 2-2. The height distribution of a Gaussian. rough surface. In the figure the curve is the distribution function of a Gaussian rough surface; the dots are the height distribution computed from a 3000 correlation-length long section of generated surface.

We present in fig. 2-3 the autocorrelation function of a Gaussian rough surface, and the computed correlation coefficients for a 3000 correlation-length long section of the generated surface. The dots in the figure are the correlation coefficients of the generated surfaces, curve (A) is the Gaussian autocorrelation function, and curve (B) is twice the RMS error in the estimate (Priestley, 1987) for a 3000 correlation-length long sample of a Gaussian rough surface (Appendix B). The autocorrelation function of the surfaces used in our numerical simulations of rough surface scattering are consistent at the 5% significance level with the autocorrelation function of a sample of a Gaussian rough surface. In fig. 2-3, for example, it can be easily

verified that the difference between the correlation coefficients of the generated surface and their theoretical values, curve (A), is less than the error in the estimate, curve (B).

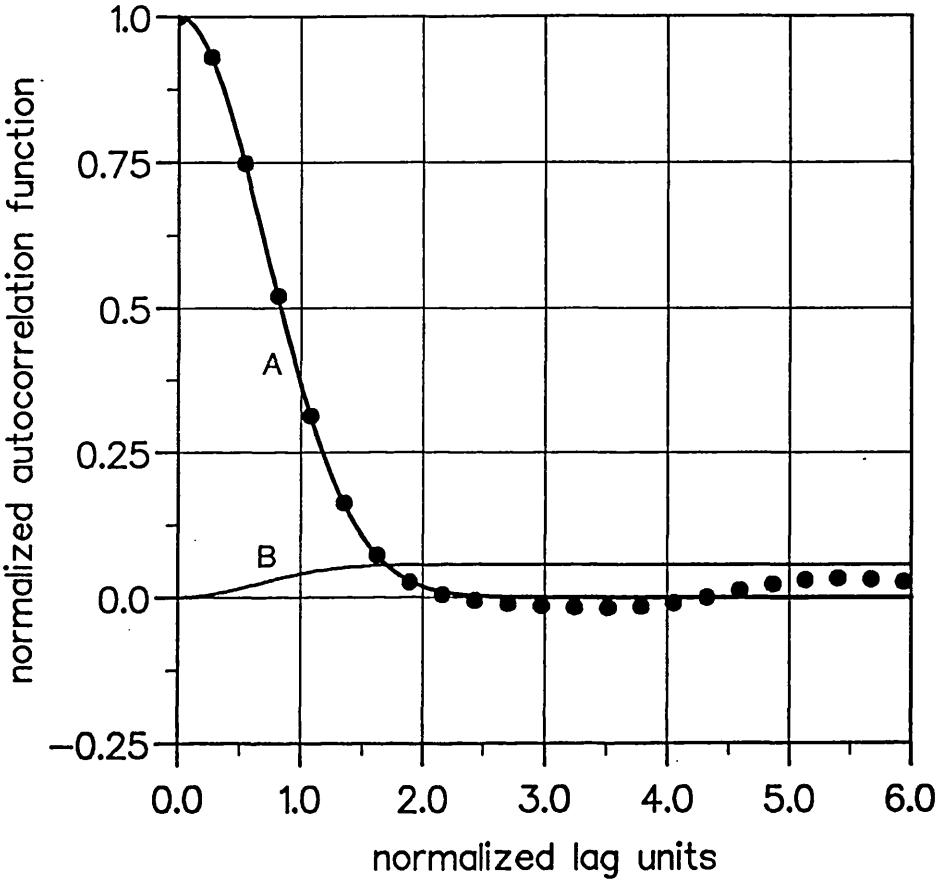

Fig. 2·3. The autocorrelation function of a Gaussian. rough surface. In the figure curve (A) is a Gaussian autocorrelation function, (B) is the error in the estimate; the dots are the computed correlation coefficients for a 3000 correlation-length long section of generated surface.

2·3 The discrete equation.

The starting-point for the numerical solution of the MFIE (1·1) is the approximation of the continuous equation by a discrete equation. We approximate the MFIE at sample points x_n n = 0, 1, ..., N-1, by a 3-point, Gaussian quadrature (Abramowitz and Stegun, 1970) over subsections Δx along the x-axis (Baker, 1977). In this manner, the MFIE is replaced by an equation of the form

$$2H^i(x_n) = J(x_n) + \sum_{m=0}^{N-1} K(x_n,x_m)J(x_m). \qquad (2\cdot4)$$

Here, $K(x_n,x_m)$ is the weighted value of the kernel of (1·1), J is the surface current density, and H^i is the value of the first term on the RHS of the MFIE at the sample points. A Δx with a variable length is used. The length of Δx is determined by requiring subsections along the surface contour Δl to be fixed, (see fig. 2·4). This ensures that, even when the surface is very rough, the incident field at the surface boundary and the integral in the MFIE are sufficiently sampled along the surface contour.

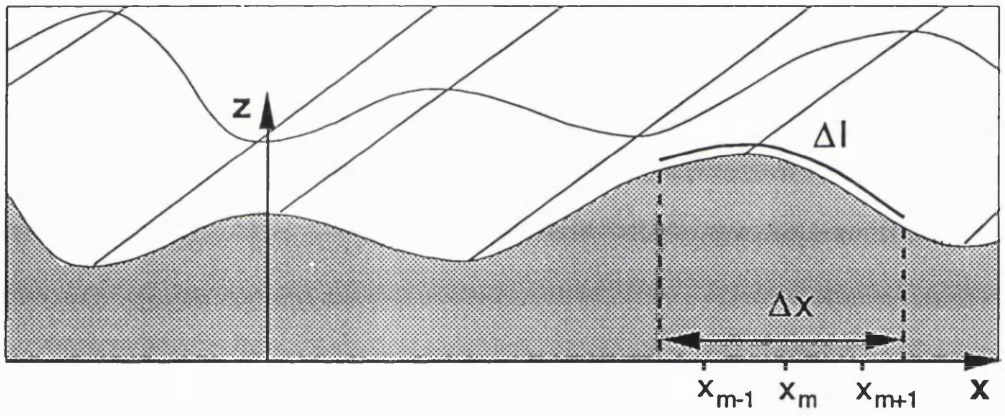

Fig. 2·4 Locating the sample points.

We may be able to solve the discrete equation (2·4) exactly, but there is no guarantee that solution to (2·4) will be a good solution to the MFIE (1·1). There are at least three sources of error. By projecting the integrand of (1·1) onto a finite basis we introduce error in the quadrature. Also, the left-hand-side (LHS) of (1·1) is approximated in (2·4) with its value at a discrete number of points. Finally, we commit further numerical errors in the evaluation of (2·4). We seek to minimise the first error by using a Gaussian quadrature to approximate the integrals in (1·1); the first two errors by having dense sampling; and we minimize the third by evaluating the sums in double-precision.

Aside from the errors incurred in the discretization of the continuous equation, is the accuracy with which we can numerically solve the matrix-equation (2·4). One hopes that when the error in the numerical values of the incident field is small, the error in the solution of (2·4) will be small too. This is sure when the condition-number of the matrix in (2·4) is small (Wilkinson, 1963). The matrix condition-number is equal to the square-root of the ratio of its maximum and minimum singular values. We chose to solve the MFIE, because of the distribution of the matrix singular values of the operator (I + K). We could, for example, have chosen to solve the electric-field-integral-equation (EFIE), since this too would give J (Poggio and Miller, 1973). However, the undesirable property of the EFIE is that the accumulation point (Kreysig, 1978) of its matrix singular values is zero (Jones, 1979). The accumulation point of the singular values of (2·4) on the other hand is unity (Jones, 1979). Therefore, given a choice of integral equations to solve, we consider the MFIE a better bet than the EFIE (Marks, 1986), (Baker, 1977).

The length of Δl will be an important factor in determining the accuracy of (2·4). However, since there is no guarantee that increasing the density of the sample points will reduce the error between the numerical solution for J and the solution of the MFIE (Sarkar, 1983), (Reddy, 1986), it seems to us a very difficult matter to determine the error in the surface current density directly, so we have not attempted to do this. We take the view that the degree to which we can zero the total field beneath the surface boundary is the best way of determining the quality of both the numerical solution for the surface current density and the scattered field. We have found that a Δl of $0{\cdot}2\lambda$ gives a good approximation to the scattered field beneath the conductor for rough surfaces with a RMS slope as large as 45° and for angles of incidence from 0° to 70°. With a Δl of $0{\cdot}2\lambda$ the sample points along the surface contour are spaced approximately $0{\cdot}06\lambda$ apart.

In § 2·2 we described how we generated a regularly-sampled surface. To obtain the surface at the quadrature points, a cubic-spline (Wilkinson and Rheinsch, 1971) was interpolated through the regularly-sampled surface. The surface slope was found by differentiating the spline polynomial.

2·4 The scattered field near to the rough surface boundary.

At a perfectly-conducting boundary the total electric field in the plane tangent to the surface is zero (Kong, 1986),

$$\hat{n}(r) \times \left(E^s(r) + E^i(r) \right) = 0. \tag{2·5}$$

Here, $\hat{n}$ is the vector normal to the surface, E^s is the scattered electric field, E^i is the incident electric field, and r is a position vector of the surface. The magnetic field on the other hand, satisfies the boundary condition

$$J(r) + \hat{n}(r) \times \left(H^s(r) + H^i(r) \right) = 0. \tag{2·6}$$

However, for a two-dimensional surface the polarization of the scattered and incident fields are the same and the boundary conditions (2·5) and (2·6) reduce to scalar equations. In the horizontal polarization case, the electric field lines are perpendicular to the x-z plane of fig. 2·1 and the boundary condition (2·5) reduces to the scalar equation

$$E^s(x) + E^i(x) = 0. \tag{2·7}$$

This is the scalar Dirichlet boundary condition. In the vertical polarization case, the magnetic field lines are perpendicular to the x-z plane and (2·6) reduces to the scalar equation

$$J(x) - H^i(x) + H^s(x) = 0. \tag{2·8}$$

A more often quoted boundary condition for the vertical polarization case is the scalar Neumann boundary condition,

$$\frac{d\left(H^s(x) + H^i(x)\right)}{dn} = 0. \tag{2·9}$$

Here, $d/dn = \hat{n}.\nabla$. The boundary condition (2·9) is derived in the following manner. For a vertically polarized wave the electric field above the surface boundary is from Maxwell's equations

$$E(R) = \frac{1}{i\omega\varepsilon_0}\left(-\frac{\partial H(R)}{\partial z}\hat{x} + \frac{\partial H(R)}{\partial x}\hat{z}\right). \tag{2·10}$$

The boundary condition (2·9) is obtained by substituting (2·10) into the electric field boundary condition (2·5).

The scattered field beneath the boundary of an infinite, perfectly-conducting, surface is equal to minus the incident field, a result known as the extinction theorem (Kong, 1986). We have used the extinction theorem to check our numerical solution of the MFIE. We consider that examining the degree to which the scattered field cancels the incident field beneath the surface boundary gives the best indication to the quality of the numerical solution of the MFIE. We have found that the solutions for the surface current density give a good approximation to the scattered field beneath the perfect-conductor for rough surfaces with a RMS slope as large as 45° and for angles of incidence from 0° to 70°. This will be illustrated in this section with contour plots of the total field in the vicinity of the surface boundary. The contour plots also show how the field at the surface boundary is in agreement with the Dirichlet boundary condition in the horizontal

polarization case, and the Neumann boundary condition in the vertical polarization case.

The electric-field scattered by a perfectly-conducting, two-dimensional, rough surface illuminated by a horizontally polarized wave is obtained from the integral (Poggio and Miller, 1973), (see Appendix C),

$$E^S(R) = \frac{kZ_0}{4}\int_{-\infty}^{\infty} J(x')\,\frac{H_0^{(2)}[k\,|R - r'|]}{|R - r'|}\,\left|\, z - x\,\frac{dz'}{dx}\,\right| dx'. \qquad (2\cdot11)$$

Here, J is the solution of the MFIE (2·2), z' and dz'/dx are the height and slope of the surface at x', r' is position vector of the surface at x', R is the vector to a point at (X, Z) above or below the surface boundary, $H_0^{(2)}$ is the zero-order Hankel function of the second-kind (Abramowitz and Stegun, 1970), Z_0 is the characteristic impedance of free space, k is the electromagnetic wavenumber and θ^i is the angle of incidence. In the vertical polarization case, the scattered magnetic field is computed from the integral (Poggio and Miller, 1973),

$$H^S(R) = \frac{ik}{4}\int_{-\infty}^{\infty} J(x')\,\frac{H_1^{(2)}[k\,|R - r'|]}{|R - r'|}\,((Z - z') - (X - x')\,\frac{dz'}{dx})\,dx'. \qquad (2\cdot12)$$

Here, $H_1^{(2)}$ is the first-order Hankel function of the second-kind (Abramowitz and Stegun, 1970) and J is the solution of the MFIE (2·1).

The quadrature used to approximate the MFIE is also used to approximate the scattered field integrals. For example, the integral (2·11) is approximated with the sum

$$E^S(R) = \sum_{m=0}^{N-1} K(R, x_m)J(x_m), \qquad (2\cdot13)$$

where $K(R,x_m)$ is the weighted value of the kernel of (2·11). The scattered fields were computed with the solution for surface current density obtained by LU decomposition. For the geometries we have considered, the discrete approximation of the MFIE is not ill-conditioned, and J solves the discrete equation to within the numerical accuracy of the double-precision, floating-point arithmetic used in its computation.

In fig. 2·5 we show one example of a grey scale plot of the normalized modulus of the total electric field,

$$\frac{|E^s + E^i|}{E_0}, \tag{2·14}$$

for a horizontally polarized wave incident at an angle of 45° on a Gaussian rough surface with a RMS slope of 45° and a correlation-length ξ of $0{\cdot}8\lambda$. The white line in the plot is the surface boundary. It can be easily verified from fig. 2·5 that the total electric field beneath the perfect-conductor is zero to within the resolution of the plot of $0.1\,|E_0|$. Furthermore, to a good approximation the total electric field just above the surface boundary is correctly zero

In fig. 2·6 we show one example of a grey scale plot of the normalized modulus of the total magnetic field,

$$\frac{|H^s + H^i|}{H_0}, \tag{2·15}$$

for the same surface considered in fig. 2·5 illuminated by a vertically polarized wave. Here, the total magnetic field beneath the perfect-conductor is zero to within the resolution of the plot of $0.1\,|H_0|$. Near to the perfect-conductor

Fig. 2·5. The normalized modulus of the total electric field in the vicinity of a rough surface with a RMS slope of 45° and a correlation-length of 0·8λ, when a horizontally polarized wave is incident from the right with an incidence angle of 45°.

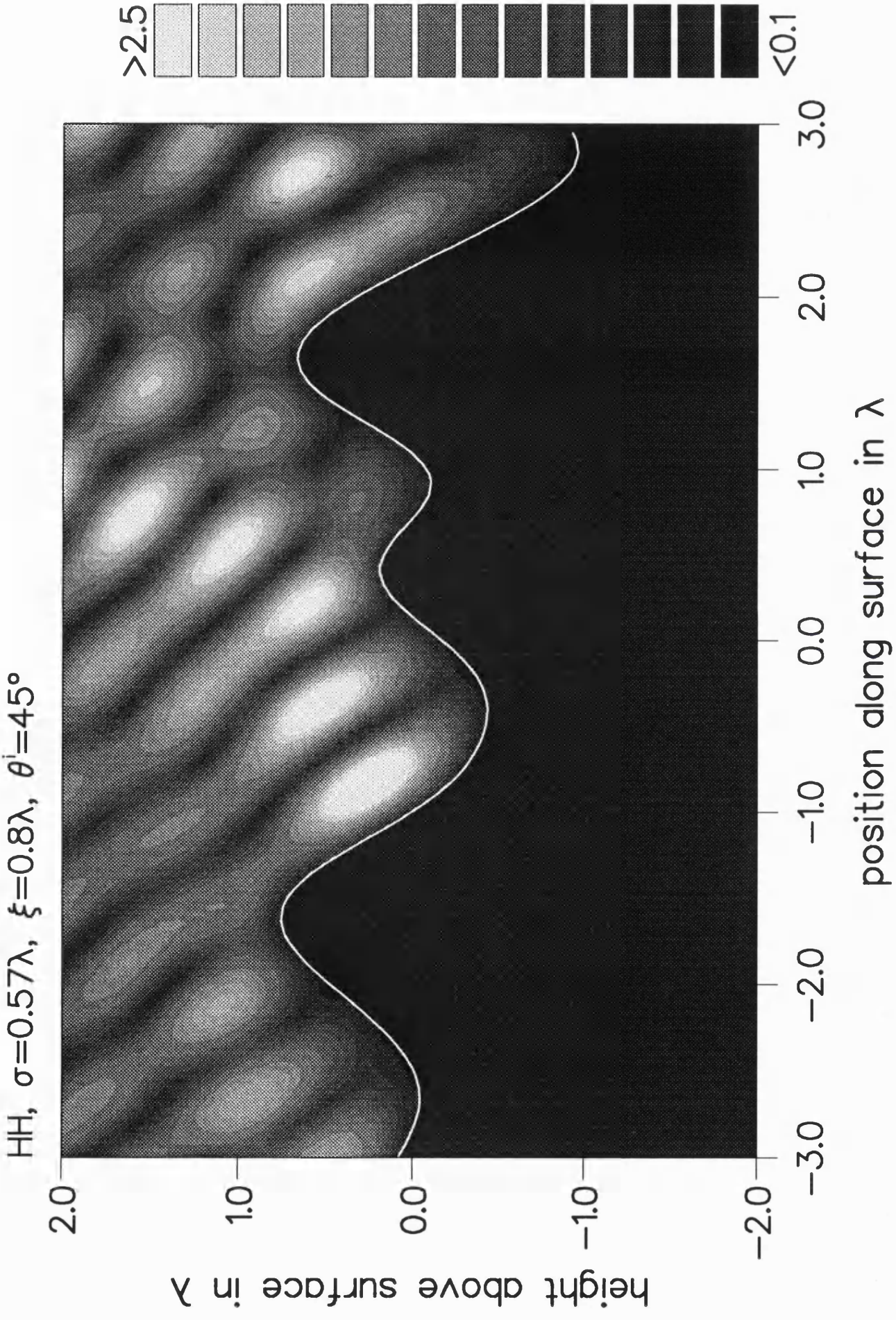

Fig. 2·6. The normalized modulus of the total magnetic field in the vicinity of a rough surface with a RMS slope of 45° and a correlation-length of 0·8λ, when a vertically polarized wave is incident from the right with an incidence angle of 45°.

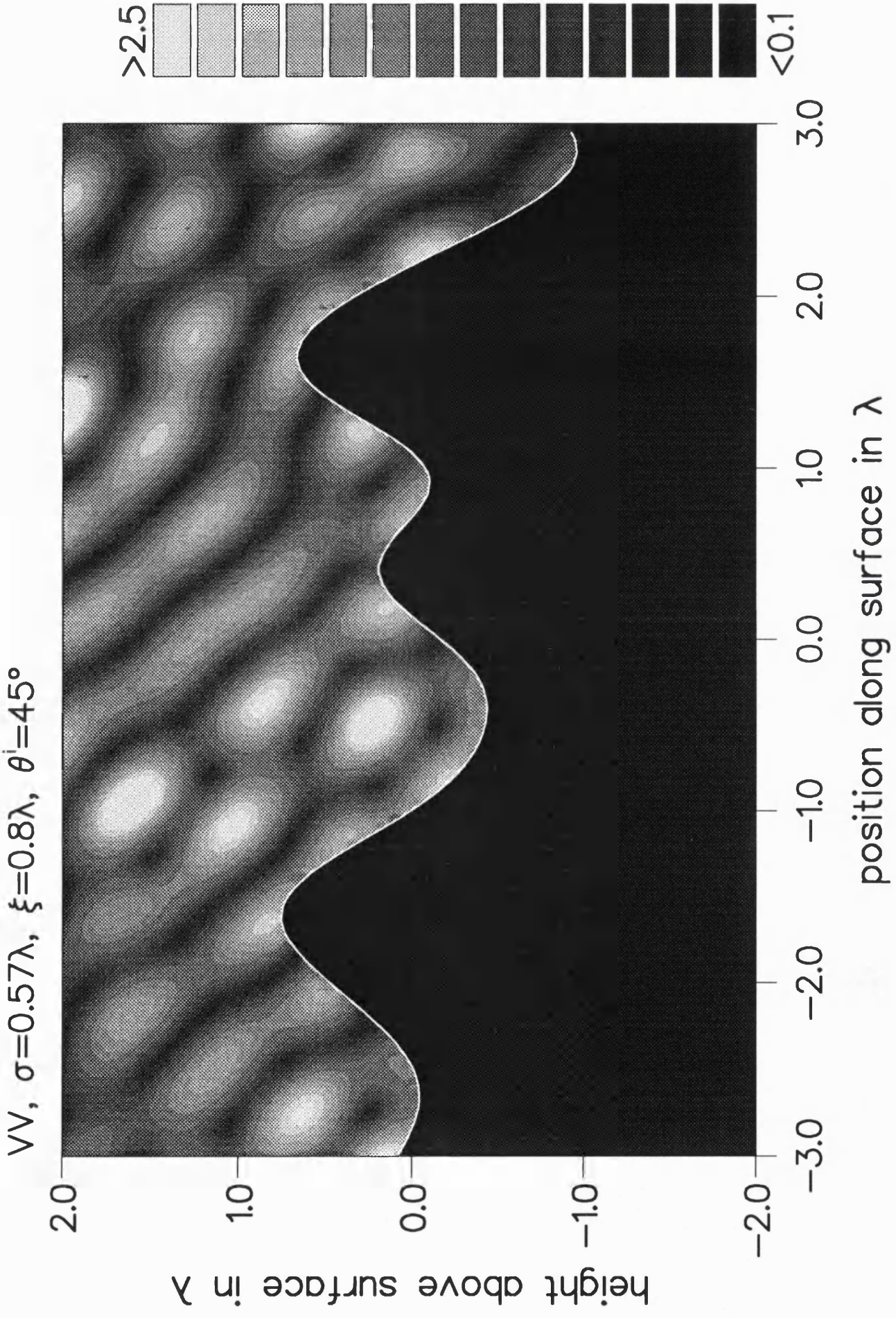

the Neumann boundary condition requires the total magnetic field to have the same value at points along the vector normal to the surface. It can be verified from fig. 2·6 that the contours intersecting the perfect-conductor are correctly perpendicular to the surface boundary.

2·5 Chapter Summary.

In this chapter we presented the numerical method used to solve magnetic-field-integral-equation for a two-dimensional, Gaussian rough surface. A quadrature that accommodates rough surfaces with large slopes is used to represent the continuous equation as a matrix-equation. For the surfaces we have considered, the matrices generated in the discretization of the continuous equation are not ill-conditioned, and we have found that LU decomposition solves the discrete equation to within the numerical accuracy of the double-precision, floating-point-arithmetic used in its computation. Contour-plots of the total electromagnetic field in the vicinity of the surface boundary were used to show how our numerical solution for the scattered field closely equals minus the incident field beneath the perfect-conductor. We consider that the closeness of the scattered field to minus the incident field, a property of the exact solution of the MFIE, is strong evidence that our discrete approximation of the MFIE is a good one.

3
Iterative solution of the magnetic-field-integral-equation

The principal problem in the numerical solution of the electromagnetic-field integral equations is that very large matrices are generated, even for moderately sized two-dimensional surfaces. Direct-methods of solving large matrix-equations can consume substantial computer resources, and there is considerable interest in using iterative-methods to solve these equations that one hopes will give a good estimate of the solution in relatively few iterations, thereby reducing the computational requirement.

In this chapter we examine two iterative methods of solving the magnetic-field-integral-equation (MFIE); the Neumann expansion, which has been used to formally represent the solution to the continuous MFIE; and the conjugate-gradient method, a procedure for solving matrix-equation whose convergence is in theory sure.

3·1 The numerical calculation of rough surface scattering by the Neumann expansion.

A natural candidate for an iterative solution of the discrete representation of the MFIE is the Neumann expansion used by Holliday (1985), and Holliday *et al* (1987). However, although the expansion has been used to formally represent the solution to the MFIE (Brown, 1982), there is no proof that the expansion, either of the MFIE or its discrete representation converges. The convergence or otherwise of the discrete case cannot prove the convergence or otherwise of the continuous case

and *vice versa*. On the other hand, the failure of the discrete case to converge would provide strong evidence that the convergence of the continuous case was not generally true. Moreover, if the convergence of the discrete case is unsure, it would be better in numerical work to replace it with an iteration whose convergence was certain. We have examined the convergence and rate of convergence of the Neumann expansion applied to the discrete representation of the MFIEs for Gaussian, rough surfaces. We have found that when the surface structure is of the same dimensions as the electromagnetic wavelength, the series diverges rapidly.

To solve the MFIE numerically, (1·1) is approximated with the discrete equation

$$2H^i(x_n) = J(x_n) + \sum_{m=0}^{N-1} K(x_n,x_m)\, J(x_m). \tag{3·1}$$

The matrix K is bounded, so for every J there is a positive constant α such that (Stakgold, 1979),

$$\left[\sum_{n=0}^{N-1}\left|\sum_{m=0}^{N-1} K(x_n,x_m)\, J(x_m)\right|^2\right]^{1/2} \le \alpha\left[\sum_{m=0}^{N-1} |J(x_m)|^2\right]^{1/2},$$

$$\equiv ||KJ|| \le \alpha ||J||. \tag{3·2}$$

In the Neumann expansion the solution $J(x_n)$ of the matrix-equation (3·1) is the limit of the sequence J_k, k = 0, 1, ..., ∞, obtained from the iteration

$$J_{k+1}(x_n) = 2H^i(x_n) - \sum_{m=0}^{N-1} K(x_n,x_m)\, J_k(x_m) \tag{3·3}$$

The iteration converges if $\alpha < 1$. This is true for arbitrary J_0 (Kreysig, p. 375, 1978). Furthermore,

$$\alpha \le \max \frac{||KJ||}{||J||} \equiv ||K||. \tag{3·4}$$

Therefore, a norm of K less than unity is a sufficient condition for convergence. The only algorithmic method we are aware of to determine the norm of K directly is to determine its singular values, (K is not Hermitian symmetric), (Schilling and Lee, 1988), (Wilkinson and Rheinsch, 1978). Numerically, this requires essentially the same effort as computing the inverse of K; if it was easy to determine *a-priori* the norm of K we would not require an iterative solution to (3·1).

We need a step-by-step method of identifying divergence. At each iteration we substitute J_k in (3·3) to generate the quantity

$$2H_k^i(x_n) = J_k(x_n) + \sum_{m=0}^{N-1} K(x_n,x_m)\, J_k(x_m). \tag{3·5}$$

We then form the normalized error

$$\varepsilon_k = \frac{\| H_k^i - H_k^i \|}{\| H_k^i \|} \tag{3·6}$$

We will show that ε_k satisfies the inequality

$$\varepsilon_k \leq \alpha^k \varepsilon_0, \tag{3·7}$$

and if the iteration (3·5) is initialised by setting $J_0 = 2H^i$, ε_0 satisfies the inequality

$$\varepsilon_0 \leq \alpha\,. \tag{3·8}$$

The inequalities (3·7) and (3·8) provide sufficient step-by-step tests for divergence. If $\varepsilon_k > \varepsilon_0$, or $\varepsilon_0 > 1$, then $\alpha > 1$ and the iteration diverges. The inequalities (3·7) and (3·8) are obtained as follows. From (3·6), (3·3) and (3·5) we have

$$\varepsilon_k = \frac{\| H^i_k - H^i \|}{\| H^i \|}. \tag{3·9}$$

But, from (3·3)

$$\| J_{k+1} - J_k \| = \| K(J_k - J_{k-1}) \|$$

$$\leq \alpha \| J_k - J_{k-1} \|$$

$$= \alpha \| K(J_{k-1} - J_{k-2}) \|$$

$$\ldots \leq \alpha^k \| J_1 - J_0 \|, \tag{3·10}$$

and (3·7) then follows by reusing (3·9). We have from (3·9) and (3·3) that if

$$J_0 = 2H^i$$

$$\varepsilon_0 = \frac{\| J_1 - J_0 \|}{2 \| H^i \|}$$

$$= \frac{\| 2H^i + J_0 + KJ_0 \|}{2 \| H^i \|}$$

$$= \frac{\| KH^i \|}{\| H^i \|} \tag{3·11}$$

and (3·8) follows using (3·2). From (3·9) it is also apparent that ε_k does not measure the closeness of J_k to the solution $J(x_n)$. However, $\varepsilon_k \rightarrow 0$ when $J_k \rightarrow J(x_n)$, and we take the smallness of ε_k to indicate that J_k is close to the solution of (3·1)

In fig. 3·1 we show the normalized error ε_k generated by the Neumann expansion at each iteration, for a vertically polarized, electromagnetic wave (2·3), normally incident on a Gaussian rough surface. The figure

shows four cases with the same correlation-length of 0·4λ, but with different RMS heights. The RMS slope of the surface is given by $\arctan(\sqrt{2}\sigma/\xi)$; and (A) illustrates a RMS slope of 20°, (B) a RMS slope of 25°, (C) a RMS slope of 35°, and (D) a RMS slope of 45°.

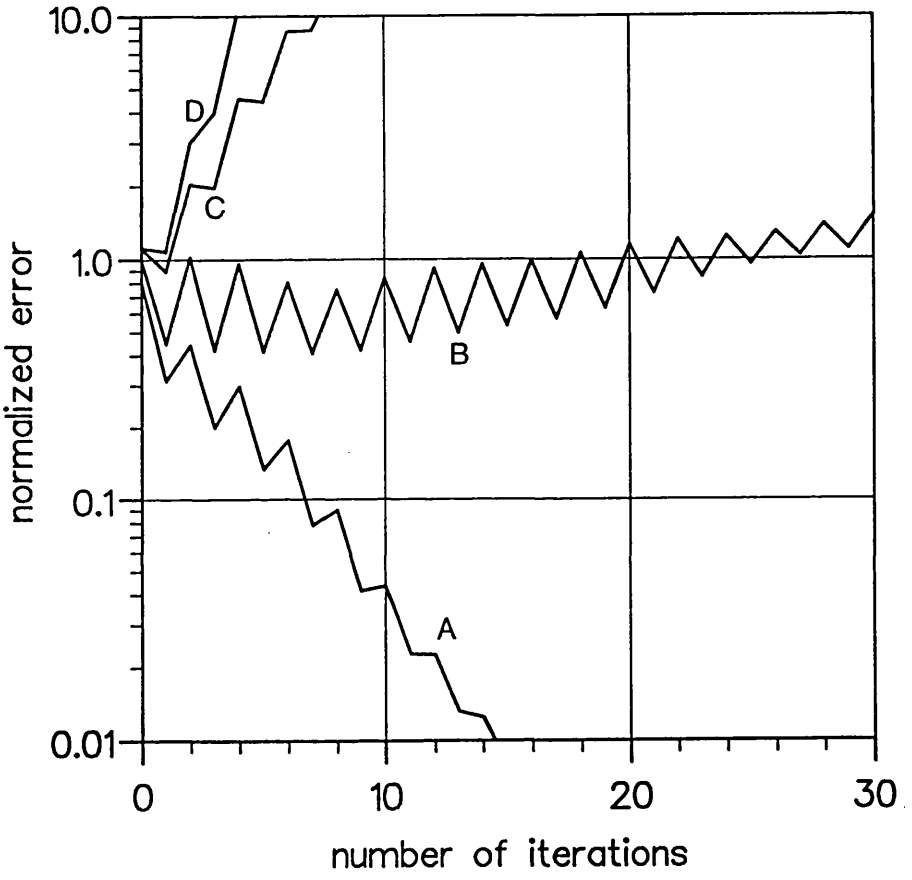

Fig. 3·1. The convergence of the Neumann expansion. The graph shows the normalized error ε_k with the number of iterations k. The correlation-length is 0·4 wavelengths and (A) the RMS slope is 20°; (B) the RMS slope is 25°; (C) the RMS slope is 35°; and (D) the RMS slope is 45°.

Three curves, (B), (C) and (D) clearly diverge. With $\alpha < 1$ one of the cases, curve (B), satisfies the inequality (3·8), but fails at the second iteration to satisfy the inequality (3·7), the remaining two fail to satisfy both the inequality (3·7) and (3·8). One of the cases curve (A) does apparently converge. Moreover the convergence is rapid; the normalized error is less than 0.01 within 13 iterations.

The RMS slope is clearly a factor in determining whether the expansion diverges, but we have found that the rate of divergence depends upon the surface correlation-length too. In fig. 3·2 we show four cases with a correlation-length of 0·8λ. The RMS slope of curves (A) - (D) in fig. 3·2 is the same as curves (A) - (D) in fig. 3·1.

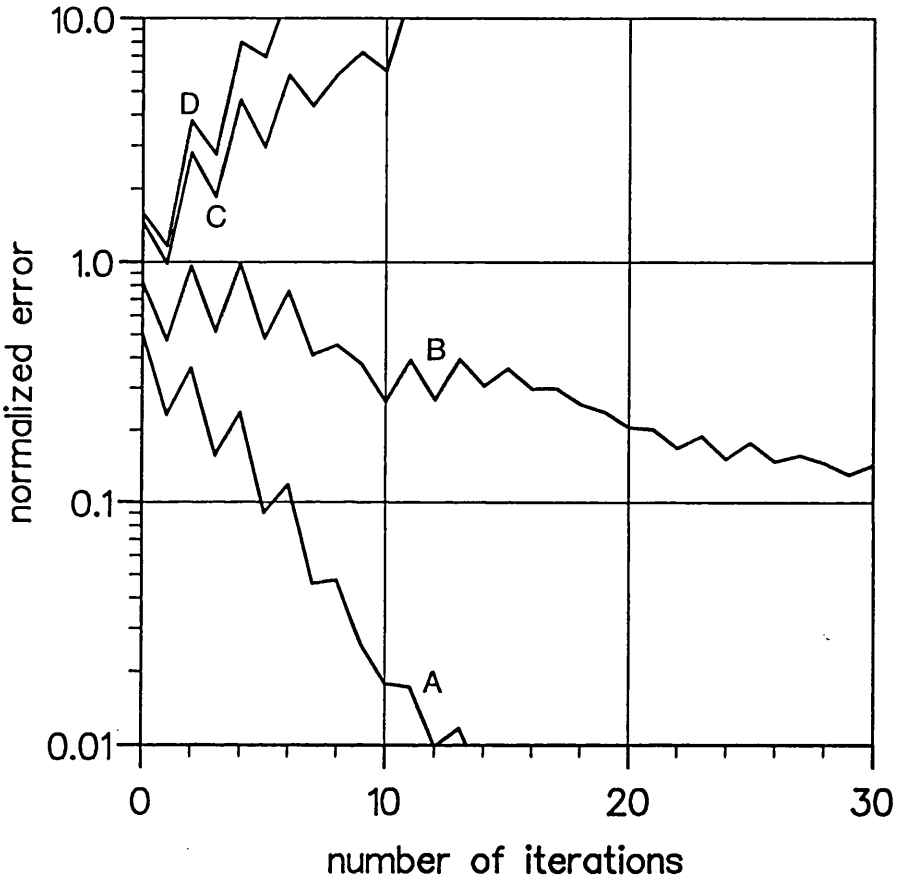

Fig. 3·2. The convergence of the Neumann expansion. The graph shows the normalized error ε_k with the number of iterations k. The correlation-length is 0·8 wavelengths and (A) the RMS slope is 20°; (B) the RMS slope is 25°; (C) the RMS slope is 35°; and (D) the RMS slope is 45°

In fig. 3·2 two of the curves, (C) and(D) clearly diverge, but at a rate which is marginally slower than curves (C) and (D) in fig. 3·1. The apparent convergence of curve (A) in fig. 3·2 is rapid, and marginally faster than curve (A) in fig. 3·1. The expansion also apparently converges in fig. 3·2(B), whereas in fig. 3·1(B) it does not. However, since fig. 3·2(B) marginally fails at the second step to satisfy the inequality (3·7) with $\alpha < 1$, we suspect that it

would diverge if we took sufficient iterations.

We have shown that when the surface structure is of the same dimensions as the electromagnetic wavelength, the Neumann series may diverge rapidly. The restriction normally placed on the Neumann expansion, *i.e.* $\sigma/\lambda << 1$ and $\sigma/\xi << 1$, are limitations that permit us to ignore all but the first two terms. In our work here, we have concentrated on cases where the RMS height and correlation length are of the same order, and of the same order of the electromagnetic wavelength, because we anticipated that this would be a region of the parameter space where the Neumann expansion may have difficulties converging. We have found that the expansion may provide a rapid numerical solution for small values of σ/ξ.and σ. To the extent that the numerical representation is a good approximation to the MFIE (1·1), we also consider that our results provide strong evidence that the Neumann expansion cannot be used without qualification to provide a formal solution to the rough surface MFIE.

3·2 The conjugate-gradient method, and avoiding rounding errors by using Gram-Schmidt orthogonalization.

The conjugate-gradient methods (Hestenes, 1980), (Sarkar *et al*, 1988) are iterative methods of solving matrix-equations whose convergence are in theory sure. There are many different conjugate-gradient methods to choose from. Some conjugate-gradient methods require the matrix in the equation to be positive-definite. The matrices in electromagnetic scattering problems are not positive-definite, and for the non-positive-definite case a suitable conjugate-gradient method to use is given in (Hestenes, 1980, eqn. 12.7(a) - (d), p. 297). We will refer to this method as the least-square-conjugate-gradient (LSCG) method.

In spite of the theoretical assurance of convergence, it is not uncommon to find in the literature references to the iteration diverging (Peterson and Mittra, 1984), (Peterson and Mittra, 1985), (Sarkar *et al*, 1988). We have ourselves been applying the LSCG method to the problem of scattering from rough surfaces, and have found that for large surfaces convergence is not sure. The LSCG method proceeds by generating at each iteration a conjugate-vector that satisfies some orthogonality properties in theory. The convergence is sure by virtue of these properties. However, the conjugate-vectors are generated recursively, and as a consequence of rounding errors, may fail to satisfy their theoretical properties (Scott and Peterson, 1988). In this section we use Gram-Schmidt orthogonalization to enforce the orthogonality properties at each iteration. In fact, a Gram-Schmidt conjugate-gradient method for the positive-definite case was given sometime ago by Hestenes (1980), and we have adapted this procedure for the non-positive-definite case. We call this modified LSCG method the Gram-Schmidt, least-square, conjugate-gradient (GS-LSCG) method. We will show that in the absence of rounding errors, the GS-LSCG method and the LSCG method will determine the same sequence of conjugate-vectors. In this respect the GS-LSCG method is not a new conjugate-gradient method. However, in the presence of rounding errors we have found the GS-LSCG method to be very much less susceptible to rounding errors than the LSCG method.

The LSCG and the GS-LSCG methods are applied to solving the matrix-equation

$$Lu = f. \tag{3·12}$$

In this study we shall only consider the case where the operator L is an N by N, non-singular matrix. The conjugate-gradient methods are iterative methods of solving the matrix-equation (3·12). At the k^{th} iteration, the methods determine a conjugate-vector p_k in the domain of L, and a vector

Lp_k in the range of L. The estimate u_k to the solution of the matrix-equation is determined as an expansion of the vectors p_j, j = 0, ..., k-1,

$$u_k = \sum_{j=0}^{k-1} a_j p_j \tag{3·13}$$

The coefficients a_j, j = 0, ..., k-1, of the expansion (3·13) are calculated to force the error

$$r_k = f - Lu_k, \tag{3·14}$$

between f and Lu_k orthogonal to the vectors Lp_j, j = 0, ..., k-1, *i.e.*

$$< r_k, Lp_j > = 0, \text{ for } j = 0, ..., k-1. \tag{3·15}$$

This is the natural criterion to choose for determining the coefficients a_j, j = 0, ..., k-1, for the following reason. Any set of N, linearly independent vectors in the range R(L) of L are a basis spanning R(L) (Kreysig, 1978). At the Nth iteration of the conjugate-gradient method, the N vectors Lp_j, j = 0, ..., N-1, in the range of L will have been determined. Moreover, as we will show later these vectors are linearly independent, and, therefore, span R(L). At the N^{th} iteration, the estimate u_N to the solution of the matrix-equation (3·12), the difference between the vectors f and Lu_N is the error r_N. With the coefficients of the expansion determined according to (3·15), the error r_N is either orthogonal to the space spanned by Lp_j, j = 0, ..., N-1, else it is zero. However, since the vectors Lp_j, j = 0, ..., N-1, span R(L), the only vector in R(L) that can satisfy (3·15) is the zero vector. With zero on the left-hand-side (LHS) of (3·14), u_N solves the matrix-equation (3·12) uniquely for non-singular L. In this manner, the conjugate-gradient method determines the exact solution of the matrix-equation in at most N iterations.

The condition (3·15) can be written in terms of the coefficients a_j, i = 0, ..., k-1, by substituting the right-hand-side (RHS) of (3·14) into the LHS of (3·15),

$$\langle r_k, Lp_j \rangle = \langle f, Lp_j \rangle - \langle Lu_k, Lp_j \rangle$$

$$= \langle f, Lp_j \rangle - \sum_{i=0}^{k-1} a_i \langle Lp_i, Lp_j \rangle = 0, \text{ for } j = 0, \ldots, k-1. \qquad (3\cdot16)$$

The second line of (3·16) is obtained from the first line by using the expansion (3·13) for the solution u_k. As (3·16) stands, the coefficients a_j, j = 0, ..., k-1, are themselves the solution of a system of linear equations. However, the vectors p_j, j = 0, ..., k-1, determined by the conjugate-gradient method are termed "conjugate-vectors", because they satisfy the orthogonality property

$$\langle Lp_i, Lp_j \rangle = 0, \text{ for } i \neq j. \qquad (3\cdot17)$$

This property diagonalizes (3·16). It also guarantees that the vectors Lp_j, j = 0, ..., k-1, are linearly independent, as we had required earlier. Applying the property (3·17) to the RHS of (3·16), the coefficients a_j, j = 0, ..., k-1, are determined according to

$$\langle r_k, Lp_j \rangle = \langle f, Lp_j \rangle - a_j \| Lp_j \|^2 = 0, \text{ for } j < k. \qquad (3\cdot18)$$

The solution

$$a_j = \langle f, Lp_j \rangle / \| Lp_j \|^2, \text{ for } j < k, \qquad (3\cdot19)$$

solves (3·18), as may be verified by substitution. An important fact to recognize from (3·19) is that only the vector p_k is used to compute a_k. Therefore, if we have already generated the sequence of vectors p_j, j = 0, ...,

k-2, and by some means generate a new vector p_{k-1}, we need only deduce the coefficient a_{k-1} to augment the solution (3·13) according to

$$u_k = u_{k-1} + a_{k-1} p_{k-1}. \tag{3·20}$$

Thus we have an iterative method of solving (3·12). Similarly, the error r_k is determined recursively

$$r_k = f - Lu_{k-1} - a_{k-1} Lp_{k-1}$$

$$= r_{k-1} - a_{k-1} Lp_{k-1}. \tag{3·21}$$

The first line of (3·21) is obtained by substituting the RHS of (3·20) into the LHS of (3·14). The second line follows from the definition of the error vector r_{k-1}. We will make use of (3·21) below. The conjugate-gradient method starts with an initial guess u_0 at the solution to (3·12), and determines the first conjugate-vector as

$$p_0 = L^a r_0. \tag{3·22}$$

Here, L^a is the complex-conjugate transpose of L.

The difference between the LSCG and the GS-LSCG algorithms is the manner in which the conjugate-vectors p_j, j = 1, ..., n < N are determined. At the k^{th} iteration, the GS-LSCG method determines the conjugate-vector p_k as

$$p_k = L^a r_k - \sum_{j=0}^{k-1} \gamma_j p_j \tag{3·23}$$

$$= L^a r_k - \gamma_{k-1} p_{k-1} - \sum_{j=0}^{k-2} \gamma_j p_j.. \tag{3·24}$$

The coefficients γ_j, j = 0, ..., k-1, in (3·23) are determined to force Lp_k orthogonal to Lp_j, j = 0, ..., k-1. This guarantees that the vector p_k satisfies the orthogonality property (3·17). The property (3·17) in terms of the coefficients γ_j, j = 0, ..., k-1, is

$$< Lp_k, Lp_j > = <LL^a r_k, Lp_j > - \sum_{i=0}^{k-1} \gamma_i < Lp_i, Lp_j >, \text{ for } j = 0,..., k-1. \quad (3·25)$$

The RHS of (3·25) is obtained by operating on both sides of (3·23) with L, and then forming the innerproduct on the LHS of (3·25). However, if, by assumption, the vectors Lp_j, j = 0, ..., k-1, having been determined by the GS-LSCG prior to the k^{th} iteration, satisfy the orthogonality property (3·17), then

$$< Lp_k, Lp_j> = < LL^a r_k, Lp_j > - \gamma_j \| Lp_j \|^2 = 0, \text{ for } j = 0,..., k-1. \quad (3·26)$$

The RHS of (3·26) is obtained by applying the property (3·17) to the argument of the sum in (3·25). From (3·26), the orthogonality property (3·17) is guaranteed by determining the coefficients according to

$$\gamma_j = \frac{< LL^a r_k, Lp_j>}{\| Lp_j \|^2}, \text{ for } j = 0,..., k-1. \quad (3·27)$$

Thus, if (3·17) is true for the vectors Lp_j, j = 0, ..., k-1, then by determining the coefficients γ_j, j = 0, ..., k-1, according to (3·27), it is also true for Lp_j, j = 0, ..., k. But, for k = 1,

$$<Lp_1, Lp_0> = <LL^a r_1, Lp_0> - \frac{< LL^a r_1, Lp_0>}{\| Lp_0 \|^2} \| Lp_0 \|^2 = 0, \quad (3·28)$$

and thus by induction (3·25), and hence (3·17) is true for all k. In fact, the vector Lp_k is the component of $LL^a r_k$ orthogonal to the orthogonal vectors Lp_j, j = 0, ..., k-1, (Schilling and Lee, 1985). This is a special case of Gram-Schmidt orthogonalization, where the Gram-matrix for the vectors Lp_j, j = 0, ..., k-1, is diagonalized by virtue of the orthogonality property (3·17).

In the case of the LSCG method, the conjugate-vector p_k is determined from the first two terms on the RHS of (3·24) with γ_{k-1} computed according to (3·27). The only difference between the LSCG method and the GS-LSCG method is due to the last term on the RHS of (3·24). However, we will show that this term is in theory zero, because the coefficients

$$\gamma_j = 0, \text{ for } j = 0, ..., k-2. \tag{3·29}$$

In other words we will now show that the GS-LSCG method and the LSCG method are in theory the same. From (3·21), the vector Lp_j in terms of the error vectors r_{j+1} and r_j is

$$Lp_j = (r_j - r_{j+1}) / a_j. \tag{3·30}$$

With (3·30) substituted into (3·27),the coefficients γ_j, j = 0, ..., k-1, are determined according to

$$\gamma_j = \frac{< LL^a r_k, (r_j - r_{j+1})>}{a_j \, || \, Lp_j \, ||^2}$$

$$= \frac{< L^a r_k, L^a r_{j+1}> - < L^a r_k, L^a r_j>}{a_j \, || \, Lp_j \, ||^2}. \tag{3·31}$$

From (3·23),

$$L^a r_j = p_j + \sum_{i=0}^{j-1} \gamma_i \, p_i \, , \tag{3·32}$$

and using (3·32), the innerproduct

$$< L^a r_k, p_j + \sum_{i=0}^{j-1} \gamma_i p_i >$$

$$= < r_k, Lp_j > + \sum_{i=0}^{j-1} \gamma_i < r_k, Lp_i >$$

$$= 0, \text{ for } j<k. \tag{3·33}$$

The last line of (3·33) is a consequence of (3·15). Finally, applying (3·33) to the innerproducts on the RHS of (3·31), we have (3·29).

The subtlety of the LSCG method is it is only necessary to determine the one coefficient γ_{k-1} to guarantee the orthogonality property (3·17). This property of the conjugate-gradient methods was proved some time ago by Hestenes (1980). Hestenes considered a general form of the conjugate-gradient algorithm, and derived many of the results in a general way using a geometric interpretation of the iteration. The algebraic proof presented here, although less general than the one in (Hestenes, 1980), allows us to contrast the methods explicitly. Whilst the LSCG method and the GS-LSCG method are in theory the same, we have found that in practice the GS-LSCG method is less susceptible to rounding errors than the LSCG method. This point will be illustrated later on in this section.

The solution of the matrix-equation (3·12) will not be known. So the best guide we have to the rate of convergence of the LSCG method is to compute at each iteration the normalized error,

$$\varepsilon_k = \frac{||f - Lu_k||}{||f||}. \tag{3·34}$$

The normalized error ε does not measure the closeness of u_k to the solution u. However, $\varepsilon_k \to 0$ when $u_k \to u$, and we take the smallness of the error ε_k to indicate that u_k is close to the solution of (3·12). This point was discussed in § 3·1. In theory, the LSCG method guarantees that the normalized error satisfies the inequality (Sarkar, *et al*, 1981)

$$\varepsilon_k < \varepsilon_{k-1}. \tag{3·35}$$

Furthermore, in the absence of rounding errors the solution of (3·12) is obtained in at most N iterations,

$$\varepsilon_N = 0. \tag{3·36}$$

We have applied the LSCG algorithm to the discrete approximation of the magnetic-field-integral-equation (MFIE) for a Gaussian rough surface where the RMS height and correlation-length are of the same order, and are of the same order as the electromagnetic wavelength. The procedure used to represent the MFIE as a matrix-equation is described in § 2·3. In the following examples, the rough surface was 50 electromagnetic wavelengths long and the matrix size N ~ 800 - 1000. In fig. 3·3 we show the normalized error ε_k, generated at each iteration. The figure shows four cases with the same correlation-length ξ of 0·6 electromagnetic wavelengths, but with different RMS height σ. The RMS surface slope is given by $\arctan(\sqrt{2}\sigma/\xi)$ and curve (A) illustrates a RMS slope of 20°; (B) a RMS slope of 25°; (C) a RMS slope of 35°; and (D) a RMS slope of 45°. For the first 16 iterations the normalized error satisfies the inequality (3·35). However, by the 21st iteration the normalized error has failed the inequality (3·35) in all four cases.

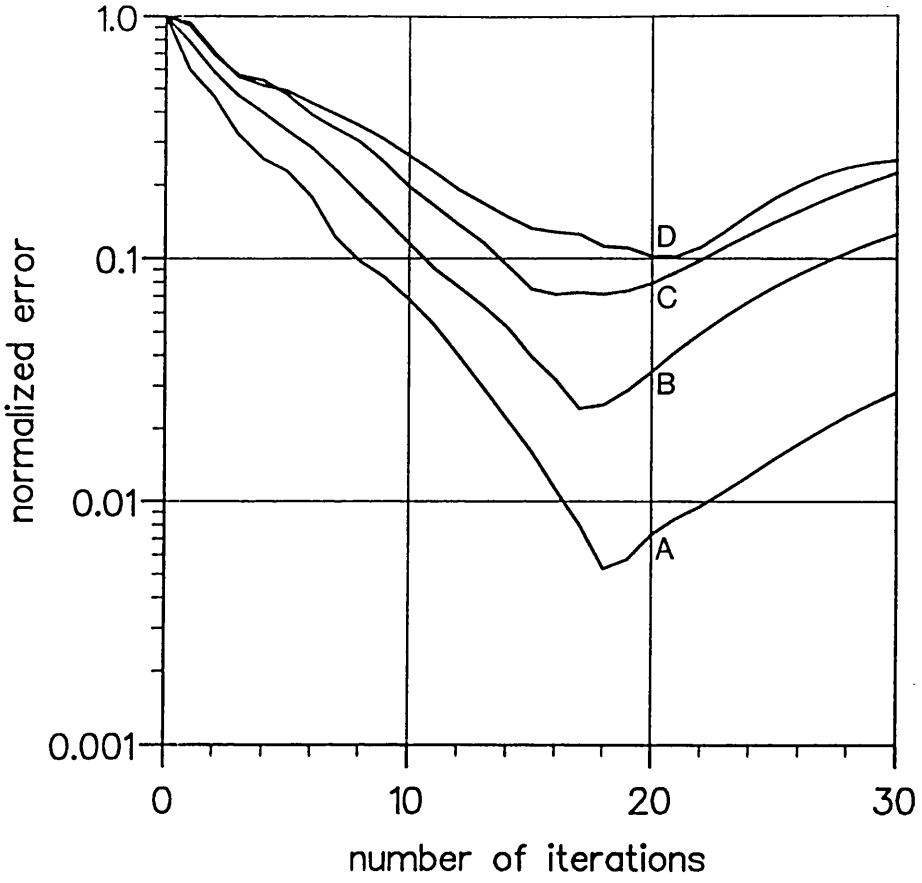

Fig. 3·3. The convergence of the least-square-conjugate-gradient method. The graph shows the normalized error ε_k with the number of iterations k. The correlation-length is 0·6 wavelengths and (A) the RMS slope is 20°; (B) the RMS slope is 25°; (C) the RMS slope is 35°; and (D) the RMS slope is 45°

In fig. 3·4 we show the normalized error ε_k generated by the GS-LSCG algorithm applied to the same four cases shown in fig. 3·3. For the first 16 iterations the error in fig. 3·4(A) - (D) is the same as the error in fig. 3·3(A) - (D). However, in contrast to fig. 3·3 the normalized error in fig. 3·4 converges in all cases. In fact, in all the cases we have considered, we have never experienced any difficulties in the convergence of the GS-LSCG method. Furthermore, we have always found the GS-LSCG method to reduce the normalized error at each iteration, a theoretical property of the LSCG method. We have found that using Gram-Schmidt orthogonalization to determine the conjugate-vectors ensures, at least when N ~ 1000, the innerproduct (3·17) is nominally zero to 15 decimal

places, the numerical accuracy of the double-precision, floating-point arithmetic used in the computations

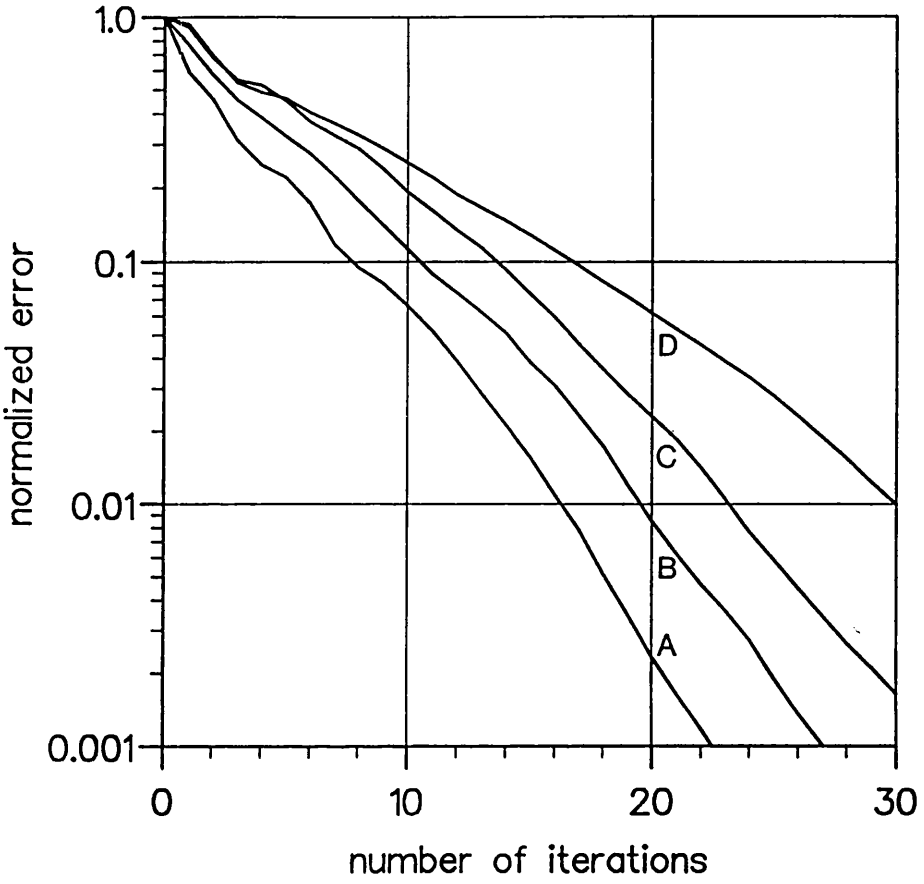

Fig. 3·4. The convergence of the Gram-Schmidt, least-square, conjugate-gradient method. The graph shows the normalized error ε_k with the number of iterations k. The correlation-length is 0·6 wavelengths and (A) the RMS slope is 20°; (B) the RMS slope is 25°; (C) the RMS slope is 35°; and (D) the RMS slope is 45°

The GS-LSCG method does require nN floating-point-operations per iteration more than the LSCG method, where n is the number of conjugate-vectors determined up to that point, because there are n of the coefficients γ_j to calculate. The storage requirement is larger too, because the vectors Lp_j, j = 0, ..., n-1 and p_j, j = 0, ..., n-1 , must be stored. This may prove to be a problem when the number of iterations required to obtain a good solution to (3·12) is of the order of the matrix size N. However, in these situations direct solution methods would be more appropriate.

A second problem associated with the convergence of the conjugate-gradient method is the problem of the iteration stagnating, (Peterson and Mittra, 1985). Although rounding errors may *apriori* be suspected as causing the iteration to stagnate, we have found that the effect of rounding errors is to initiate divergence, rather than stagnation. For the cases we have considered we have not experienced the problem of stagnation. We suspect that the nature of the scattering problem, and the method used to approximate the continuous equation by a matrix-equation are the factors that determine whether or not the iteration will stagnate.

3·3 The conjugate-gradient method for scattering problems that require solutions for several incident fields.

In many electromagnetic scattering problems the solutions to the field-integral-equation for a surface with a particular geometry are required for several incident fields. LU decomposition is a method that allows the numerical solution for any incident field to be directly obtained. Also once N iterations of the LSCG method have been implemented for a particular incident field, the solution for an arbitrary incident field can also be directly obtained (Sarkar, 1983). However, the conjugate-gradient method is advantageous when a good solution is obtained in $n << N$ iterations. So, in practice the method is implemented for each incident field in turn in the hope that the total number of iterations will still be much less than N.

In this section we describe how the conjugate-gradient method is applied to scattering problems where solutions are required for several incident-fields (Smith *et al*, 1989). In the following discussion we will assume that the Gram-Schmidt, least-square, conjugate-gradient method (GS-LSCG) method, or, in the absence of rounding errors, the least-square, conjugate-gradient (LSCG) method has been applied to the matrix-equation

$$Lu = f, \tag{3·37}$$

for a vector $f = f_1$. In determining a solution to (3·37) for f_1, we determine a basis p_{i1}, $i = 0, ..., q$, spanning a subspace of the domain of L, and an orthogonal basis Lp_{i1}, $i = 0, ..., q$, spanning a subspace of the range of L. The best linear estimate (Papoulis, 1984) in terms of the conjugate-vectors p_{i1}, $i = 0, ..., q$, to the solution of (3·37) for $f = f_2$, is the vector u_{02} that forces the error

$$r_{02} = f_2 - Lu_{02}, \tag{3·38}$$

orthogonal to the subspace spanned by Lp_{i1}, $i = 0, ..., q$,

$$< r_{02}, Lp_{i1}> = 0, \text{ for } i = 0, ..., q. \tag{3·39}$$

As was discussed in § 3·2, the condition (3·39) is true for the initial-guess determined according to

$$u_{02} = \sum_{j=0}^{q-1} a_{j1}\, p_{j1},$$

$$a_{j1} = < f_2, Lp_{j1} > / \, || \, Lp_{j1} \, ||^2. \tag{3·40}$$

In solving for f_1 we have determined the inverse of L on the basis Lp_{i1}, $i = 0, ..., q$. If f_2 occupies the subspace spanned by this basis, then u_{02} is the unique solution of (3·37) for non-singular L. In the likely event of this being not the case, there is some solace from the fact that the search for other vectors p_{j2}, $j = 0, ..., n$, can be confined to those that satisfy the orthogonality property

$$< Lp_{i1}, Lp_{j2} > = 0, \text{ for } i = 0, ..., q, \text{ and } j = 0, ..., n. \tag{3·41}$$

Initialized with the initial-guess (3·40), the vectors p_{j2}, j = 0, ..., n, determined by the LSCG method will in theory satisfy (3·41), (Smith *et al*, 1989). However, due to the effect of rounding errors, we have found it necessary to use Gram-Schmidt orthogonalization to guarantee (3·41). The algorithm that results is the GS-LSCG method initialized with u_{02}. In this case, Gram-Schmidt orthogonalization is used to force the vector Lp_{k2} orthogonal to the vectors Lp_{i1}, i = 0, ..., q, and Lp_{j2}, j = 0, ..., k-1. In this manner the GS-LSCG method is applied to solving the matrix-equation (3·37) for each additional incident field.

We have applied this method to solving the rough surface scatter problem for six waves incident at angles from 0° to 70°. The method provides a moderate improvement in the rate of convergence with each additional incident field. However, this is offset by the increase in the storage and computation requirement discussed at the end of § 3·2.

3·4 The numerical calculation of rough surface scattering by the conjugate-gradient method.

The LSCG method has been used to solve the matrix-equations that represent the scattering of waves from thin wire antennae (Sarkar and Rao, 1984) and conducting and dielectric cylinders (Peterson and Mittra, 1984). For some of these structures they have shown rapid convergence, but there is no wide understanding of the range of geometries for which this is true, (Sarkar *et al*, 1981), (Peterson and Mittra, 1985). This section is concerned with the rate of convergence of the GS-LSCG method applied to the discrete approximation of the MFIE for a Gaussian rough surface where correlation-length and RMS surface height are of the same order, and of the same order as the electromagnetic wavelength. For the surfaces we have considered, N is typically 800 - 1000, and good solutions may be

obtained within 20 to 40 iterations. We have observed that the rate of convergence depends less upon the particular value of the RMS height and correlation-length of the surface, but more upon their ratio. This ratio is proportional to the RMS surface slope. We suppose that the reduction in the rate of convergence with increasing RMS surface slope is related to the degree of multiple-scattering at the surface boundary. We have found that the size of the surface, which determines the matrix size N, does not affect the rate of convergence. This is important, because the advantages of the the GS-LSCG method then grows with N. The GS-LSCG method generates a solution J_k at the kth iteration. To determine the closeness of the iterative solution to the solution of the matrix-equation (3·1), we calculate the normalized error

$$\varepsilon_k = \left[\frac{\sum_{m=0}^{N-1} | J(x_m) - J_k(x_m) |^2}{\sum_{m=0}^{N-1} | J(x_m) |^2} \right]^{1/2}$$

$$\equiv \frac{||J - J_k||}{||J||} \qquad (3\cdot42)$$

Here, J is the solution of the matrix-equation obtained by LU decomposition. The matrix (I + K) in (3·1) is not ill-conditioned and we have found that LU decomposition solves the matrix-equation to within the numerical accuracy of the double-precision, floating-point arithmetic used in its computation. In this section, we present the behaviour of the average value of the normalized error ε_k (3·42). The average error is computed from a sample size of 20.

We present in fig. 3·5 and 3·6 the average error for a vertically polarized wave incident at an angle of 45°. In all, six cases are shown. The three cases in fig. 3·5 have a correlation-length of 0·4λ and the three cases in fig. 3·6

have a correlation-length of 0·8λ. The RMS slope is given by arctan($\sqrt{2}\sigma/\xi$) and curve (A) is for a RMS slope of 25°, (B) a RMS slope of 35° and (C) a RMS slope of 45°. The figures show how the iteration yields an average error of less than 0·01 within 35 iterations. The figures also show how the RMS surface slope is a dominant factor in determining the rate of convergence of the GS-LSCG method. The rate of convergence of the GS-LSCG method is related to the conditioning of the matrix (I + K), (Sarkar and Arvas, 1985). Physically, we consider that the degree of ill conditioning is related to the degree of multiple-scattering at the surface boundary.

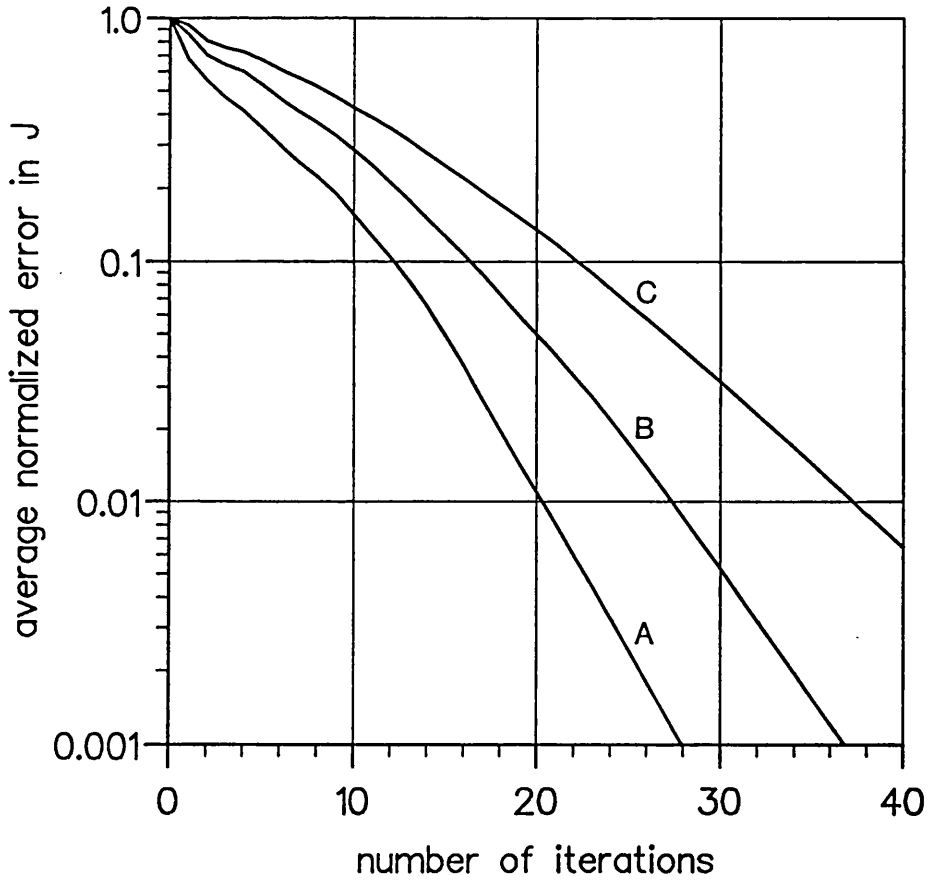

Fig. 3·5. The convergence of the conjugate-gradient method. The graph shows the normalized error ε_k with the number of iterations k for a vertically polarized wave incident at 45°. The correlation-length is 0·4 wavelengths and (A) the RMS slope is 25°; (B) the RMS slope is 35°; and (C) the RMS slope is 45°.

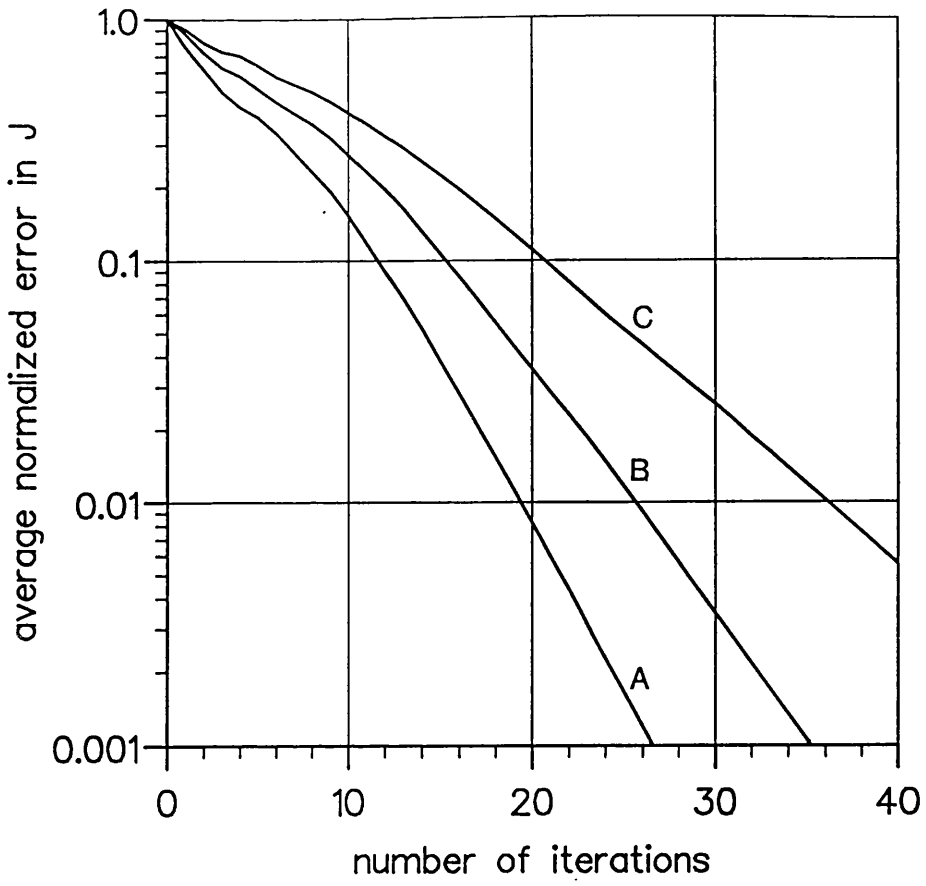

Fig. 3·6. The convergence of the conjugate-gradient method. The graph shows the normalized error $\varepsilon(k)$ with the number of iterations k for a vertically polarized wave incident at 45°. The correlation-length is 0·8 wavelengths and (A) the RMS slope is 25°; (B) the RMS slope is 35°; and (C) the RMS slope is 45°.

We have found that the polarization of the incident wave does not significantly effect the rate of convergence. We illustrate this point in fig, 3·7 where we present the average normalized error for a horizontally polarized wave incident at an angle of 45°. The three cases in fig. 3·7 have the same geometries as the three cases in fig. 3·5. It can be easily verified by comparing fig. 3·7 with fig. 3·5, that in cases (A) - (C) the error at each iteration is marginally smaller in the horizontal polarization case than in the vertical polarization case. However, after the 10^{th} iteration the rate of convergence is about the same for both polarizations.

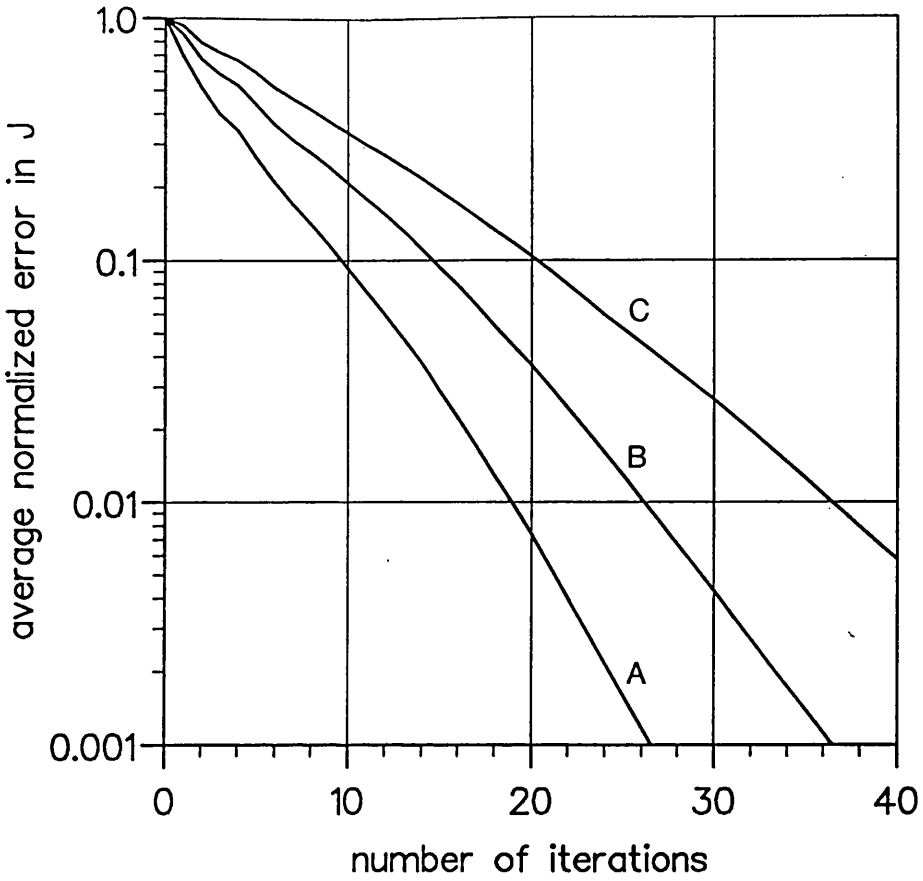

Fig. 3·7. The convergence of the conjugate-gradient method. The graph shows the average normalized error ε_k with the number of iterations k for a horizontally polarized wave incident at 45°. The correlation-length is 0·8 wavelengths and (A) the RMS slope is 25°; (B) the RMS slope is 35°; and (C) the RMS slope is 45°.

We have applied the GS-LSCG method to the discrete approximation of the MFIE for waves incident at angles from 0° to 70°. We have found that the angle of incidence does not significantly affect the rate of convergence. In fig. 3·8 we present three cases of the average normalized error for a vertically polarized wave, normally incident on a Gaussian rough surface with a correlation-length of 0·8λ. Curve (A) is for a RMS slope of 25°, (B) a RMS slope of 35° and (C) a RMS slope of 45°. The same three cases for a wave incident at an angle of 70° are presented in fig. 3·9 and the three cases for a wave incident at an angle of 45° are shown in fig. 3·6. It can be easily verified by comparing fig. 3·6, fig. 3·8 and fig. 3·9, that the average normalized error at each iteration is similar to all three angles of incidence.

We have applied the GS-LSCG method to surfaces where N is as large as 1800. We have found that the rate of convergence is largely unaffected by the size of the matrix. Figure 3·6(B), for example, shows the average error for a Gaussian rough surface with a correlation-length of 0·8λ and a RMS slope of 35°, illuminated by a vertically polarized wave incident at an angle of 45°. For the case in fig. 3·6(B) the matrix size N is on average ~800, and the average normalized error is less than 0·01 after 26 iterations. We found that when the GS-LSCG method was applied to the MFIE for the same RMS slope, but with N = 1755 the normalized error was reduced to less than 0·01 within 30 iterations.

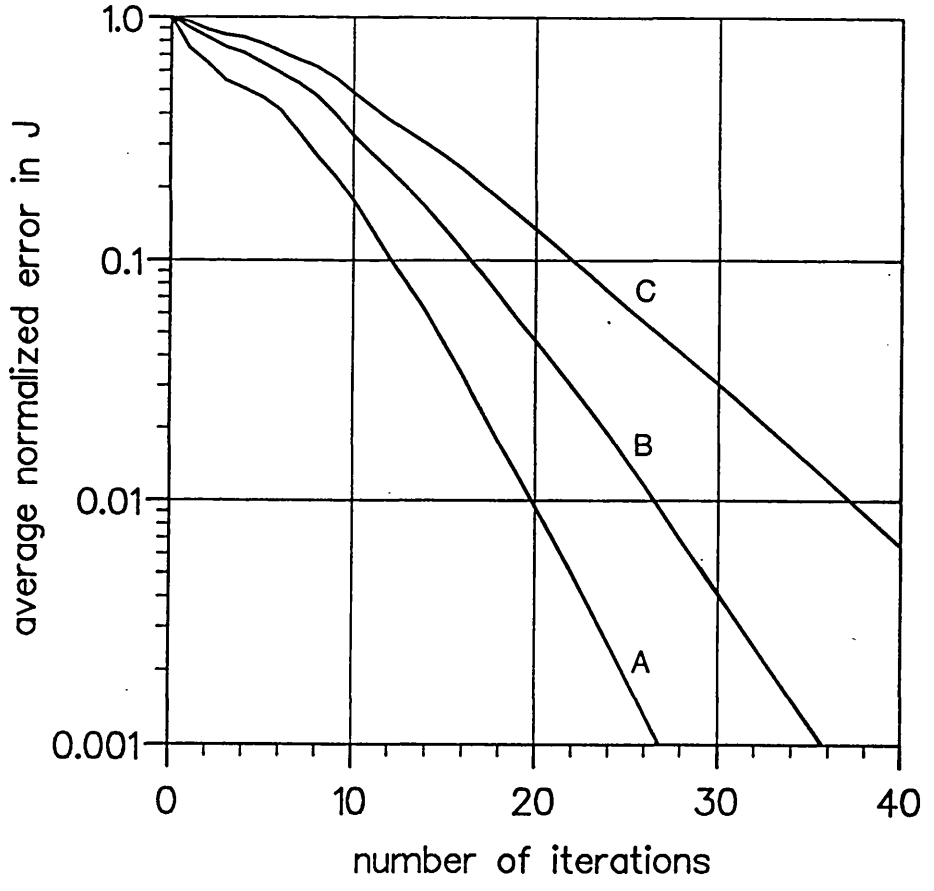

Fig. 3·8. The convergence of the conjugate-gradient method. The graph shows the average normalized error ε_k with the number of iterations k for a vertically polarized wave incident at 0°. The correlation-length is 0·8 wavelengths and (A) the RMS slope is 25°; (B) the RMS slope is 35°; and (C) the RMS slope is 45°.

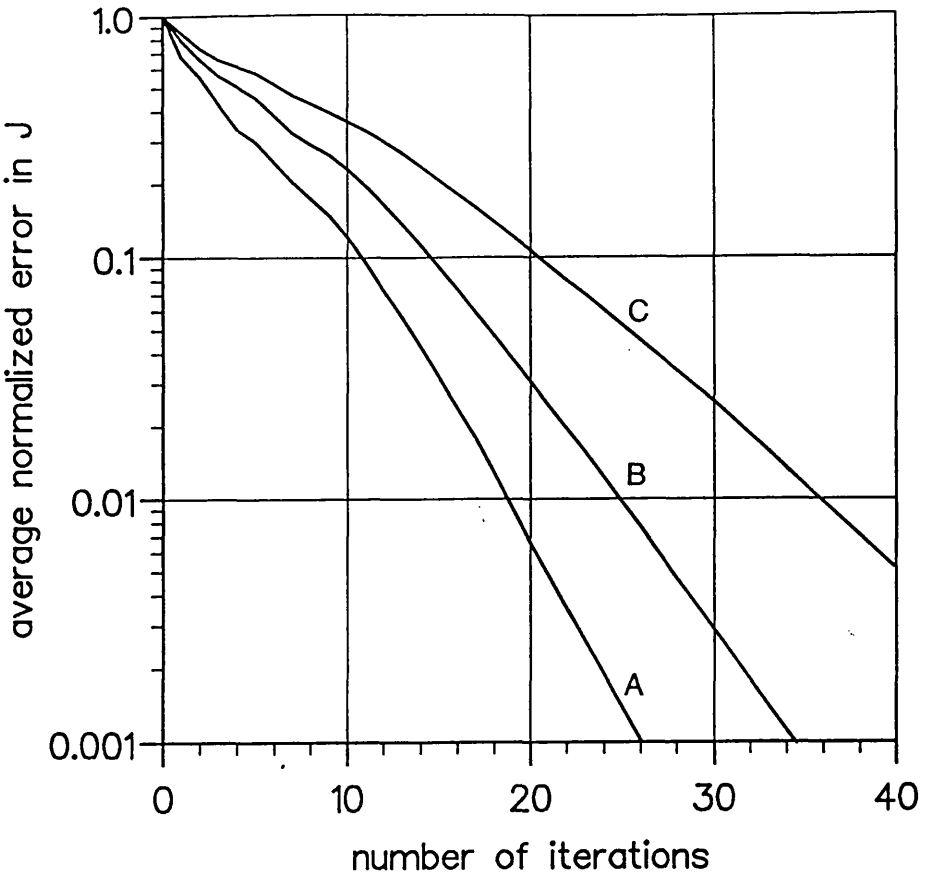

Fig. 3·9. The convergence of the conjugate-gradient method. The graph shows the average normalized error $\varepsilon(k)$ with the number of iterations k for a horizontally polarized wave incident at 70°. The correlation-length is 0·8 wavelengths and (A) the RMS slope is 25°; (B) the RMS slope is 35°; and (C) the RMS slope is 45°.

The fact that the rate of convergence does not depend on the matrix size N, but only upon the surface geometry, is important because the advantages of the conjugate-gradient method then grows with N.However, before discussing the computational advantages of the GS-LSCG method it necessary to first establish what is a "good solution". This is the subject of the next section.

3·5 Errors in the scattered far-field.

The principal quantity of interest to us, is the far-field scattered power. The calculation of the scattered far-field is described in Chapter 4.

Although the differences between our iterated solution to the discrete equation and its exact solution are small, it is possible that these differences may result in large errors in the scattered far-field, particularly when the scattered far-field is small. However, we have found that when the normalized error between these currents is less than 0·01, the difference between the scattered powers is small, even when the dynamic range of the scattered power is as large as 50dB.

We present in figs. 3·10 the scattered power for a horizontally polarized wave incident at angle of 45° on a Gaussian rough surface with a correlation-length of 0·8λ and a RMS slope of 25°.

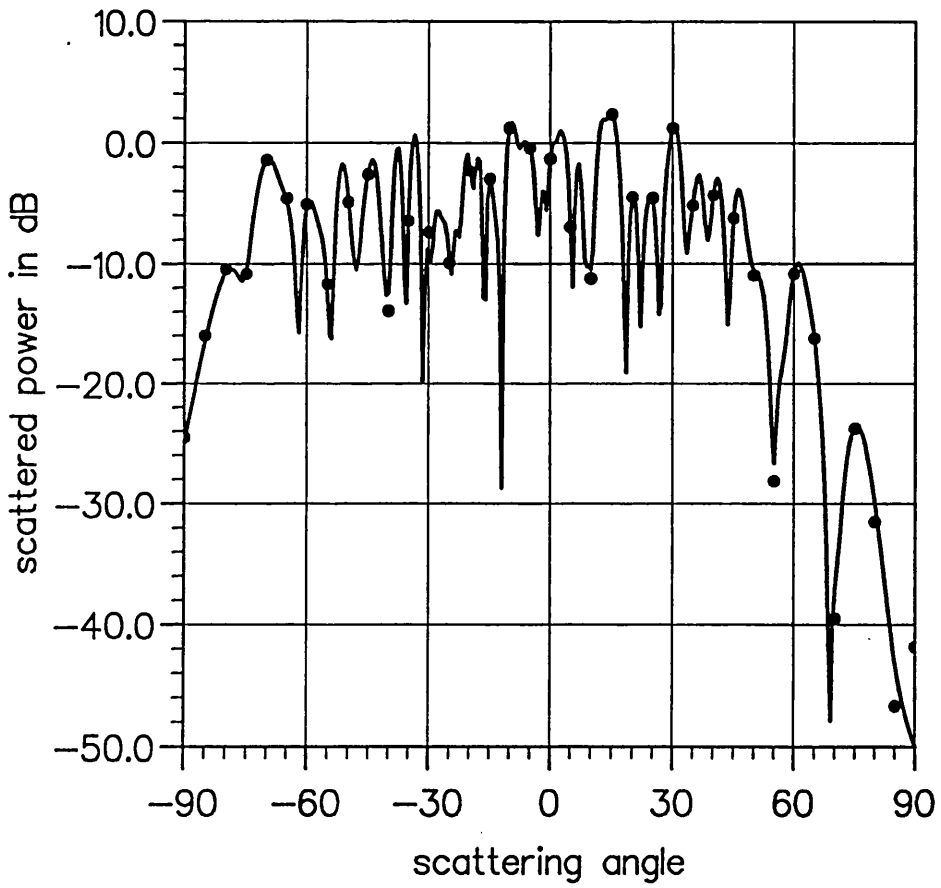

Fig. 3·10. The scattered powers for a Gaussian, rough surface with a correlation length of 0·8 wavelengths and a RMS slope of 25° illuminated by a horizontally polarized wave incident at an angle of 45°. The curve is computed using the solution for J obtained by LU decomposition, and the dots are computed using the solution J_{12} obtained by the GS-LSCG method.

The curve in the figure is the scattered power computed using the exact solution to the matrix-equation (3·1) obtained by LU decomposition, and the dots show the scattered power computed with the solution J_{12} obtained by the GS-LSCG method. In this case the normalized error ε_{12} is approximately 0·05. It can be verified from fig. 3·10, that when the scattered power is above -20dB there is small difference between the scattered powers computed with the exact and iterated solutions. However, below -20dB there is a clear difference between the scattered powers.

In fig. 3·11 we present the scattered power for the same surface, computed with the solution J_{20}.

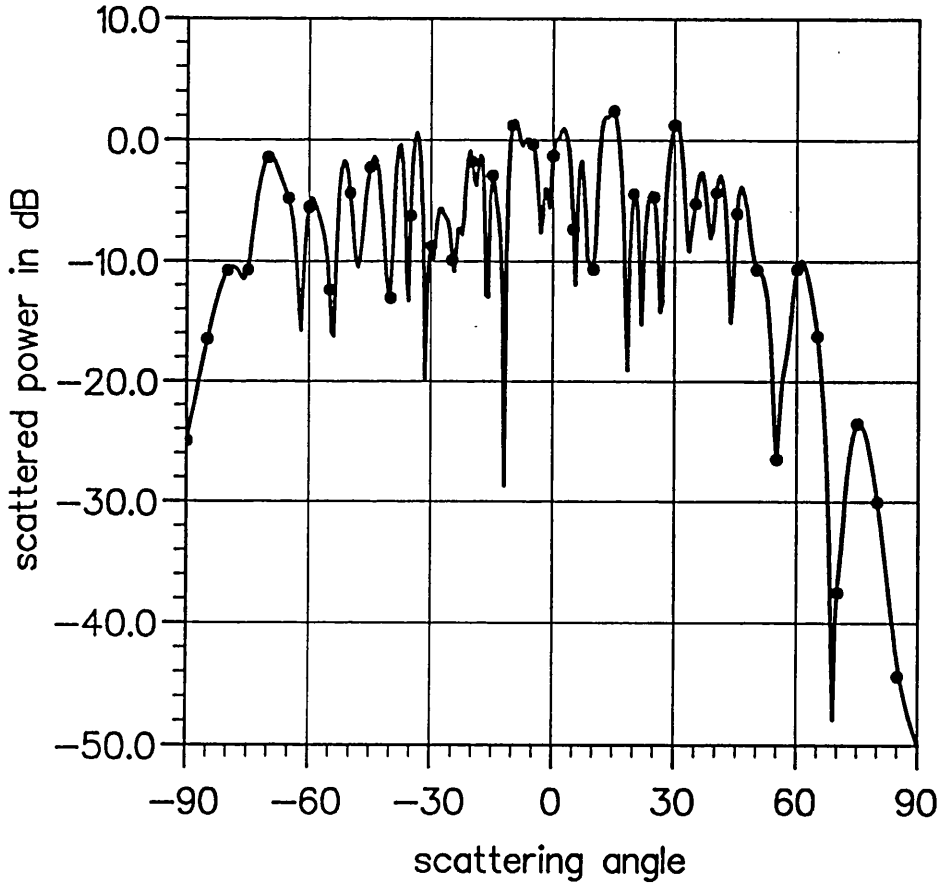

Fig. 3·11. The scattered powers for a Gaussian, rough surface with a correlation length of 0·8 wavelengths and a RMS slope of 25° illuminated by a horizontally polarized wave incident at at an angle of 45°. The curve is computed using the solution for J obtained by LU decomposition, and the dots are computed using the solution J_{20} obtained by the GS-LSCG method.

The normalized error ε_{20} is approximately 0·01. It can be easily verified from fig. 3·11 that with this value of error there is small difference between the two scattered powers, even though the dynamic range of the scattered power is as large as 50dB. It would appear from this result that small errors in J are mapped to small errors in the scattered field at each and every scattering angle.

3·6 Computational issues.

When the GS-LSCG method is used in practice, we do not know the exact solution to the matrix-equation. The best guide we have to the rate of convergence is the error in the incident field at the sample points. For the cases we have considered, when the average normalized error in J is less than 0·01 the average normalized error in the incident field at the sample points is less than 0·002. Although the error in J lags behind the error in the incident field at the surface, when one of these errors is small the other is too.

The computations were done on a Sun Sparcstation IPC. In fig. 3·12 we present the CPU seconds to (A) compute the N^2 elements of the matrix; (B) perform one iteration of the GS-LSCG method; and (C) factorize the matrix into its LU form. The CPU-time is roughly proportional to the number of floating-point-operations required by each task. One iteration of the GS-LSCG method requires approximately $2N^2$ floating-point-operations; LU decomposition requires $N^3/3$. We have found that the rate of convergence of the GS-LSCG method applied to solving the MFIEs for Gaussian, rough surfaces depends upon the RMS surface slope. For the surfaces we have considered good solutions are obtained in 20 - 30 iterations. It can be verified from fig. 3·12 that when N ~ 800 - 1000 the GS-LSCG method requires ~1/5 of the CPU-time required by LU-decomposition. We have found that the size of the surface, which determines N, does not effect the

rate of convergence. This is important, because the advantage of the GS-LSCG method then grows with N. With N ~ 2000, the GS-LSCG requires ~1/10 of the CPU-time required by LU decomposition.

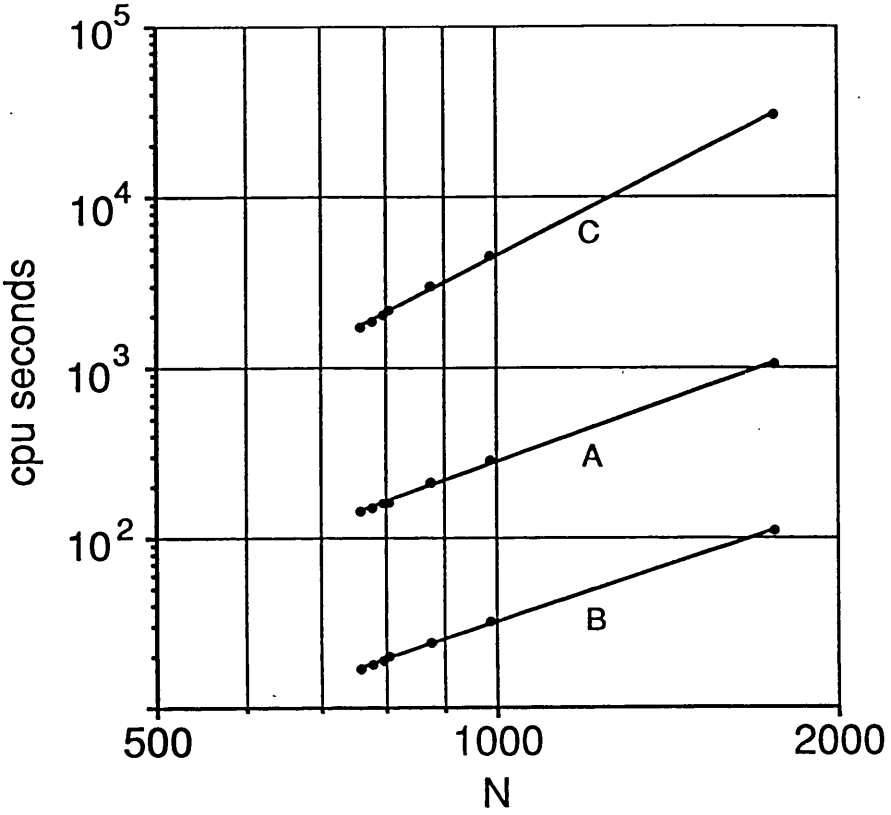

Fig. 3·12. The CPU-seconds required to (A) compute the N^2 elements of the matrix, (B) perform one iteration of the GS-LSCG method and (C) factorize the matrix into its LU form.

The CPU-time does not include the seconds spent swapping data between the hard-disc and the random-access-memory (RAM). When the RAM is large enough to accommodate the computational task, the time taken to do the computation is about the same as the CPU-time. The RAM available on the Sun Sparcstation was 24 mega-bytes. This was large enough for the computations on the matrices with N < 1000 to be done in real time. However, with N ~ 2000, ~95% of the time was spent swapping data to disc. With the GS-LSCG method the storage requirement can be reduced by not storing the matrix. Instead, the rows of the matrix are recomputed as the algorithm requires them. We have applied this

approach to solving the matrix-equations with N ~ 2000. We found that due to the reduction in the time spent swapping to disc, recomputing the matrix at each iteration made little difference to the time taken to obtain a solution, in spite of a 20 fold increase in the CPU-time used.

3·7 Chapter summary.

The numerical solution of the MFIE for rough surface scattering problems generates large matrices. We have found that the Neumann expansion applied to the discrete representation of the MFIE for Gaussian, rough surfaces with moderate slopes may provide a rapid numerical solution. It however fails to converge for rough surfaces in general. To the extent that the numerical representation is a good one, we also consider that our results provide strong evidence that the Neumann expansion cannot be used without qualification to provide a formal solution to the rough surface MFIE.

The least-square-conjugate-gradient (LSCG) method is an iterative method of solving matrix-equations whose convergence is in theory sure. We have applied the LSCG method to the problem of scattering from Gaussian, rough surfaces and have found that, due to rounding errors, convergence is not sure. In this chapter we presented a numerically robust form of the LSCG method, which we call the Gram-Schmidt, least-square, conjugate-gradient (GS-LSCG) method. In all the cases that we have considered, we have never experienced a problem with the convergence of the GS-LSCG method. We have found that the rate of convergence of the GS-LSCG method depends upon the RMS surface slope. Moreover, the size of the surface, which determines the matrix size N, does not significantly affect the rate of convergence. This is important, because the advantages of the GS-LSCG method then grows with N. When N is very large, or when

the slope of the surface is small, good solutions are obtained with an order of magnitude reduction in the computation required by LU decomposition.

In Chapters 4 and 6 we consider the scattering of waves incident at six angles between 0° and 70°. The disadvantage of the GS-LSCG method is that it is implemented for one incident field at a time. LU decomposition is a method that allows the solution for any incident field to be directly obtained. We have presented in this chapter a numerically robust conjugate-gradient method for scattering problems that require solutions for several incident fields. However, for the cases we have considered the solution for the surface current for each of the incident fields are too distinct for the method to provide any significant gain over LU decomposition. For this reason the solutions for the surface current used in Chapters 4 and 6 were obtained by LU decomposition. We consider that the work presented in this chapter, is relevant to the numerical solution of wave scattering from rough surfaces when solutions are required for a few incident fields, or when the size of the matrices generated in the discretization of the continuous equation prohibit the use of direct solution methods.

4
The expected scattered power for a patch of rough surface.

To solve the MFIE numerically the integral in (1·1) must be truncated at some point. The scattering problem described by the truncated integral-equation is that of a wave scattered from a patch of surface. The point at which the integral is truncated is important, because it is one of the factors that determines the size of the matrix used to approximate the MFIE, and hence the computation required to obtain the surface current density. From a computational standpoint a small patch size is preferable. However, since it is hoped that the normalized incoherent scattered power computed for an ensemble of rough surface patches will apply to the infinite surface too, the patch size must be large enough to accommodate the average scattering properties of the infinite surface. In the chapter, we investigate how the patch size effects the value of the normalized incoherent scattered power.

4·1 The scattered far-field.

When the length of surface illuminated by the incident wave is much larger than the distance from the surface to the observation point R, the scattered field is obtained from the integrals (Fung and Chen, 1985);

$$E^S(\theta^S) = Z_0\sqrt{\frac{k}{8\pi R}}\exp\left(-\frac{i\pi}{4}\right)\exp\ (-ikR)$$

$$\int_{-\infty}^{\infty} J(x')\exp\left(ik\left(z'\cos\theta^S - x'\sin\theta^S\right)\right)\left(\cos\theta^S - dz'/dx\sin\theta^S\right)\sqrt{1+(dz'/dx)^2}\,dx'$$

(4·1)

and

$$E^s(\theta^s) = Z_0 \sqrt{\frac{k}{8\pi R}} \exp\left(-\frac{i\pi}{4}\right) \exp(-ikR)$$

$$\int_{-\infty}^{\infty} J(x') \exp\left(ik\left(z' \cos\theta^s + x' \sin\theta^s\right)\right) \sqrt{1 + (dz'/dx)^2}\, dx' \quad (4\text{-}2)$$

The integral (4·1) is appropriate when the incident wave is vertically polarized, and the integral (4·2) is appropriate when the incident wave is horizontally polarized. Here, $E^s(\theta^s, \theta^i)$ is the scattered far-field in the direction of the scattering angle θ^s for a wave incident at θ^i, z' and dz'/dx are the height and slope of the surface at x', J is the surface current density, Z_0 is the characteristic impedance of free space, and k is the electromagnetic wavenumber. The geometry of the scattering problem is illustrated in fig. 4·1.

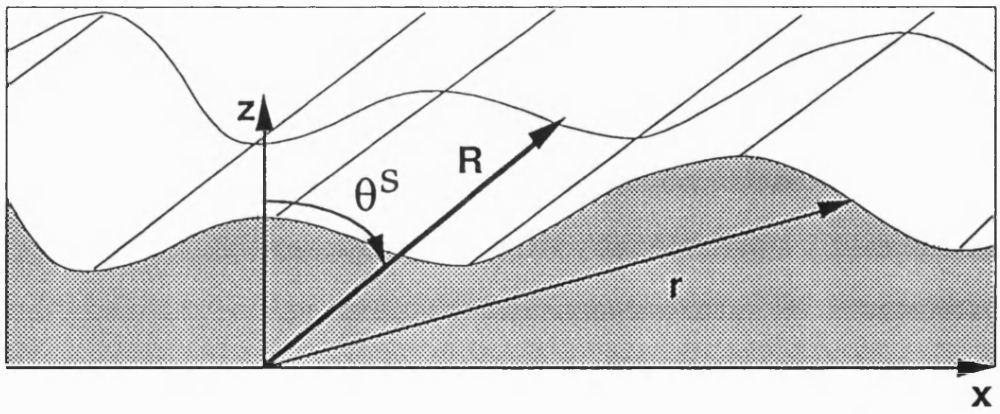

Fig. 4·1 The geometry of the scattering problem.

In this study the scattered powers are normalized with respect to the power incident on the surface. The normalized power scattered from the m^{th} surface realization, for example, is,

$$\sigma_S(m:\theta^s,\theta^i) = \frac{|\,E^s(m:\theta^s,\theta^i)\,|^2}{Z_0\,P^i(\theta^i)}. \qquad (4\cdot3)$$

Here, $E^s(m:\theta^s,\theta^i)$, m = 1, ..., M, is the far-field scattered from the m^{th} surface realization, and $P^i(\theta^i)$ is power incident on the surface. For the incident wave used our numerical simulations (Thorsos, 1988)

$$P^i(\theta^i) = H_0^2 Z_0 \sqrt{\frac{\pi}{2}}\gamma\left[1 - \frac{0\cdot5\,(1+2\tan^2\theta^i)}{\left(k\gamma\cos\theta^i\right)^2}\right]\cos\theta^i. \qquad (4\cdot4)$$

Here, γ is the parameter that controls the tapering of the incident wave. To simplify the notation used in the following text, we will assume that the scattered field computed with the integrals (4·1) and (4·2), have been multiplied by the factor $\sqrt{(R/Z_0P_i(\theta^i))}$.

4·2 The expected scattered power.

A description of the scattering behaviour of a randomly, rough surface involves associating some expected property to an ensemble of surface realizations. We are interested in the expected value of the scattered power,

$$\sigma_S(\theta^s,\theta^i) = E\left[\;\left|\,E^s(\theta^s,\theta^i)\right|^2\;\right]. \qquad (4\cdot5)$$

There are two components to the angular pattern of radiation scattered from an ensemble of randomly, rough surfaces, a coherent component and an incoherent component. The coherent scattered power is defined as

$$\left|\mu_S(\theta^s,\theta^i)\right|^2 = \left|E\left[\;E^s(\theta^s,\theta^i)\;\right]\right|^2 \qquad (4\cdot6)$$

Here, E [u] is the mean value of the random variable u(m), m = 1, ..., ∞,

and is read as the expected u. The coherent component contributes to the angular radiation pattern over a range of scattering angles centred on the specular angle. Its angular width is dependent upon the size of the illuminated surface, and in the limit of a plane wave illuminating a surface of infinite extent reduces to a delta function.

The incoherent or diffuse scattering component is defined as

$$\sigma^0(\theta^s, \theta^i) = \sigma_s(\theta^s, \theta^i) - \left|\mu_s(\theta^s, \theta^i)\right|^2. \tag{4.7}$$

As the term diffuse would suggest, the incoherent scattered power contributes to the radiation pattern in all directions, albeit that the diffuse scattering is greater in some directions than in others. In the following text, the dependence of the scattered far-field on the angle of incidence and the scattering angle has been omitted. We have also normalized the scattered powers with respect to the power incident on the surface.

We compute the average power scattered from M, uncorrelated, sections of a Gaussian rough surface,

$$\hat{\sigma}_s = \frac{1}{M} \sum_{m=1}^{M} \left| E^s(m) \right|^2 \tag{4.8}$$

Here, $E^s(m)$ m = 1, ..., M, is the field scattered from the m^{th} surface realization. In this manner, we obtain the estimate $\hat{\sigma}_s$ of the expected scattered power (4.5). The number of observations of the scattered power will be an important factor in determining the closeness of the estimate to its expected value. To determine the error in the estimate, let $\hat{\sigma}_s(j : M)$, j = 1,..., ∞, denote the random variable of estimates of the expected scattered power each made from M, independent, observations. It is well known that irrespective of the distribution of $\left| E^s(m) \right|^2$, m = 1, ..., ∞, the mean-square-error in the estimate is (Priestley, 1987)

$$E\left[\left(\hat{\sigma}_S(M) - \sigma_S\right)^2\right] = \frac{E\left[\left(|E^S|^2 - \sigma_S\right)^2\right]}{M}. \qquad (4\cdot9)$$

When the surface illuminated by the incident wave is many surface-correlation-lengths long the random variable $|E_S(m)|^2$, m = 1, ..., ∞, is Ricean distributed (Beckmann and Spizzichino, 1963). However, when the coherent component of the scattered power is small $|E_S(m)|^2$, m = 1, ..., ∞, is exponentially distributed (Rice, 1951), (Macaskill and Kachoyan, 1988), and

$$\frac{E\left[\left(|E^S|^2 - \sigma_S\right)^2\right]}{\sigma_S^2} = 1. \qquad (4\cdot10)$$

Using (4·10) in (4·9), the normalized RMS error in the estimate of the expected scattered power is

$$\frac{\sqrt{E\left[\left(\hat{\sigma}_S - \sigma_S\right)^2\right]}}{\sigma_S^2} = \frac{1}{\sqrt{M}}. \qquad (4\cdot11)$$

This is an unfortunate, but hardly unexpected result. By increasing the sample size by a factor of four, the error in the estimate is only reduced by a factor of two.

In this study we average the scattered powers for 60, uncorrelated, 50 wavelength long sections of a Gaussian rough surface. Waves incident at angles from 0° to 70° are considered. For normal incidence, the estimate of the average scattered power is determined from 60 independent observations. Away from normal incidence, we compute for each surface realization the scattered power at θ^S for a wave incident at θ^i, and the scattered power at $-\theta^S$ for a wave incident at $-\theta^i$; in total 120 independent observations are averaged. Assuming that the random variable of scattered powers is exponentially distributed, the normalized error in the estimate is

~0·13 for 60 independent observations, and ~0·1 for 120 independent observations. We would obviously like to average a larger number of observations, and thereby reduce the error in the estimate. However, time has prevented us from doing so.

4·3 The size of a patch.

To solve the MFIE numerically the integral in (1·1) must be truncated at some point. The scattering problem described by the truncated integral-equation is that of a wave scattered from a patch of surface. The point at which the integral is truncated is important, because it is one of the factors that determines the size of the matrix used to represent the MFIE, and hence the computation required to determine the surface current density. From a computational standpoint a small patch size is preferable. However, since it is hoped that the normalized incoherent scattered power computed for an ensemble of rough surface patches will apply to the infinite surface too, the patch size must be large enough to accommodate the second-order scattering properties of the infinite surface.

The scattered far-field is obtained by integrating the field scattered by each point on the surface boundary. We will refer to the function describing the spatial distribution of scattered fields along the infinite surface as the scattering-function. Furthermore, we will use the term "scattering-function" to refer to the specific case of the infinite surface illuminated by a uniform plane wave. In this section, we present an equation for the incoherent power scattered from a wide-sense-stationary, randomly, rough surface as a function of the size of the illuminated area. We will show that the separation required for the random component of the scattering-function to decorrelate, is the factor determining the size of a patch.

The field scattered from an infinite surface illuminated by a uniform,

plane wave is obtained from the integral

$$E^s(m:\theta^i,\theta^s) = \int_{-\infty}^{\infty} J(m:\theta^i, x')\, K(m:\theta^s, x')\, dx'. \qquad (4\cdot12)$$

Here, $E^s(m:\theta^i, \theta^s)$ is the scattered field in the direction of θ^s, for a uniform plane wave incident at θ^i, K(m: x') is the kernel of the scattered far-field integral (4·1), or (4·2), and J(m: x') is the surface current density. The integrand of (4·12) is the field scattered from the surface at x'. This will be represented by the function $E^s(m: x')$, which we refer to as the scattering-function. The dependence of the scattering-function on the angle of incidence and the scattering angle has been omitted from the notation. We shall also take for granted that the scattered power has been normalized with respect to the power incident on the surface.

The scattering-function

$$E^s(m: x) = A(m: x)\, e^{ikx(\sin\theta^i + \sin\theta^s)}. \qquad (4\cdot13)$$

is the product of a stochastic process and a deterministic process (Ulaby *et al*, 1982). The deterministic process, which is the complex-exponential in (4·13), is due to the periodic phase modulation of the incident wave along the x-axis. The random component A(m: x), m = 1, ..., ∞, describes the phase and amplitude modulation of the scattering-function by the random surface profile. The objective of this section is to determine the incoherent scattered power for an incident wave

$$H^i(x) = W(x)e^{ik(x\sin\theta^i + z\cos\theta^i)}, \qquad (4\cdot14)$$

in terms of the random process A(m: x). In (4·14), W(x) is the footprint of the incident wave on a flat surface. We shall assume that the affect of the

footprint W(x) is to linearly weight the scattering-function along the x-axis. Based on this assumption, the far-field scattered from a surface illuminated by the tapered wave (4·14), is

$$E^S(m) = \int_{-\infty}^{\infty} W(x')\ E^S(m: x')\ dx' \qquad (4\cdot15)$$

We will examine the validity of this assumption later. We will also make the assumption that for wide-sense stationary, random rough surface the random process A(m: x), m = 1, ..., ∞, is wide-sense stationary too (Ulaby *et al*, 1982). On this assumption, the expected scattered power in terms of the scattering function is (see Papoulis, 1984)

$$\sigma_S = \int_{-\infty}^{\infty} R_W(\tau)\ R(\tau)\ e^{ik(\sin\theta^i + \sin\theta^S)\,\tau}\ d\tau \qquad (4\cdot16)$$

where,

$$R(\tau) = E\left[\ A(x'+\tau)\ ,\ A^*(x')\ \right], \qquad (4\cdot17)$$

and

$$R_W(\tau) = \int_{-\infty}^{\infty} W(x'+\tau)\ W^*(x')\ dx'\ . \qquad (4\cdot18)$$

Here, R(τ) is the autocorrelation-function of the stochastic process A(m: x'), m = 1, ..., ∞, which we will call the scattering-autocorrelation-function.

A similar expression for the coherent scattered power

$$|\mu_S|^2 = \int_{-\infty}^{\infty} R_W(\tau)\,|\mu_A|^2\ e^{ik(\sin\theta^i + \sin\theta^S)\,\tau}\ d\tau, \qquad (4\cdot19)$$

is derived using (4·15). Here, μ_A is $E[A(x)]$, which for a wide-sense-stationary process is by definition constant for all x (Papoulis, 1984). Finally, the incoherent scattered power (4·7) is obtained by subtracting (4·19) from (4·16),

$$\sigma^0 = \int_{-\infty}^{\infty} R_W(\tau)\ (\ R(\tau) - |\mu_A|^2\ )\ e^{ik(\sin\theta^i + \sin\theta^s)\,\tau}\ d\tau. \qquad (4\cdot20)$$

It can be recognized from (4·20) that the effect of the footprint W(x) on the incoherent scattered power is to weight ($R(\tau) - |\mu_A|^2$) by the function $R_W(\tau)$. Furthermore, for non-pathological, wide-sense-stationary, random processes (Papoulis, 1984)

$$R(\tau) \rightarrow \mu_A \ \text{ as } \tau \rightarrow \infty. \qquad (4\cdot21)$$

If follows from (4·21) that if the scattering-autocorrelation-function (4·17) obtains its asymptotic value within a separation very much smaller than the width of the illumination, the finite width of the footprint will have small affect on the incoherent scattered power. The separation required for the scattering-autocorrelation-function to obtain its asymptotic value, is by definition the separation required for the the random component of the scattering-function to decorrelate.

A result that is immediately available, is the incoherent scattered power obtained with the Kirchhoff approximation for a Gaussian rough surface illuminated by a tapered incident wave. The scattering-autocorrelation-function obtained with the Kirchhoff approximation is derived in (Ulaby *et al*, 1982),

$$R_K(\tau) = R_K(0)\ \exp\left[-\sigma^2 k^2 \left(\cos\theta^i + \cos\theta^s\right)^2 (1 - c(\tau))\right], \qquad (4\cdot22)$$

$$c(\tau) = \exp\left[-\frac{\tau^2}{\xi^2}\right]. \qquad (4\cdot23)$$

Here, σ is the RMS surface height, ξ is the surface correlation-length and $c(\tau)$ is the normalized autocorrelation-function of the surface. The asymptotic value of $R_K(\tau)$ is obtained by setting $c(\tau)$ to zero, (with $c(\tau) = 0$, $R_K(\tau)$ is the rough surface reflection coefficient discussed in § 5·1). It can be easily recognized from (4·22), that $R_K(\tau)$ obtains its asymptotic value after about two surface correlation-lengths. For an incident wave with a Gaussian, footprint,

$$W(x) = e^{-x^2/\gamma^2}, \qquad (4\cdot24)$$

and

$$R_W(\tau) = R_W(0)\, e^{-\tau^2/2\gamma^2}. \qquad (4\cdot25)$$

The function R_W obtains its half power point for $\tau \sim 0{\cdot}8\gamma$. Therefore, the the footprint (4·24) will have small affect on the normalized incoherent scattered power provided the tapering parameter γ is several surface correlation-lengths long.

For the surfaces we have considered, the Kirchhoff approximation is inappropriate and the MFIE must be solved. In the next section we will present examples of the scattering-autocorrelation-functions computed from our numerical solutions of the MFIE.

4·4 Examples of scattering-autocorrelation-functions.

In this section we present examples of the backscattering-autocorrelation-functions computed from our numerical simulations of rough surface scattering. The estimates of the scattering-autocorrelation-

functions (4·17) were obtained in the following manner. Using the numerical solution for the surface current density, the scattering-function was computed according to (4·12), and the stochastic process $A(m: x_n)$ determined by multiplying the scattering-function by the conjugate of the complex exponential in (4·13). The autocorrelation-function of $A(m: x_n)$ was determined for each surface realization according to,

$$\hat{R}(m: r) = \frac{1}{N} \sum_{r=1}^{N-r} A(m: x_{n+r})\ A^*(m: x_n)\ . \qquad (4\cdot26)$$

Finally, the estimate of the scattering-autocorrelation-function was obtained by averaging the autocorrelations (4·26) computed for a number of surface realizations (see. § 4·2),

$$\hat{R}(r) = \frac{1}{M} \sum_{m=1}^{M} \hat{R}(m: r)\ . \qquad (4\cdot27)$$

In most of the cases we have considered the scattering-autocorrelation-function (4·27) obtains a constant value within a few surface correlation-lengths, and well within the half power point of the incident wave used in our numerical simulations. We consider that the results presented in this section provide evidence that a relatively small patch size can accurately represent the second-order scattering properties of the infinite surface. This is possible because of the small correlation-length of the random component of the scattering function. The assumption that the footprint of the incident wave linearly weights the scattering-function, which was used to obtain equation (4·15), is examined by comparing the normalized, incoherent scattered power computed for two tapered waves, one with a tapering parameter of 12 wavelengths, and the other with a tapering parameter of 6 wavelengths. For the surfaces we have considered we have

found small difference between these two incoherent scattered powers.

To illustrate these remarks, we present in figs. 4·2 - 4·4 the backscattering-autocorrelation-functions for a Gaussian rough surface with a RMS slope of ~25° and a correlation-length of 0·8λ. The Gaussian, tapered incident wave (2·3) was used in the numerical simulations. In the following examples the tapering parameter was 12λ, and unless otherwise stated the integral in the MFIE was truncated at ±25λ. In the figures curve (A) is for a horizontally polarized wave, and curve (B) is for a vertically polarized wave. The figures show how the backscattering-autocorrelation-functions decay to an approximately constant value within a few surface correlation-lengths. In three cases, figs. 4·2(A), 4·2(B) and 4·3(B), the autocorrelation-functions decay to zero. In the remaining three cases the autocorrelation-functions decay to a non-zero value within the range of the plot.

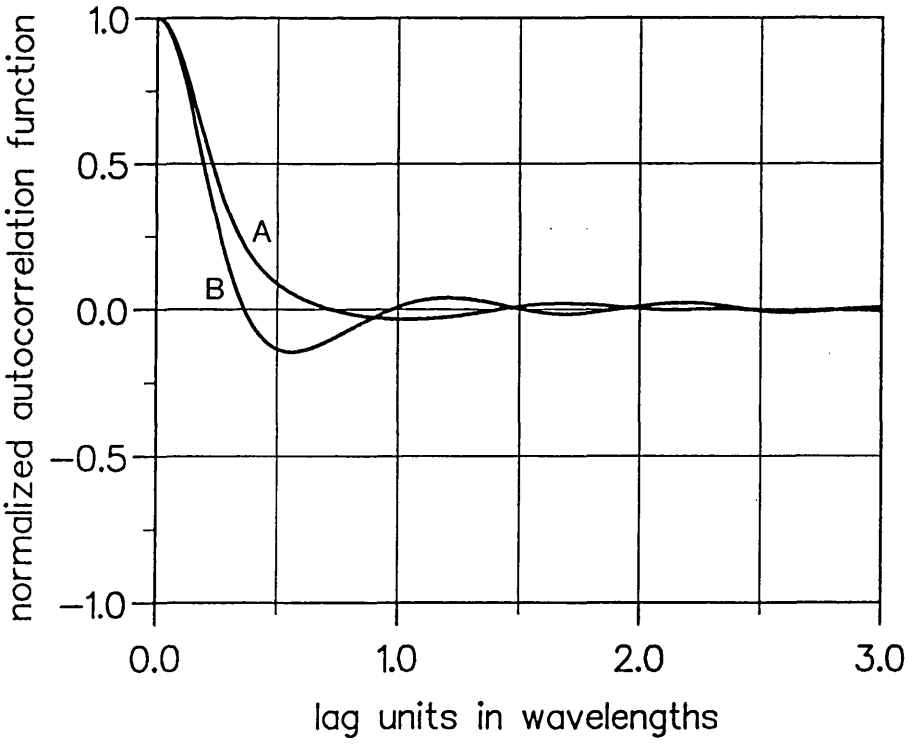

Fig. 4·2. The backscattering-autocorrelation-functions for a Gaussian rough surface with a RMS slope of 25° and a correlation-length of 0·8λ illuminated by a wave incident at an angle of 0°. Curve (A) is for a horizontally polarized wave and curve (B) is for a vertically polarized wave.

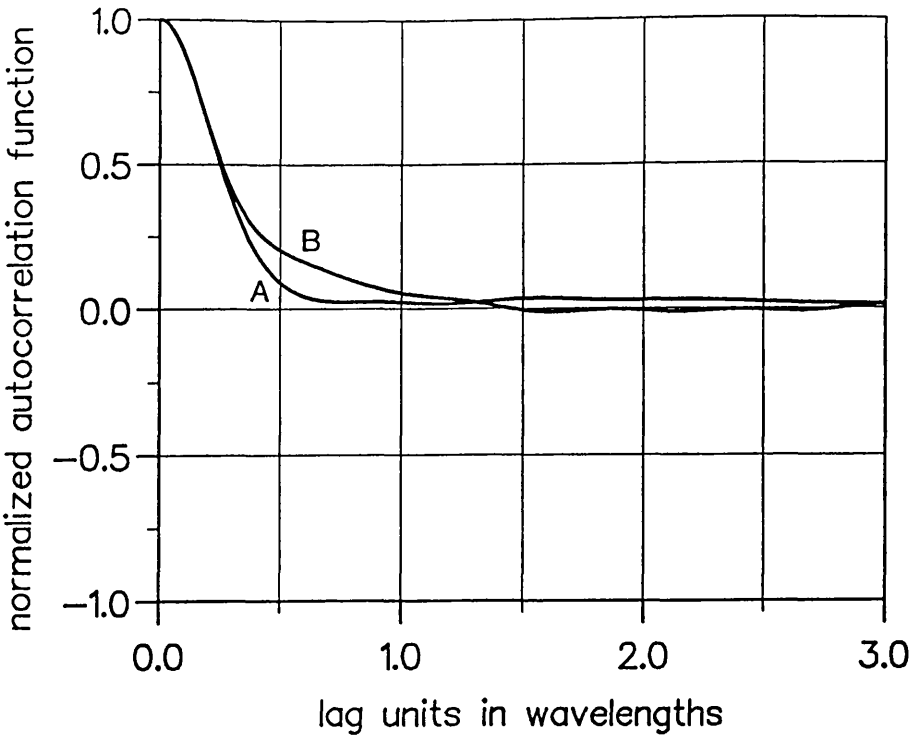

Fig. 4·3. The backscattering-autocorrelation-functions for a Gaussian rough surface with a RMS slope of 25° and a correlation-length of 0·8λ illuminated by a wave incident at an angle of 45°. Curve (A) is for a horizontally polarized wave and curve (B) is for a vertically polarized wave.

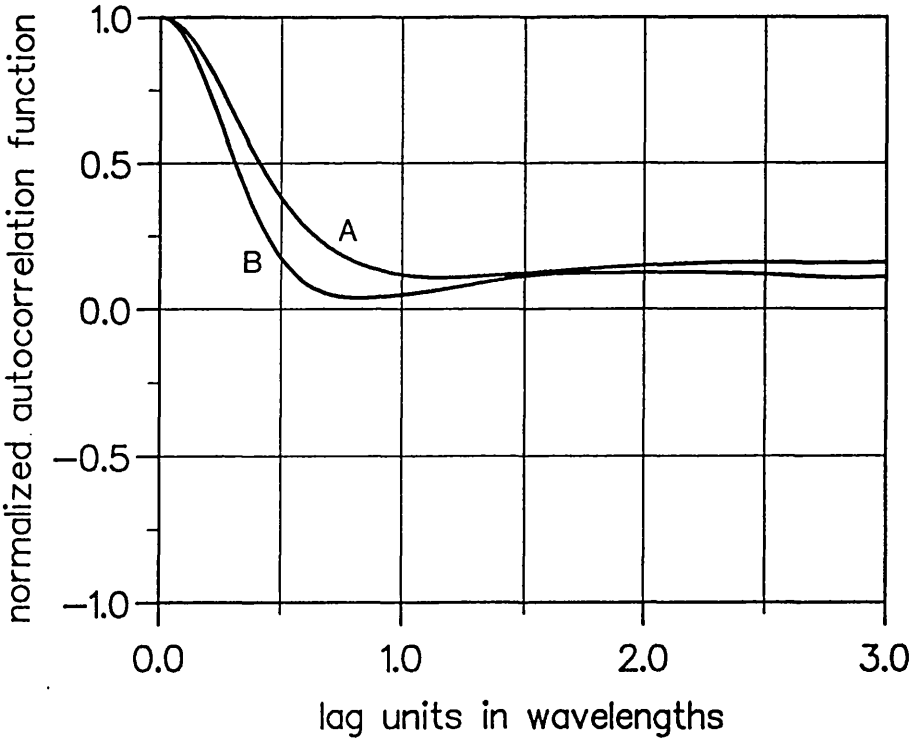

Fig. 4·4. The backscattering-autocorrelation-functions for a Gaussian rough surface with a RMS slope of 25° and a correlation-length of 0·8λ illuminated by a wave incident at an angle of 70°. Curve (A) is for a horizontally polarized wave and curve (B) is for a vertically polarized wave.

We have found small difference between the incoherent scattered power computed for the incident wave (2·3) with a tapering parameter of 12λ and with a tapering parameter of 6λ. Given that the scattering-autocorrelation-functions obtain a constant value within a few surface correlation-lengths, and well within the half power point of these two incident waves, this result is not entirely unexpected. To illustrate this point we present in figs. 4·5 and 4·6 the incoherent scattered power for a wave incident at an angle of 45° on a Gaussian rough surface with a RMS slope of 25° and a correlation-length of 0·8λ. The curve in the figures is computed for an incident wave with a tapering parameter $\gamma = 12\lambda$ and the dots are computed for a $\gamma = 6\lambda$. In fig. 4·5 the incident wave is vertically polarized, and in fig. 4·6 the incident wave is horizontally polarized, and it can be verified that in both figures there is small difference between the two scattered powers.

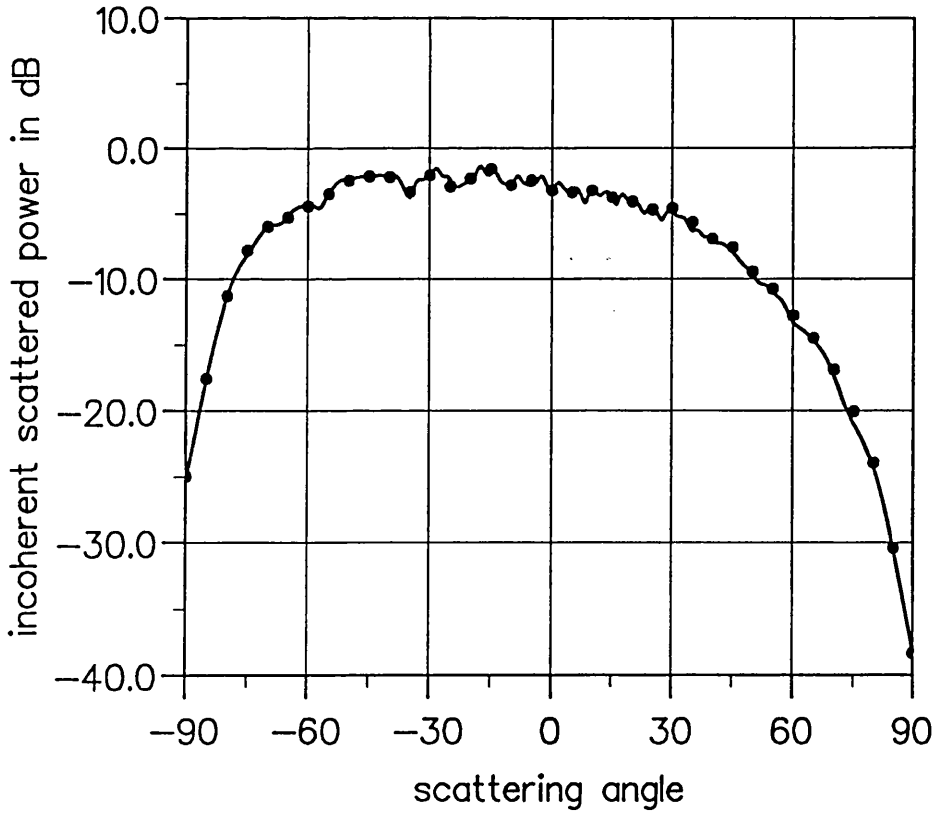

Fig. 4·5. The incoherent scattered power for a Gaussian rough surface with a RMS slope of 25° and a correlation-length of 0·8λ illuminated by a horizontally polarized wave incident at an angle of 45°. The curve is for a tapering parameter of 12λ; and the dots are for a tapering parameter of 6λ.

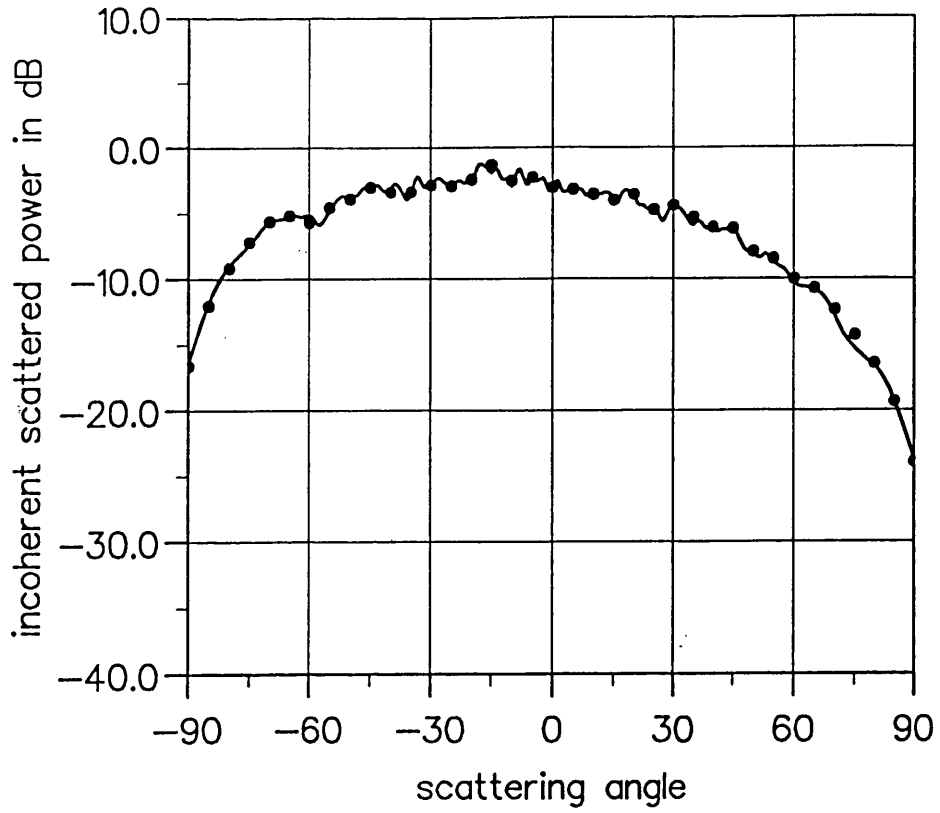

Fig. 4·6. The incoherent scattered power for a Gaussian rough surface with a RMS slope of 25° and a correlation-length of 0·8λ illuminated by a vertically polarized wave incident at an angle of 45°. The curve is for a tapering parameter of 12λ; and the dots are for a tapering parameter of 6λ.

For rough surfaces with small heights we have found cases where the scattering-autocorrelation-functions have a periodic component over the entire length of the footprint. An example of this phenomenon is presented in fig. 4·7. The figure shows the backscattering-autocorrelation-function for a normally incident wave, a RMS slope of 25°, a RMS height of 0·13λ, and a correlation-length of 0·4λ. It can be easily verified from fig. 4·7(B) that the backscattering-autocorrelation-function has a periodic component over the entire range of the plot. We suspect that this phenomenon, which we have found to occur only in the vertical polarization case, is due to a wave propagating along the length of the surface. It is well known that a surface wave can be excited on a conducting rough surface illuminated by a vertically polarized wave. A surface wave is

not excited in the horizontal polarization case, because the electric field is in the plane tangent to the surface boundary and is "short-circuited" by the surface conductivity.

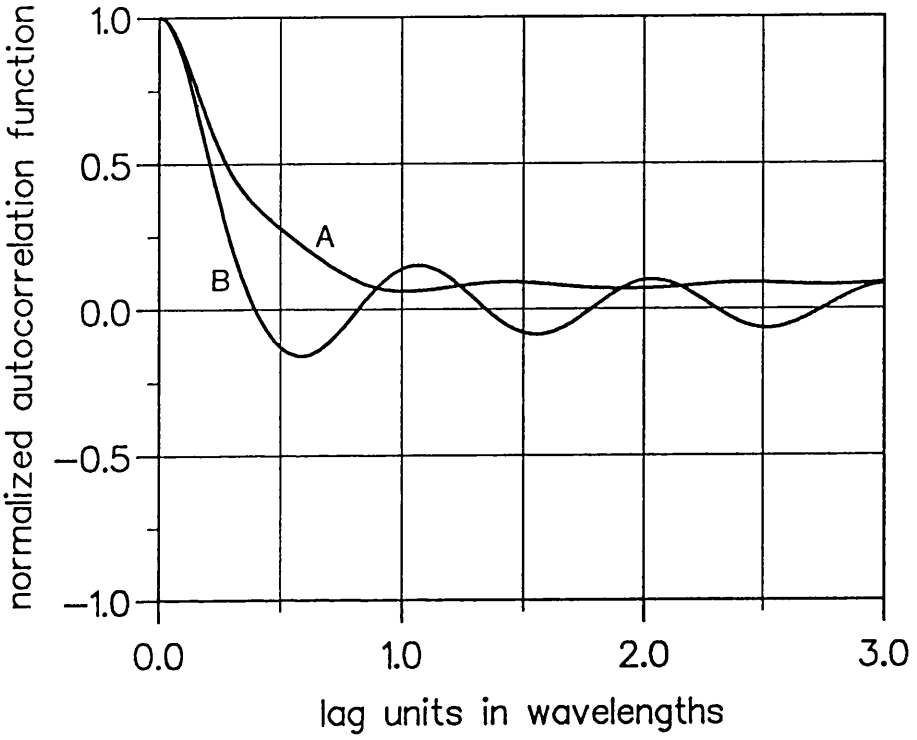

Fig. 4·7. The backscattering-autocorrelation-functions for a Gaussian rough surface with a RMS slope of 25° and a correlation-length of 0·4λ illuminated by a wave incident at an angle of 0°. Curve (A) is for a horizontally polarized wave and curve (B) is for a vertically polarized wave.

The presence of a slowly decaying oscillatory component to the autocorrelation-functionmight appear to invalidate the assumption that the random component of the scattering function is wide-sense-stationary. However, the surface wave is a spatially deterministic event, and we can remove its effect from the stochastic process A(m: x) by multiplying (4·13) by a second complex exponential. For the case in fig. 4·7(B) the period of this exponential would be one wavelength. A more serious implication of a surface wave concerns the truncation of the MFIE and the scattered field integrals. The presence of a wave propagating along the length of the surface clearly complicates the issue of where to truncate these integrals.

Nevertheless, for the surfaces we have considered we have found small change in the incoherent scattered power as the limits on the integrals are changed. To illustrate this point we present in fig. 4·8 the incoherent scattered powers for the case considered in fig. 4·7(B) computed for the tapered incident wave with $\gamma = 6\lambda$. The curve in the figure is computed by truncating the integrals at $\pm 25\lambda$, and the dots are computed by truncating the integrals at $\pm 12{\cdot}5\lambda$.

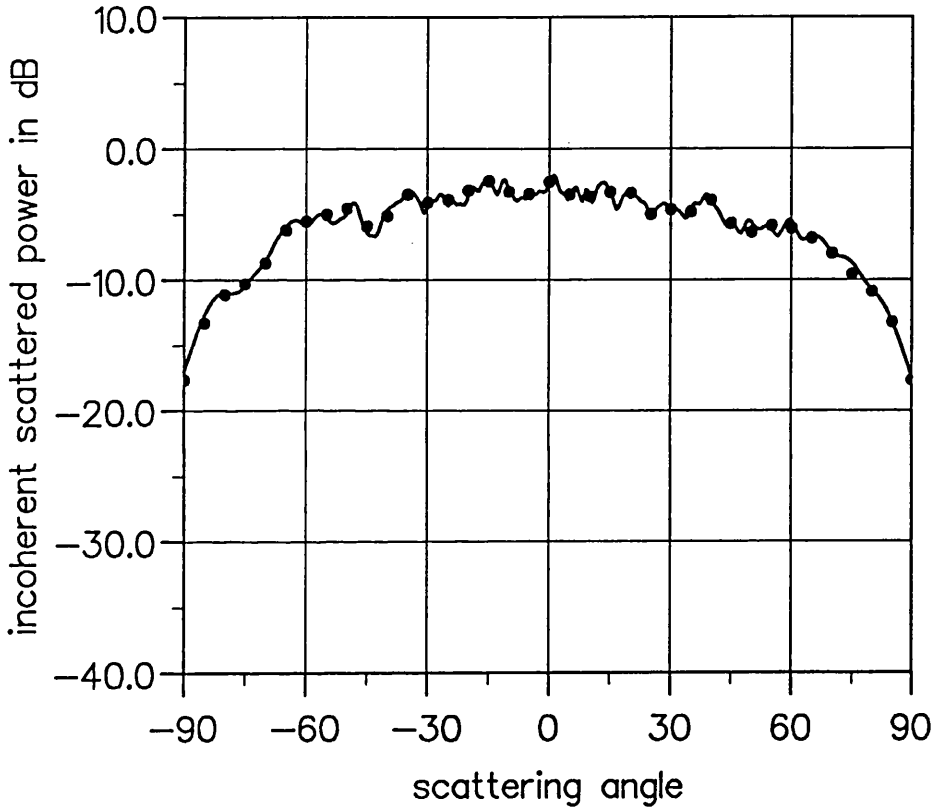

Fig. 4·8. The bistatic, incoherent scattered power for a Gaussian rough surface with a RMS slope is 25° and a correlation-length of $0{\cdot}4\lambda$ illuminated by a vertically polarized wave incident at an angle of 45°. The curve in the figure is computed by truncating the integrals at $\pm 25\lambda$; and the dots are computed by truncating the integrals at $\pm 12{\cdot}5\lambda$.

It can be verified from the figure that there is small difference between the two scattered powers. We suspect that for the very rough surfaces considered in this study the diffuse scattering of the surface wave is relatively small. Indeed, it is well known that surface waves have their largest effect in the region of the parameter space "FP" of fig. 1·1 (Ishimaru

and Chen, 1990 b), (Celli *et al*, 1985). Here, the incoherent scattered power is itself small and we suppose, therefore, that the diffuse scattering of the surface wave cannot be neglected.

4·5 Chapter summary.

To solve the MFIE numerically the integral in the equation must be truncated at some point. The scattering problem described by the truncated integral-equation is that of a wave scattered from a patch of surface. From a computational standpoint a small patch size is preferable. However, since it is hoped that the normalized incoherent scattered power computed for an ensemble of rough surface patches will also apply to the infinite rough surface, the patch size must be large enough to accommodate the average scattering properties of the infinite surface. In this chapter, we have placed the point at which to truncate the MFIE into a mathematical context. The incoherent scattered power for an illuminated patch of surface was presented as the integral of the weighted autocorrelation-function of the random component of the field scattered by each point of the surface. By representing the incoherent scattered power in this manner, the factor determining the size of a patch was identified as the separation required for this random process to decorrelate. We presented examples of backscattering-autocorrelation-functions for a perfectly-conducting, Gaussian rough surface. In the horizontal polarization case, the autocorrelation-functions obtain a constant value within a few surface correlation-lengths. This is also true of most of the cases for vertical polarization. The exceptions occur when the RMS surface height is small. For these geometries the autocorrelation-functions have an oscillatory component over the entire length of the footprint. We suspect this phenomenon is due to a surface wave. The presence of a surface wave

clearly complicates the issue of where to truncate the MFIE. However, for the surfaces considered in this study we suspect that the diffuse scattering of the surface wave is relatively small.

In conclusion, the results presented in this section provide evidence that a relatively small patch size can accurately represent the second-order scattering properties of the infinite surface. This is possible because of the small correlation-length of the random component of the scattering function. In fact, we consider that the limit on the patch size relates more to the method used to reduce the scattering from the patch edges. The tapered incident wave used in our numerical simulations, for example, is less consistent with the wave equation as the tapering is increased.

5
Corrections to the Kirchhoff approximation.

The surface current induced on a perfectly-conducting, rough surface can be separated into two components; the Kirchhoff component; and the component due to the integral in the magnetic-field-integral-equation (MFIE). We refer to the scattered far-field obtained with the Kirchhoff approximation as the Kirchhoff-field, and the far-field due the integral component of the surface current, we refer to as the integral-field. In the high-frequency limit the physical significance of these two components of the scattered field are understood. The Kirchhoff-field is due to single reflections of incoming rays from the surface, including the fictitious reflections from those parts of the surface in shadow. The integral-field is required to account for shadowing, and multiple-reflections at the surface boundary. In this chapter we present a procedure for determining from the solution of the MFIE two corrections to the expected scattered power obtained with the Kirchhoff approximation. One of these corrections is determined from the linear-mean-square estimate of the integral-field in terms of the Kirchhoff-field. The error in estimate provides the second correction. We will justify that in the high frequency-limit the first of these two corrections is for shadowing, and the second is for multiple-reflections at the surface boundary.

5·1 The Kirchhoff approximation.

The central assumption of the Kirchhoff approximation for a perfectly-conducting surface, is that the scattered magnetic field is equal to the

incident magnetic field in the plane tangent to the surface boundary. This assumption is inappropriate for the rough surfaces considered in this study, because we cannot neglect the field due the integral in the MFIE. However, we discuss the Kirchhoff approximation for two reasons. An analytic solution for the expected scattered power obtained with the Kirchhoff approximation is available. We use this to test the computations required in the calculation of the scattered power. The Kirchhoff approximation also provides a framework for some of the discussions in this chapter and in Chapter 6.

The expected scattered power obtained with the Kirchhoff approximation for a perfectly conducting, two-dimensional, Gaussian rough surface illuminated by a plane wave, is the sum of the incoherent and coherent scattering contributions (Thorsos, 1989),

$$\sigma_K(\theta^i, \theta^s) - \left|\mu_K(\theta^i, \theta^s)\right|^2 = \frac{k}{\pi\cos\theta^i}\left(\frac{1 + \cos(\theta^i+\theta^s)}{\cos\theta^i + \cos\theta^s}\right)^2 \Psi \qquad (5\text{-}1)$$

$$\left|\mu_K(\theta^i, \theta^s)\right|^2 = P^s(\theta^i, \theta^s)\exp\left(-\chi^2\right) \qquad (5\text{-}2)$$

$$\Psi = \int_0^\infty \cos(kx(\sin\theta^i + \sin\theta^s)\left(\exp\left[-\chi^2\left\{1 - \exp\left(\frac{x^2}{\xi^2}\right)\right\}\right] - \exp -\chi^2\right)dx \qquad (5\text{-}3)$$

$$\chi = k\sigma\,(\cos\theta^s + \cos\theta^i). \qquad (5\text{-}4)$$

Here, σ_K is the expected scattered power obtained with the Kirchhoff approximation, μ_K is the expected value of the Kirchhoff-field, σ is the RMS surface height, ξ is the surface correlation-length, θ^s is the scattering angle, θ^i is the angle of incidence, and P^s is the power scattered from a flat surface. For the tapered incident wave (2·3) used in our numerical simulations

$$P^s(\theta^i, \theta^s) = \frac{H_0^2 k\gamma^2}{2P^i} \exp\left(\frac{-k^2\gamma^2 (\sin\theta^i + \sin\theta^s)^2}{2}\right) \cos^2\theta^s \qquad (5\cdot5)$$

when the incident wave is vertically polarized, and

$$P^s(\theta^i, \theta^s) = \frac{H_0^2 k\gamma^2}{2P^i} \exp\left(\frac{-k^2\gamma^2 (\sin\theta^i + \sin\theta^s)^2}{2}\right) \cos^2\theta^i, \qquad (5\cdot6)$$

when the incident wave is horizontally polarized. Here, γ is the parameter that controls the tapering of the incident wave, and P^i is the power incident on the surface. When $k\gamma >> 1$, the power scattered from a flat surface is small at scattering angles away from the specular direction. Moreover, there is small difference between (5·5) and (5·6) when $\gamma >> \lambda$. The incoherent scattered power (5·1) is the same for both polarizations (Ulaby *et al,* 1982).

We present in figs. 5·1 - 5·8 the scattered powers obtained with the Kirchhoff approximation. The smooth curve in the figures is determined from (5·1) - (5·5). The fluctuating curve is computed using the Kirchhoff approximation for the surface current density,

$$J_K(m: x) = 2H^i(m: x), \qquad (5\cdot7)$$

in the scattered far-field integral (4·1), for 60, 50 wavelength long, uncorrelated, sections of a Gaussian rough surface. The results presented in this section are for a tapering parameter of 12λ. For the surfaces we have considered we have found small difference between the analytic solution for the incoherent scattered power (5·1), and the incoherent scattered power computed with (5·7), even though (5·1) is derived for a plane wave illuminating a surface of infinite extent. However, this result was not

entirely unexpected, because of our findings in § 4·3. To illustrate this point, we present in figs. 5·1 and 5·2 the scattered powers for a wave normally incident on a Gaussian rough surface with a correlation-length of 0·8λ. The RMS surface slope is given by $\arctan(\sqrt{2}\sigma/\xi)$, and in fig. 5·1 the RMS slope is 25°, and in fig. 5·2 the RMS slope is 45°. The figures show how the numerically computed result for the average scattered power is close to its theoretical result. We consider that the differences, typically less than ~1dB, are statistical in origin, and would be reduced by taking more observations of the scattered power. The striking feature of the figures is the small dynamic range of the incoherent scattered power. In fig. 5·2, where the RMS surface slope is 45°, the dynamic range of the incoherent scattered power is less than 2dB.

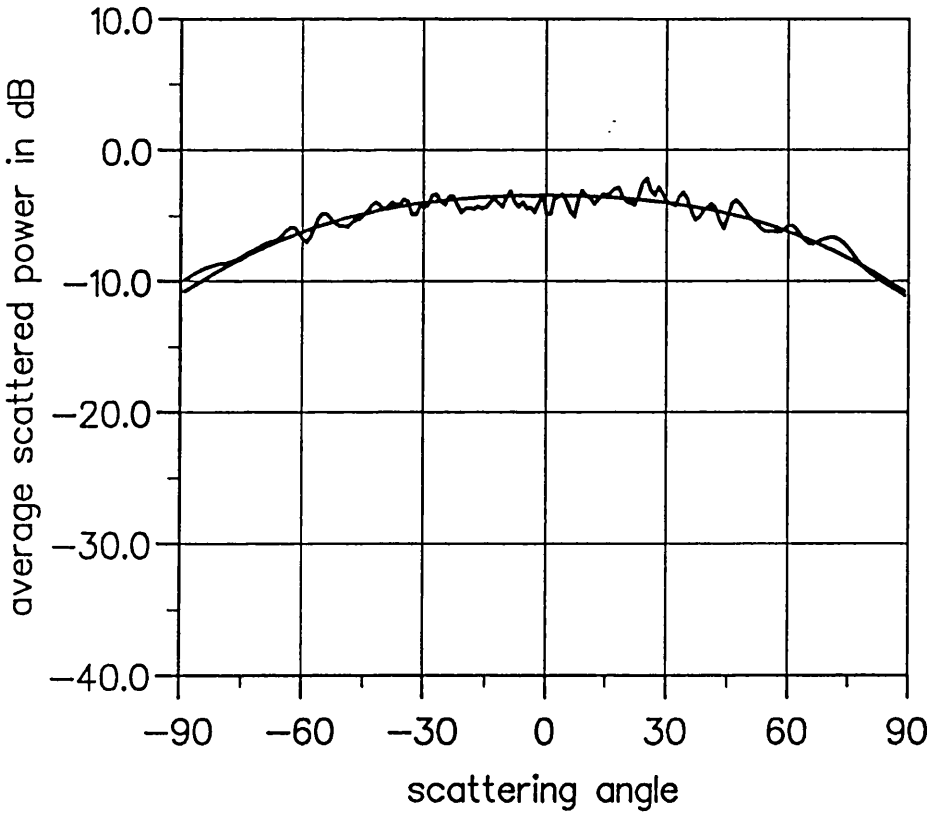

Fig. 5·1. The scattered powers obtained with the Kirchhoff approximation for a Gaussian rough surface with a RMS slope of 25° and a correlation-length of 0·8λ, illuminated by a wave incident at an angle of 0°.

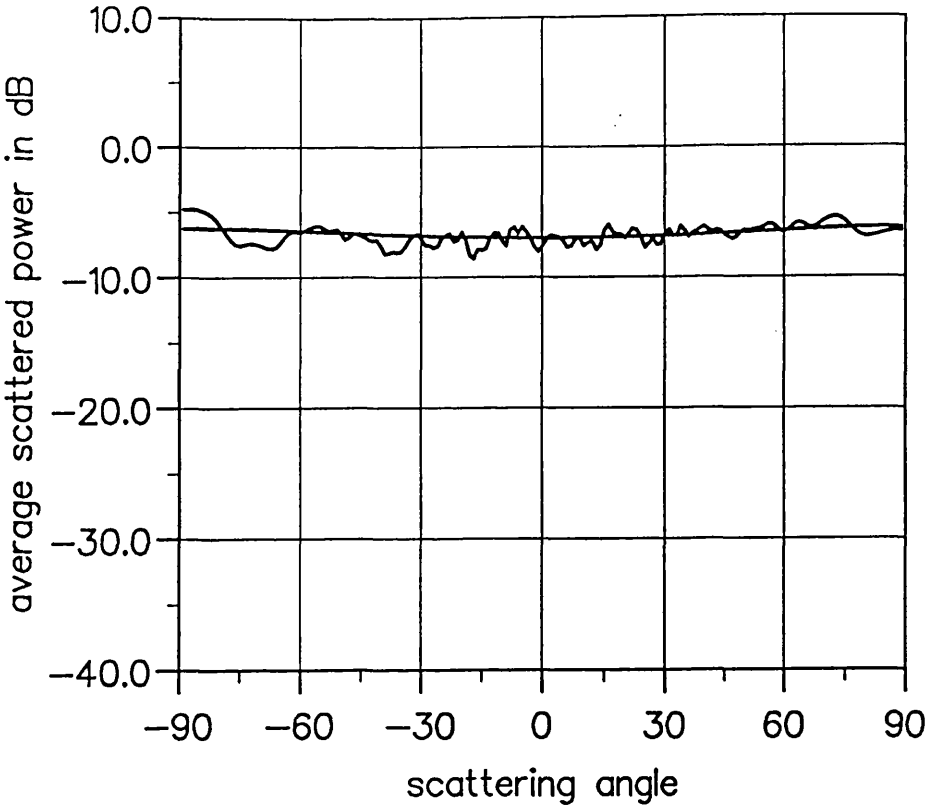

Fig. 5·2. The scattered powers obtained with the Kirchhoff approximation for a Gaussian rough surface with a RMS slope of 45° and a correlation-length of 0·8λ, illuminated by a wave incident at an angle of 0°.

The dynamic range is larger for waves incident away from normal incidence. In figs. 5·3 and 5·4 we present the expected scattered power for a wave incident at an angle of 70° on the geometries considered in figs. 5·1 and 5·2. In fig. 5·3 there is a strong coherent component to the expected scattered power. This can be recognized from the figure as the narrow angular distribution of power centred on the specular angle, θ^s = -70°. The closeness of the numerical result in fig. 5·3 to its expected value shows how our scattered far-field computation is accurate to within a fraction of a decibel, even when the dynamic range of the expected scattered power is 50dB. The error in a Gaussian quadrature used to approximate an integral over the integration interval Δx is (Abramowitz and Stegun, 1970),

$$\varepsilon_n(x) = \frac{(\Delta x)^{2n+1}(n!)^4}{2n+1\ (2n!)^3} 2^{2n+1} I^{(2n)}(\chi),\ x - \frac{\Delta x}{2} \le \chi \le x + \frac{\Delta x}{2} \qquad (5\text{·}8)$$

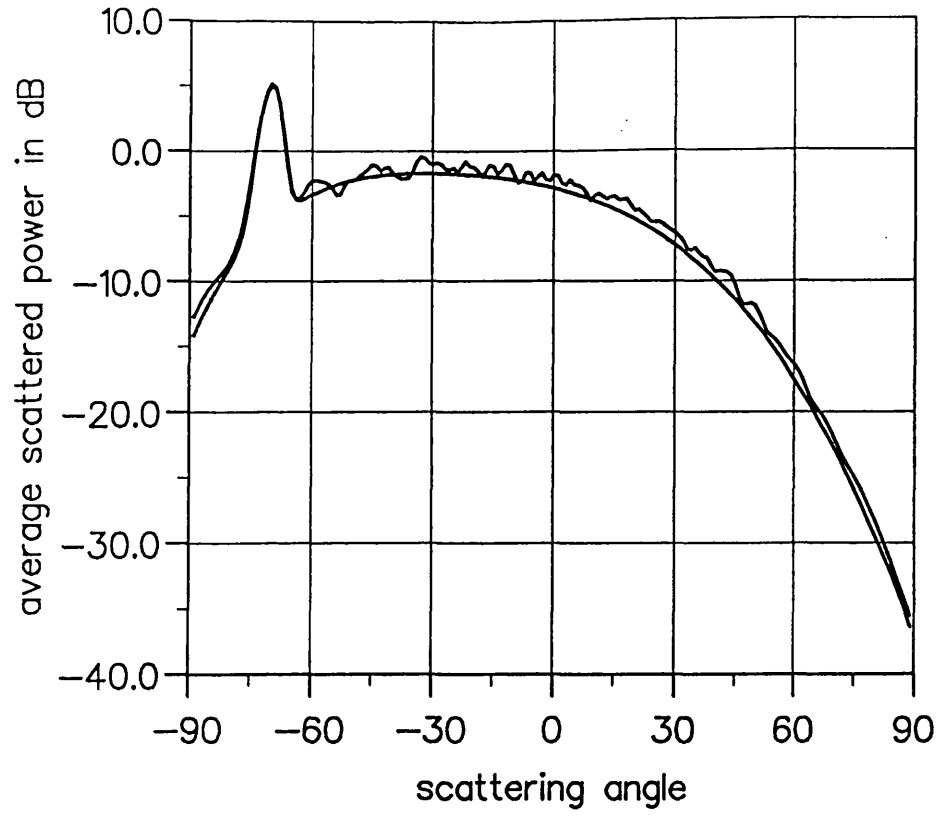

Fig. 5·3. The scattered powers obtained with the Kirchhoff approximation for a Gaussian rough surface with a RMS slope of 25° and a correlation-length of 0·8λ, illuminated by a wave incident at an angle of 70°.

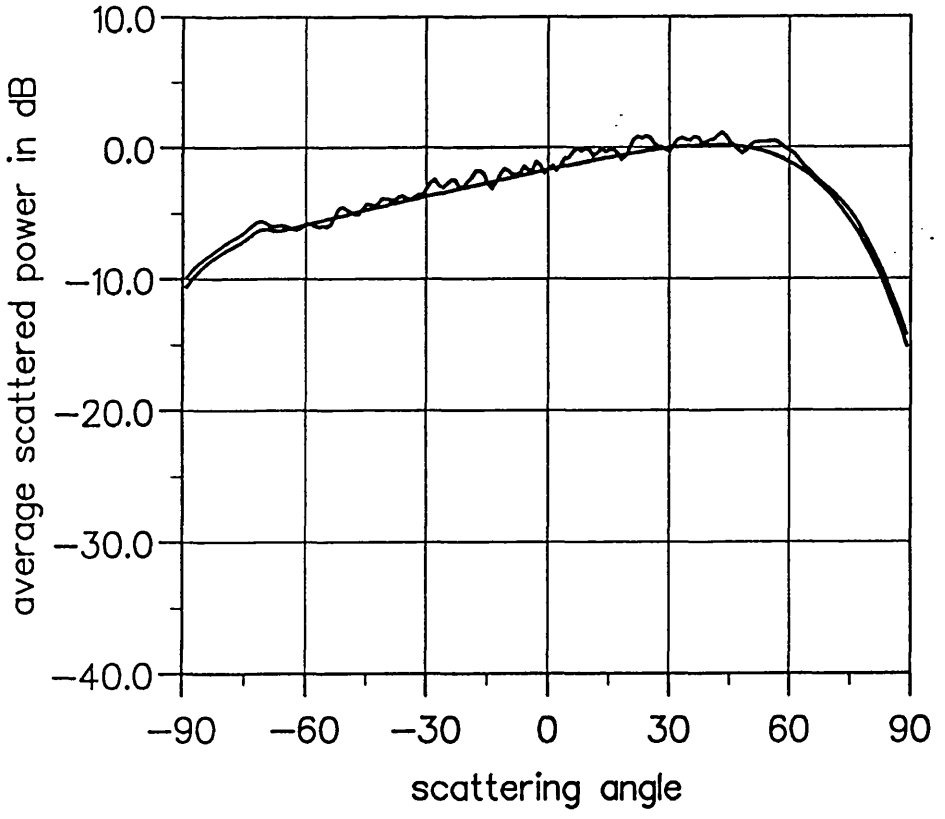

Fig. 5·4. The scattered powers obtained with the Kirchhoff approximation for a Gaussian rough surface with a RMS slope of 45° and a correlation-length of 0·8λ, illuminated by a wave incident at an angle of 70°.

Here, n is the order of the quadrature, and $I^{(2n)}$ is the $2n^{th}$ derivative of the integrand of of the integral. With a n=3 and $\Delta x=0{\cdot}2\lambda$, the error (5·8) is $\sim 10^{-9}$ times the maximum value of the 6^{th} derivative of the integrand. Since for a smooth surface we would expect the derivatives of the integrand of the scattered far-field integrals to be well behaved, the closeness of the numerical result to its theoretical value is not entirely unexpected.

5·2 A correction to the Kirchhoff method for shadowing.

In common with all shadowing theories (Beckmann, 1965), (Brockelmann and Hagfors, 1966), the shadowing theory developed by Wagner (1967) uses rays to represent the incident and scattered waves, and the Kirchhoff approximation to describe the wave scattered from the illuminated parts of the surface. In spite of these high-frequency approximations, the shadow-corrected Kirchhoff method, as we will refer to it, has been successfully used for Gaussian rough surfaces in the region "KA" of fig. 1·1 (Thorsos, 1988). It is significant that the surface-correlation length in this region of the parameter space is comparable to the electromagnetic wavelength.

The correction for shadowing is applied to the expected scattered power obtained with the Kirchhoff approximation by multiplying the incoherent scattered power (5·1) by the shadow-function $S(\theta^i,\theta^s)$,

$$\sigma_{WK}(\theta^i,\theta^s) = S(\theta^i,\theta^s)\left(\sigma_K(\theta^i,\theta^s) - \left|\mu_K(\theta^i,\theta^s)\right|^2 \right) + \left|\mu_K(\theta^i,\theta^s)\right|^2 \quad (5{\cdot}9)$$

Here, σ_K is the expected scattered power obtained with the Kirchhoff approximation, and μ_K is the expected value of the Kirchhoff-field. The shadow-function derived by Wagner is given in Appendix D.

5·3 Two corrections to the Kirchhoff approximation from the solution of the magnetic-field-integral-equation.

The surface current induced on a perfectly-conducting, rough surface can be separated into two components; the Kirchhoff component; and the component due to the integral in the magnetic-field-integral-equation (MFIE). We refer to the scattered far-field obtained with the Kirchhoff approximation as the Kirchhoff-field, and the far-field due the integral component of the surface current as the integral-field. For the m^{th} surface realization, the scattered far-field $E^s(m: \theta^i,\theta^s)$ is the sum of the integral-field $E_I(m: \theta^i, \theta^s)$, and the Kirchhoff-field $E_K(m: \theta^i, \theta^s)$,

$$E^s(m: \theta^i, \theta^s) = E_K(m: \theta^i, \theta^s) + E_I(m: \theta^i, \theta^s). \tag{5·10}$$

The expected scattered power in terms of the Kirchhoff and integral-fields is,

$$\sigma_S(\theta^i,\theta^s) = \sigma_K(\theta^i,\theta^s) + \sigma_I(\theta^i,\theta^s) + 2\mathrm{Re}\,(\sigma_{KI}(\theta^i,\theta^s)), \tag{5·11}$$

where,

$$\sigma_s = E\left[\,|E^s|^2\,\right], \tag{5·12}$$

$$\sigma_K = E\left[\,|E_K|^2\,\right], \tag{5·13}$$

$$\sigma_I = E\left[\,|E_I|^2\,\right], \tag{5·14}$$

$$\sigma_{KI} = E\left[\,E_K E_I\,\right]. \tag{5·15}$$

Here, $\sigma_K(\theta^i,\theta^s)$ is the expected scattered power obtained with the Kirchhoff approximation, $\sigma_I(\theta^i,\theta^s)$ is the expected scattered power obtained with the

integral-field, and $\sigma_{KI}(\theta^i,\theta^s)$ is a measure of the degree of coherence between the Kirchhoff and integral-fields: For the set of data u(m) and v(m), m = 1, ..., ∞, (Papoulis, 1984),

$$E[\,u, v\,] = \lim_{M \to \infty} \frac{1}{M} \sum_{m=0}^{M} u(m).v(m)^*. \qquad (5\cdot16)$$

We can write down a similar equation for the coherent scattered power,

$$|\mu_s(\theta^i,\theta^s)|^2 = |\mu_K(\theta^i,\theta^s)|^2 + |\mu_I(\theta^i,\theta^s)|^2 + 2\mathrm{Re}\,(\mu_K(\theta^i,\theta^s)\,\mu_I^*(\theta^i,\theta^s)) \qquad (5\cdot17)$$

$$\mu_s = E[\,E^s\,] \qquad (5\cdot18)$$

$$\mu_K = E[\,E_K\,] \qquad (5\cdot19)$$

$$\mu_I = E[\,E_I\,] \qquad (5\cdot20)$$

Here, $\mu_K(\theta^i,\theta^s)$ is the expected value of the Kirchhoff-field, and $\mu_I(\theta^i,\theta^s)$ is the expected value of the integral-field.

Regardless of what the electromagnetic wavelength is the integral-field is required to provide a complete description of the field scattered by a rough surface. In the following discussion we will consider wave scattering in the high frequency limit. In this limit the incoming and outgoing waves can be represented as rays. Parts of the surface obstruct the path of the rays leaving areas of the surface in shadow. An outgoing ray originates from a point on an unshadowed part of the surface, either by a single reflection of an incoming ray, or else after an incoming ray has been reflected from one or more other points on the surface boundary. The field due to single reflections is the Kirchhoff-field (Beckmann, 1965), (Kodis, 1966). However, the Kirchhoff-field also includes fictitious reflections from those parts of

the surface in shadow (Beckmann, 1965), (Wagner, 1966). For this reason, and when the field due to multiple-reflections is small, the expected scattered power obtained with Kirchhoff approximation is generally an overestimate of the expected scattered power σ_s (Beckmann, 1965). The only term in (5·11) that can reduce σ_s to a value less than that obtained with the Kirchhoff approximation is the term σ_{KI}. This is easily recognized from (5·11) by the fact that σ_{KI} is the only term in the equation that can be negative. The integral-field in addition to providing the correction for shadowing via σ_{KI}, includes the field due to multiple-reflections at the surface boundary. To this end we describe the integral-field as the sum of the field responsible for shadowing $E_{sI}(m: \theta^i, \theta^s)$, and the field due to multiple-reflections $E_{mI}(m: \theta^i, \theta^s)$, $m = 1, ..., \infty$,

$$E_I(m: \theta^i, \theta^s) = E_{sI}(m: \theta^i, \theta^s) + E_{mI}(m: \theta^i, \theta^s). \tag{5·21}$$

We know of no way of determining the fields E_{sI} and E_{mI} from the solution of the MFIE. However, since we would expect the Kirchhoff-field and the field responsible for shadowing to be correlated, it seems appropriate, therefore, to make an estimate of the random variable $E_{sI}(m)$ in terms of the random variable $E_K(m)$, $m = 1, ..., \infty$. The optimality criterion that we will use to determine this estimate, is minimizing the mean-square error. The linear mean-square estimate of $E_{sI}(m)$, $m = 1, ..., \infty$, in terms of the Kirchhoff-field is (Papoulis, 1984)

$$\hat{E}_{sI}(m) = (\rho E_K(m) + \upsilon), \tag{5·22}$$

where

$$\rho = \frac{\sigma_{KsI} - \mu_K \mu_{sI}^*}{\sigma_K - |\mu_K|^2}, \tag{5·23}$$

and

$$\nu = \mu_{sI} - \rho \mu_K. \tag{5·24}$$

Here,
$$\sigma_{KsI} = E[\, E_K E_{sI}\,], \tag{5·25}$$

and
$$\mu_{sI} = E[\, E_{sI}\,]. \tag{5·26}$$

We cannot determine the constants (5·23) and (5·24) directly, because we do not know the expected value of $E_{sI}(m)$, or the covariance between $E_{sI}(m)$ and $E_K(m)$. However, we intend to show that

$$\rho = \frac{\sigma_{KI} - \mu_K \mu_I^*}{\sigma_K - |\mu_K|^2}, \tag{5·27}$$

and,
$$\nu = \mu_I - \rho \mu_K. \tag{5·28}$$

Unlike (5·23) and (5·24), (5·27) and (5·28) can be determined from the solution of the MFIE.

In the high-frequency limit the horizontal dimension of the surface roughness is necessarily large. Consequently, the difference between the path-lengths of pairs of rays adopting different multiple-reflection paths will range over several electromagnetic wavelengths. Therefore, we can safely assume that the expected scattered power due to multiple-reflections is incoherent,

$$E[\, E_{mI}\,] \equiv \mu_{mI} = 0. \tag{5·29}$$

Taking the expectation of (5·21) and using (5·29), the expected value of the integral-field is then equal to the expected value of the field responsible for shadowing,

$$\mu_I = \mu_{sI} \tag{5·30}$$

Using (5·30), (5·28) is obtained from (5·24) by substitution. A similar relationship can be deduced for the coherence between the field due to

single-reflections and the field due to multiple-reflections. The difference between the path-length of a single-reflection from a point on the surface at x and the path-length of a multiple-reflection escaping from the surface at x, will vary from point to point by several electromagnetic wavelengths. Therefore, we can safely assume that the field due to single-reflections and the field due to multiple-reflections are uncorrelated,

$$E[E_K + E_{sI}, E_{mI}] = E[E_K, E_{mI}] + E[E_{sI}, E_{mI}] = 0. \tag{5·31}$$

For precisely the same reasons that lead to (5·31), we can also assume that

$$E[E_K, E_{mI}] = 0, \tag{5·32}$$

The equality

$$\sigma_{KI} = \sigma_{KsI}, \tag{5·33}$$

is obtained by substituting (5·21) into (5·15) and then applying (5·32). Finally, (5·27) is obtained from (5·23) using (5·33) and (5·30). Thus, based on the assumption that the coherence between the field due to multiple-reflections and the field due to single-reflections is negligible, we can determine the estimate (5·22) from the solution of the MFIE. It can be recognized by comparing (5·23) with (5·27), and (5·24) with (5·28), that $\hat{E}_{sI}$ is also the linear mean-square estimate of the integral-field in terms of the Kirchhoff-field. Therefore, the difference between the integral-field and the estimate $\hat{E}_{sI}$,

$$\hat{E}_{mI}(m) = E_I(m) - (\rho E_K(m) + \upsilon), \tag{5·34}$$

is also the error in the estimate. We can show that $\hat{E}_{mI}(m)$ satisfies the properties of the field due to multiple-reflections. Taking the expectation of

both sides of (5·34) we get

$$E\left[\hat{E}_{mI}\right] = 0, \tag{5·35}$$

and the expectations

$$E\left[E_K, \hat{E}_{mI}\right] = 0, \tag{5·36}$$

and

$$E\left[\hat{E}_{sI}, \hat{E}_{mI}\right] = 0, \tag{5·37}$$

can be verified from (5·34), (5·27) and (5·28), by substitution. In fact, the properties (5·35) - (5·37) are necessarily true of the error in the mean-square estimate (Papoulis, 1984).

We have in fact derived two corrections to the scattered field obtained with the Kirchhoff approximation. The estimate of the shadowing component of the integral-field $\hat{E}_{sI}$ provides the first correction. On the assumption that the coherence between the field due to single-reflections and the field due to multiple-reflections is negligible, $\hat{E}_{sI}$ is also the estimate of the integral-field in terms of the Kirchhoff-field. The second correction to the Kirchhoff approximation is provided by the remainder of the integral-field $\hat{E}_{mI}$. The coherence properties of this contribution to the scattered field satisfy the properties that we associate with the field due to multiple-reflections.

It only remains then for us to calculate the expected scattered powers. Since $\hat{E}_{mI}(m)$ is uncorrelated with $E_K(m)$ and $\hat{E}_{sI}(m)$, $m = 1, \ldots, \infty$, the expected scattered power σ_s is the sum of

$$E\left[\,|\hat{E}_{mI}|^2\right] \equiv \sigma_{mI} = \sigma_I - |\rho|^2 \sigma_K - |\nu|^2 - 2\,\mathrm{Re}\,(\rho\,\nu\,\mu_K + \nu\,\mu_I + \rho\,\sigma_{KI}), \tag{5·38}$$

and the expected scattered power due to $\hat{E}_{sI}(m)$ plus $\hat{E}_K(m)$,

$$E\left[\left|\hat{E}_{sI}+E_K\right|^2\right]\equiv\sigma_{sK}=|1+\rho|^2\sigma_K+|\nu|^2+2\,\mathrm{Re}\left((1+\rho)\nu\,\mu_K\right). \quad (5\text{·}39)$$

The scattered powers (5·38) and (5·39) reduce to simpler expressions when the coherent scattered power is negligible; away from the specular angle, for example. With the coherent scattered powers

$$\mu_I=\mu_K=0, \quad (5\text{·}40)$$

then

$$\sigma_{mI}=\sigma_I+|\rho|^2\sigma_K, \quad (5\text{·}41)$$

$$\sigma_{sK}=|1+\rho|^2\sigma_K, \quad (5\text{·}42)$$

and

$$\rho=\frac{\sigma_{KI}}{\sigma_K}. \quad (5\text{·}43)$$

At lower frequencies wave scattering is complicated by diffraction. The significance of the scattered powers (5·38) and (5·39) at lower frequencies is investigated in the next chapter, Chapter 6.

5·4 Chapter summary.

The field scattered from a rough surface is the scattered field obtained with the Kirchhoff approximation plus the field due to the integral in the MFIE, which we call the integral-field. In the high frequency limit the role of the Kirchhoff and integral-fields are understood. In this limit wave scattering is not complicated by diffraction, which allows the incoming and outgoing rays to be represented as rays. The Kirchhoff-field is due to the single-reflections of incoming rays from the surface. While the integral-field is required to account for shadowing of the surface, and multiple-reflections at the surface boundary. In this chapter we presented a

procedure for obtaining from the solution of the MFIE two corrections to the Kirchhoff approximation. On the assumption that the coherence between the field due to single reflections and the field due to multiple-reflections is negligible, a correction for shadowing was obtained as the linear mean-square estimate of the integral-field in terms of the Kirchhoff-field. The error in the estimate, which provides the second correction to the Kirchhoff method, satisfies the coherence properties of the scattered field due to multiple-reflections. Finally, we would note that the relationship between the Kirchhoff-field and the component of the integral-field responsible for shadowing is likely to be non-linear. However, in cases where these two random variables are jointly normal, the non-linear mean-square estimate of the shadowing component of the integral-field is the same as the linear estimate, (see Papoulis, 1984).

6
Numerical results for the far-field scattered power.

In this chapter we present the numerical results for the average scattered power for 60, uncorrelated, 50 wavelength long sections of a Gaussian rough surface (see § 4·2). Curves are presented for the estimate of the expected scattered power $\sigma_S(\theta^i, \theta^s)$ and the estimate of $\sigma_{SK}(\theta^i, \theta^s)$ (5·39). The difference between these two scattered powers is the estimate of $\sigma_{mI}(\theta^i, \theta^s)$ (5·38), (see § 5·3). We have also compared our numerical results with the expected scattered power obtained using the Kirchhoff method both with, and without the correction for shadowing derived in (Wagner, 1967). We will refer to the method employing the shadowing correction as the shadow-corrected Kirchhoff method. Bearing in mind that the computed averages are estimates of their expected values, the term "estimate" has been omitted from the following text.

To compute the Kirchhoff-field $E_K(m{:}\theta^i,\theta^s)$, m = 1, ..., M, the Kirchhoff approximation for the surface current is used in the scattered far-field integrals (4·1) and (4·2). Similarly, the integral-field $E_I(m)$, m = 1,..., M, is computed using the surface current density,

$$J_I(m{:}\ \theta^i, x) = J(m{:}\ \theta^i, x) - J_K(m{:}\ \theta^i, x).$$

Here, $J(m{:}\ \theta^i, x)$ is the solution of the MFIE for the m^{th} surface realization. The results presented in this chapter are grouped according to RMS surface slope and angle of incidence. In § 6·1 we present a summary of the results for rough surfaces with moderate slopes, and in § 6·4 we present a summary of the results for rough surfaces with large slopes.

6·1 A summary of the results for rough surfaces with moderate slopes.

In § 6·2 and § 6·3 we present the scattered powers for a Gaussian rough surface with a RMS slope of 25° and a correlation-length of the same order as the electromagnetic wavelength. For these surfaces, we have found small difference between the average scattered power σ_S and the scattered power σ_{SK}. Physically we suspect that, because this difference is small, the scattered field due to the illumination of the surface by waves scattered from other parts of the surface is small too. We suspect, therefore, that for a RMS slope of less than ~25° the principal role of the integral-field is to correct the Kirchhoff-field for partial-shadowing and the diffraction by the surface of the incident and scattered waves. The results presented in § 6·2 and § 6·3 provide strong evidence that the polarization is an important factor in determining the degree of shadowing at the surface boundary. We have found, for example, that the polarization of the incident wave is a factor in determining the nature of the error in the Kirchhoff method. In the horizontal polarization case a better description of the average scattered power is obtained with the Kirchhoff method when it is used with the correction for shadowing derived in (Wagner, 1967). The results for vertical polarization on the other hand, show how the Kirchhoff method gives a better estimate to the backward scattered power when the shadowing correction is not used. We have also found that the polarization of the incident wave is an important factor in determining the coherent scattered power too. The results show how at large angles of incidence the coherent scattered power is larger for horizontal polarization than for vertical polarization. In some cases the difference between the coherent scattered powers is as large as 6dB.

We have found that the correlation-length is a factor in determining the accuracy of the Kirchhoff method. In fact, we have found that in some

cases the Kirchhoff method overestimates the average scattered power, even when the shadowing correction is not applied. We suspect that for the surfaces considered in this study the interference between neighbouring scatterers on the surface boundary, which is neglected by the Kirchhoff method, is influential in determining the pattern of scattered radiation.

6·2 Results for moderate slopes and small incident angles.

In this section we present the scattered powers for waves incident at angles of 0° to 45° on a Gaussian rough surface with a RMS slope of 25° and a correlation-length of the same order as the electromagnetic wavelength. The striking feature of the results presented in this section is the small difference between the average scattered power σ_S and the scattered power σ_{SK}. The results also show how the polarization of the incident wave is an important factor in determining the nature of the difference between σ_{SK} and the expected scattered power obtained with the Kirchhoff method.

We present in figs. 6·1 - 6·3 the scattered powers for a horizontally polarized wave incident on a Gaussian rough surface with a RMS slope of 25° and a correlation-length of 0·8λ. Curve (A) is the average scattered power σ_S; (B) is σ_{SK}; and (C) is obtained with the shadow-corrected Kirchhoff method. In all three figures the difference between σ_S and σ_{SK} is less than ~1dB. We suspect that, because this difference is small, the scattered far-field due to multiple-scattering is small too. This point will be discussed in § 6·4. For a surface with a RMS slope of 25° there is little geometric shadowing of incoming rays at angles between -40° and 40°. Furthermore, for scattering angles between -40° and 40° there is little shadowing of the outgoing rays too. In figs. 6·1 - 6·3 the value of σ_{SK} at scattering angles between -40° to 40° is described to within 1dB using the Kirchhoff approximation.

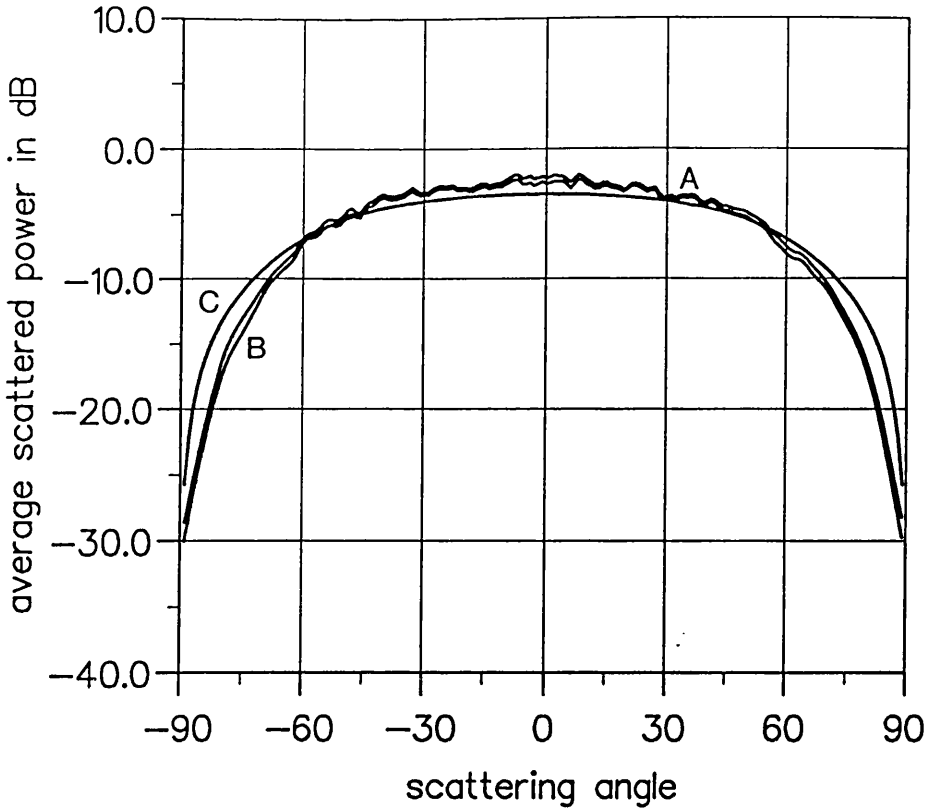

Fig. 6·1. The scattered powers for a Gaussian surface with a RMS slope of 25° and a correlation-length of 0·8λ illuminated by a horizontally polarized wave incident at 0°. Curve (A) is the average scattered power; (B) is σ_{sK}; and (C) is obtained with the shadow-corrected Kirchhoff method.

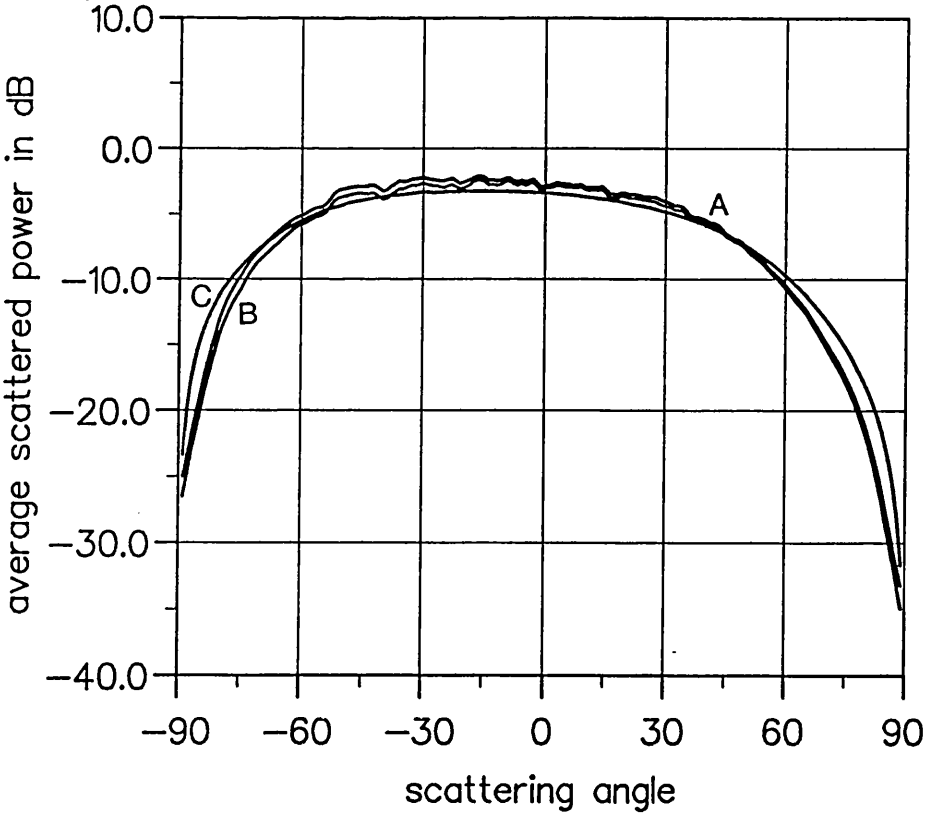

Fig. 6·2. The scattered powers for a Gaussian surface with a RMS slope of 25° and a correlation-length of 0·8λ illuminated by a horizontally polarized wave incident at 30°. Curve (A) is the average scattered power; (B) is σ_{sK}; and (C) is obtained with the shadow-corrected Kirchhoff method.

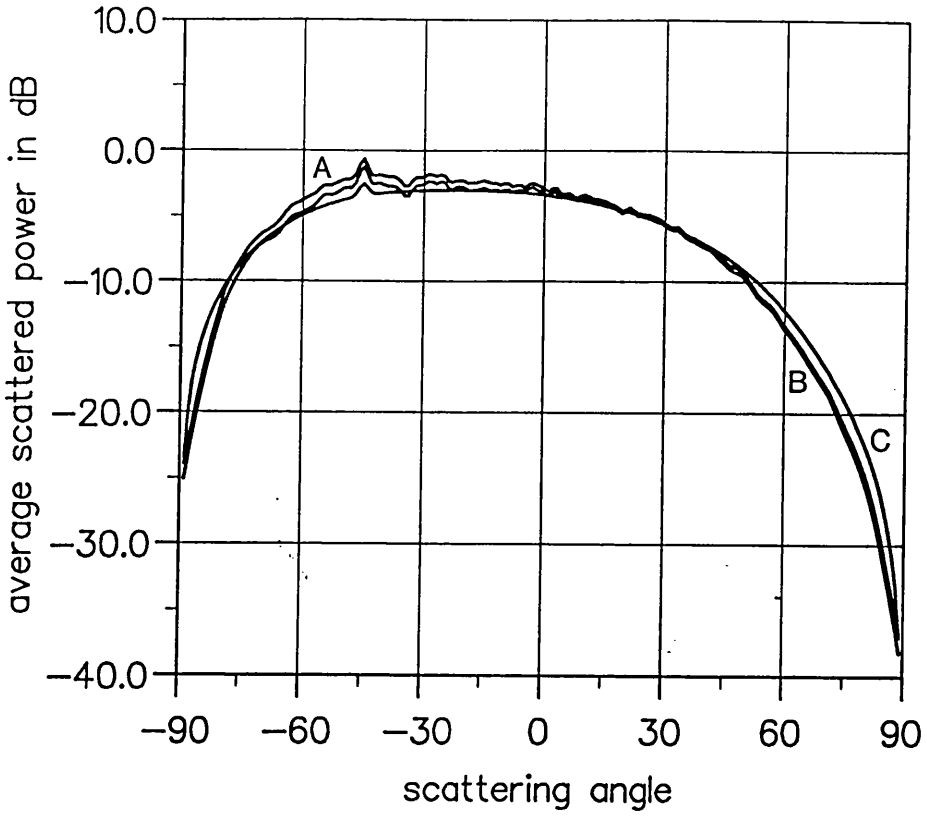

Fig. 6·3. The scattered powers for a Gaussian surface with a RMS slope of 25° and a correlation-length of 0·8λ illuminated by a horizontally polarized wave incident at 45°. Curve (A) is the average scattered power; (B) is σ_{sK}; and (C) is obtained with the shadow-corrected Kirchhoff method.

However, at larger scattering angles where we would anticipate the shadowing effect to be greater, the shadow-corrected Kirchhoff method overestimates σ_{sK}.

We have found the surface correlation-length to be an important factor in determining the accuracy of the Kirchhoff method. This point is illustrated in figs. 6·4 and 6·5 where we present the scattered powers for a horizontally polarized wave incident on a Gaussian rough surface with a RMS slope of 25° and a correlation-length of 0·4λ. In fig. 6·4 the wave is normally incident on the surface, and in fig. 6·5 the wave is incident at an angle of 45°. It can be easily verified by comparing fig. 6·1 with fig. 6·4 and fig. 6·3 with fig. 6·5, that the difference between the average scattered power and the shadow-corrected Kirchhoff method is significantly larger for a surface correlation-length of 0·4λ than for a correlation-length of 0·8λ.

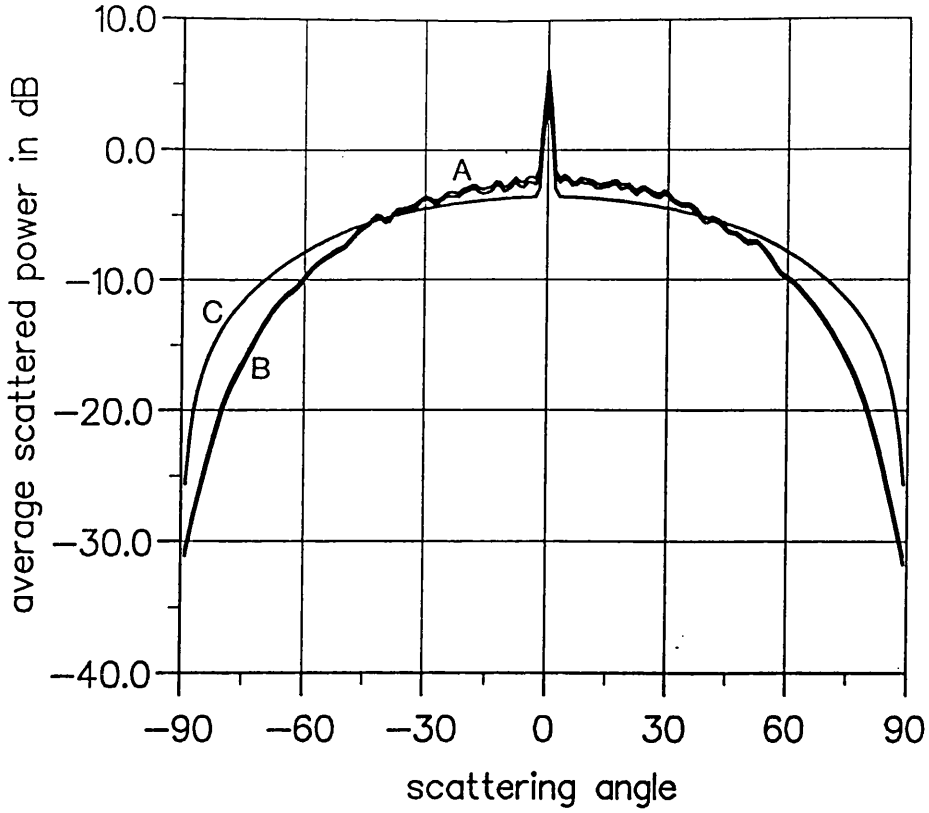

Fig. 6·4. The scattered powers for a Gaussian surface with a RMS slope of 25° and a correlation-length of 0·4λ illuminated by a horizontally polarized wave incident at 0°. Curve (A) is the average scattered power, (B) is σ_{sK} and (C) is obtained with the shadow-corrected Kirchhoff method.

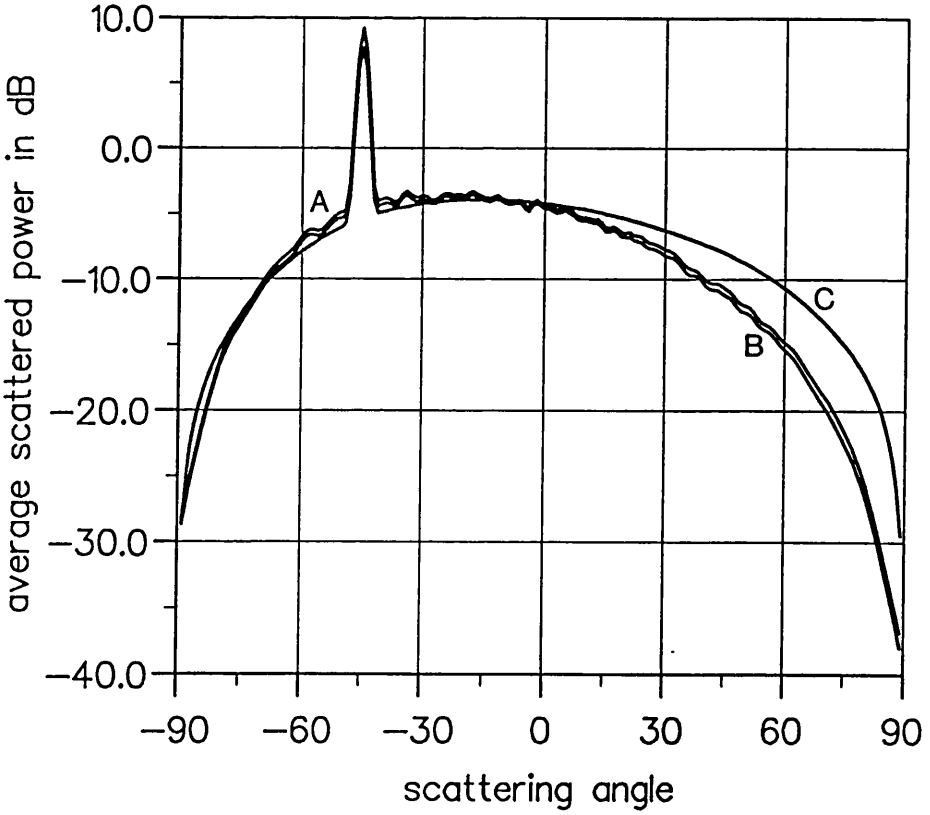

Fig. 6·5. The scattered powers for a Gaussian surface with a RMS slope of 25° and a correlation-length of 0·4λ illuminated by a horizontally polarized wave incident at 45°. Curve (A) is the average scattered power; (B) is σ_{sK}; and (C) is obtained with the shadow-corrected Kirchhoff method.

The polarization of the incident wave is also an important factor in determining the nature of the difference between average scattered power and the expected scattered power obtained with the Kirchhoff method. We present in figs. 6·6 and 6·7 the scattered powers for a vertically polarized wave incident on a Gaussian rough surface with a RMS slope of 25° and a correlation-length of 0·8λ. In the figures curve (A) is the average scattered power σ_S; (B) is σ_{SK}; and (C) is obtained with the shadow-corrected Kirchhoff method. It can be verified from the figures that there is close agreement between the Kirchhoff method and σ_{SK} at scattering angles between -40° and 40°. However, at larger scattering angles the shadow-corrected Kirchhoff method underestimates the value of σ_{SK}.

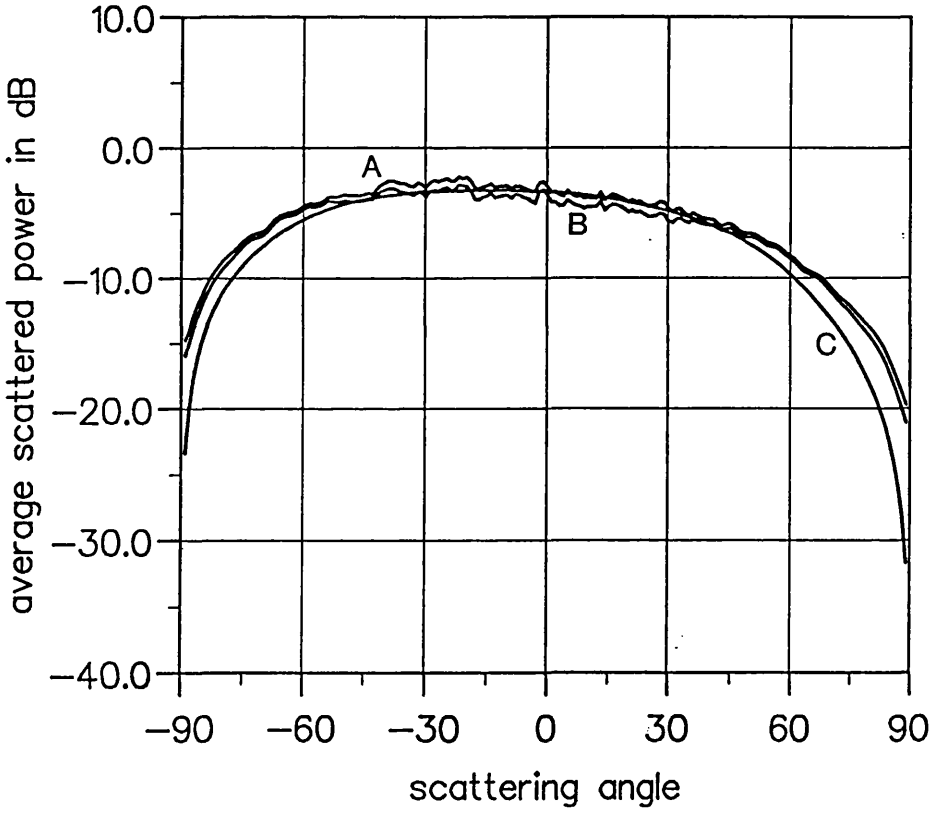

Fig. 6·6. The scattered powers for a Gaussian surface with a RMS slope of 25° and a correlation-length of 0·8λ illuminated by a vertically polarized wave incident at 30°. Curve (A) is the average scattered power; (B) is σ_{SK}; and (C) is obtained with the shadow-corrected Kirchhoff method.

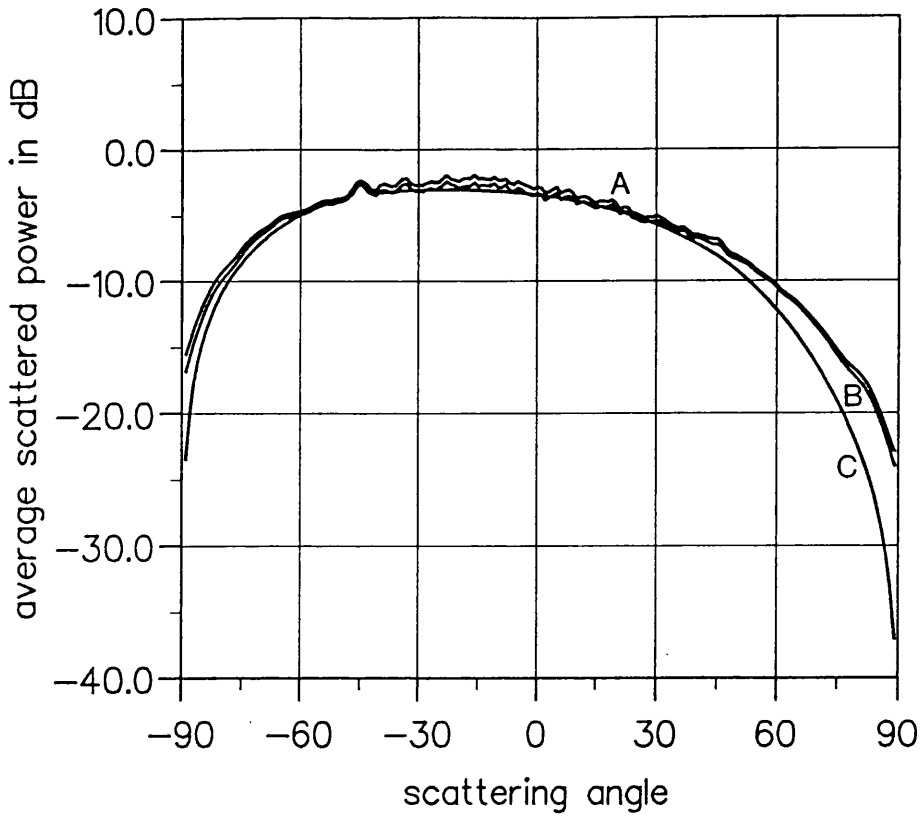

Fig. 6·7. The scattered powers for a Gaussian surface with a RMS slope of 25° and a correlation-length of 0·8λ illuminated by a vertically polarized wave incident at 45°. Curve (A) is the average scattered power; (B) is σ_{sK}; and (C) is obtained with the shadow-corrected Kirchhoff method.

In fact, we have found for the cases in figs. 6·6 and 6·7 that the Kirchhoff method gives a better estimate to the backward scattered power when the shadowing correction is not used. We illustrate this point in figs. 6·8 and 6·9 where curve (A) is σ_{sK}; curve (B) is the scattered power obtained with the Kirchhoff approximation; and curve (C) is obtained with the shadow-corrected Kirchhoff method. At a scattering angle of 80°, for example, the shadow-corrected Kirchhoff method underestimates the value of σ_{sK} by 10dB in fig. 6·9, and by 8dB in fig. 6·8. The error using the Kirchhoff method with no correction for shadowing is only 1dB in fig. 6·9, and in fig. 6·8 the error is very small. However, in both figures a better description of the scattered power σ_{sK} at large forward scattering angles is obtained by including the shadowing correction.

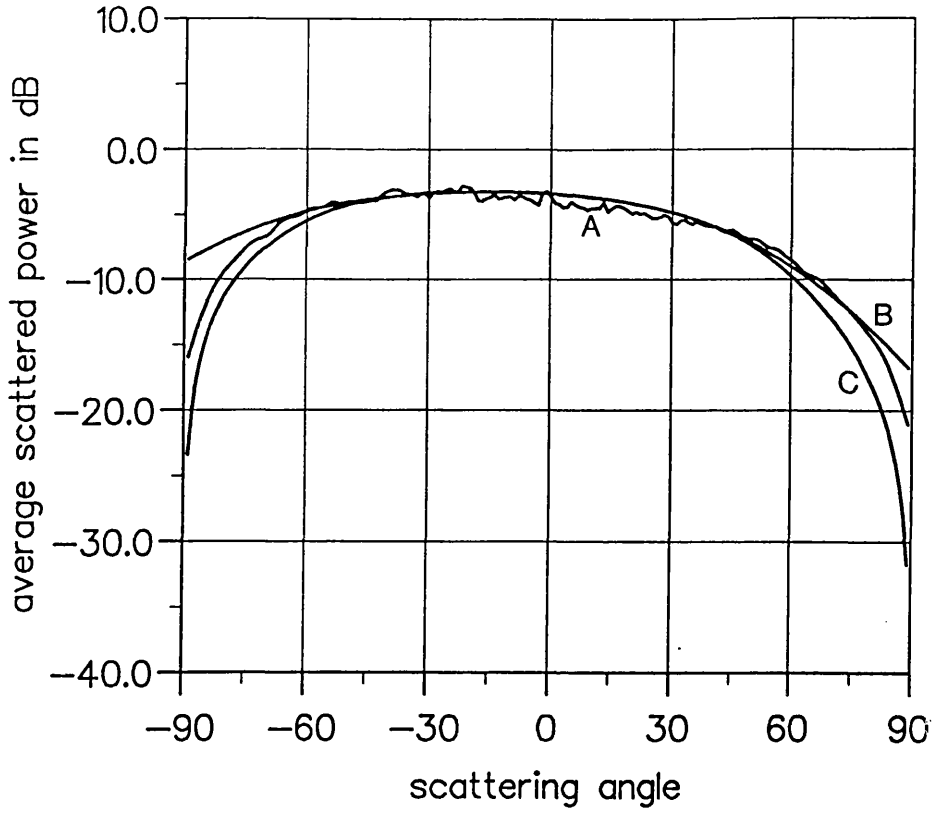

Fig. 6·8. The scattered powers for a Gaussian rough surface with a RMS slope of 25° and a correlation-length of 0·8λ illuminated by a vertically polarized wave incident at 30°. Curve (A) is σ_{sK}; (B) is obtained with the Kirchhoff approximation; and (C) with the shadow-corrected Kirchhoff method.

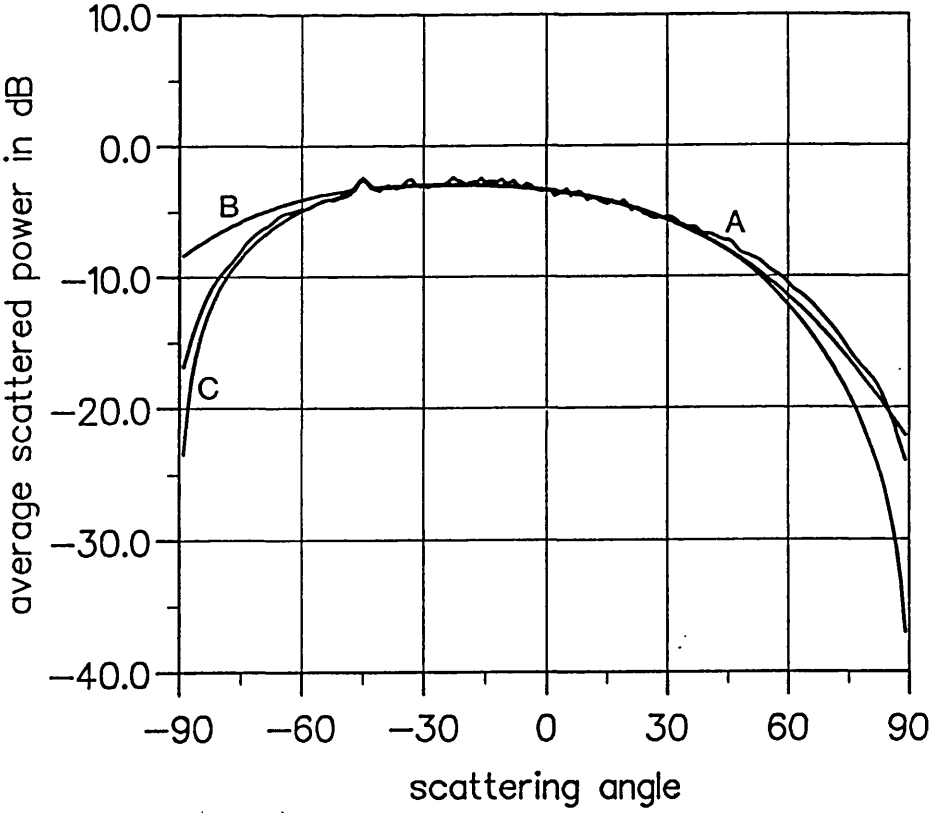

Fig. 6·9. The scattered powers for a Gaussian rough surface with a RMS slope of 25° and a correlation-length of 0·8λ illuminated by a vertically polarized wave incident at 45°. Curve (A) is σ_{sK}; (B) is obtained with the Kirchhoff approximation; and (C) with the shadow-corrected Kirchhoff method.

We have found that the correlation-length is an important factor in determining the accuracy of the Kirchhoff method in the vertical polarization case too. To illustrate this point we present in fig. 6·10 the scattered powers for a vertically polarized wave incident at an angle of 45° on a Gaussian rough surface with a RMS slope of 25° and a correlation-length of 0·4λ. In fig. 6·10 curve (A) is σ_{sK}; and curve (B) is obtained with the Kirchhoff method without using the shadowing correction. The corresponding curves for a surface correlation-length of 0·8λ are presented in fig. 6·9. It can be easily verified that where there is small difference between curves (A) and (B) in fig. 6·9, there is a large difference between curves (A) and (B) in fig. 6·10.

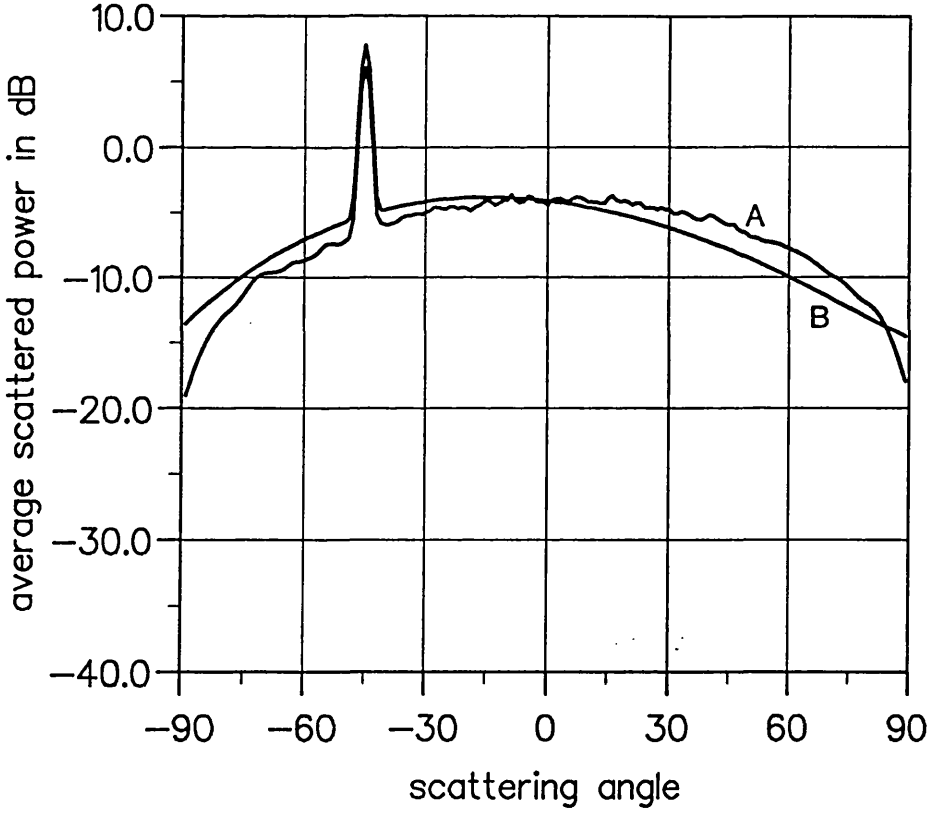

Fig. 6·10. The scattered powers for a Gaussian rough surface with a RMS slope of 25° and a correlation-length of 0·4λ illuminated by a vertically polarized wave incident at 45°. Curve (A) is σ_{sK}; and (B) is obtained with the Kirchhoff approximation.

Several points have been raised so far concerning the trends in results for vertical and horizontal polarization. These trends will be discussed further once we have presented the results for waves incident at large angles. The results for large incident angles are presented in the next section.

6·3 Results for moderate slopes and large incident angles.

In this section, we present the scattered powers for a Gaussian rough surface with a RMS slope of 25° illuminated by waves incident at angles of 60° and 70°. For these surfaces there is small difference between the scattered powers σ_s and σ_{sK} when the incident wave is horizontally polarized. However, in the vertical polarization case there is a significant difference between these two scattered powers at large forward scattering angles. This difference is the scattered power σ_{mI}. Physically, we suspect the difference is due to the illumination of the surface by waves scattered from other parts of the surface. This point will be discussed in § 6·5. A new feature of the results is the dependence of the coherent scattered power on the polarization of the incident wave. We have found that the coherent scattered power is greater for horizontal polarization than for vertical polarization. We suspect that this effect is related to the degree of shadowing at the surface boundary, and the resulting distribution of the scattering sites along the surface. We will present contour-plots of the electromagnetic field in the vicinity of the surface boundary. The contour-plots for the vertical polarization case show how the scattering sites are distributed along the surface slopes. In the horizontal polarization case the contour-plots show how the scattering sites are located near to the surface peaks. We suspect it is for this reason that the apparent roughness of the surface is smaller for horizontal polarization than for vertical polarization.

We present in figs. 6·11 and 6·12, the scattered powers for a horizontally polarized wave incident on a Gaussian rough surface with a RMS slope of 25° and a correlation-length of 0·8λ. In the figures, curve (A) is the average scattered power σ_S; (B) is σ_{SK}; and (C) is obtained with the shadow-corrected Kirchhoff method. In fig. 6·11 the wave is incident at an angle of 60°, and in fig. 6·12 the wave is incident at an angle of 70°. It can be easily verified from fig. 6·12 that the difference between σ_{SK} and the scattered power obtained with the Kirchhoff method extends to scattering angles between -40° and 40°. This is also true in fig. 6·11, although the difference is smaller. In as far as the ray model can be applied to our surfaces, figs. 6·11 and 6·12 could be interpreted to show how the correction for shadowing derived by Wagner (1967) underestimates the degree of shadowing of the incident wave; numerically at least the correction is too small.

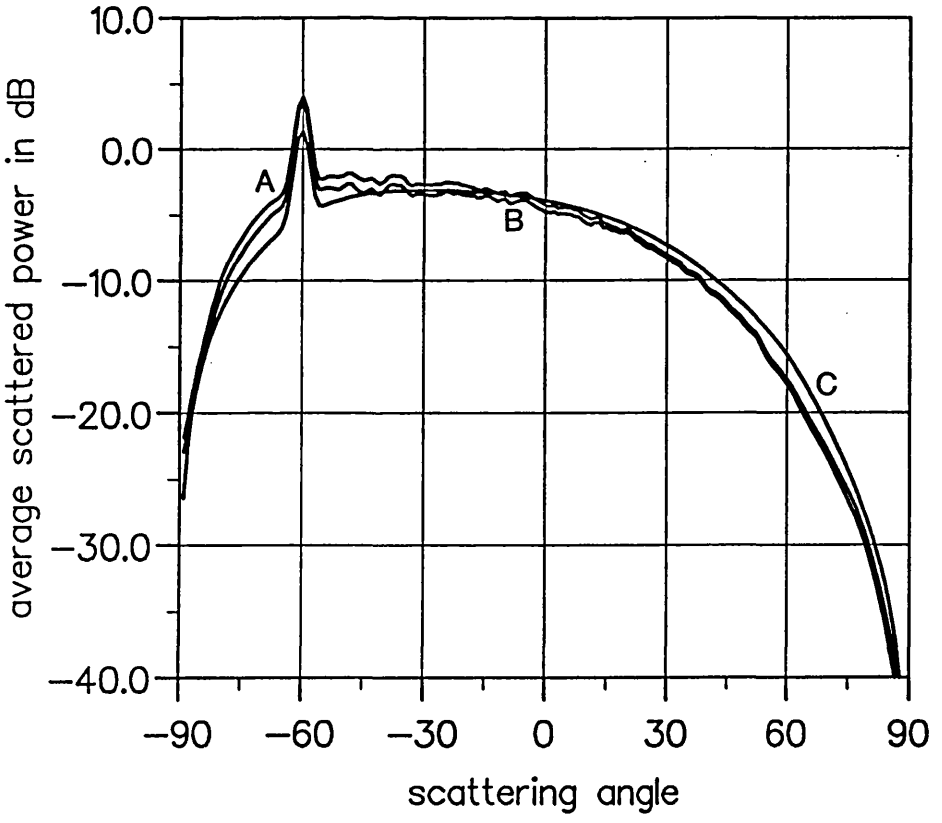

Fig. 6·11. The scattered powers for a Gaussian surface with a RMS slope of 25° and a correlation-length of 0·8λ illuminated by a horizontally polarized wave incident at 60°. Curve (A) is the average scattered power; (B) is σ_{SK}; and (C) is obtained with the shadow-corrected Kirchhoff method.

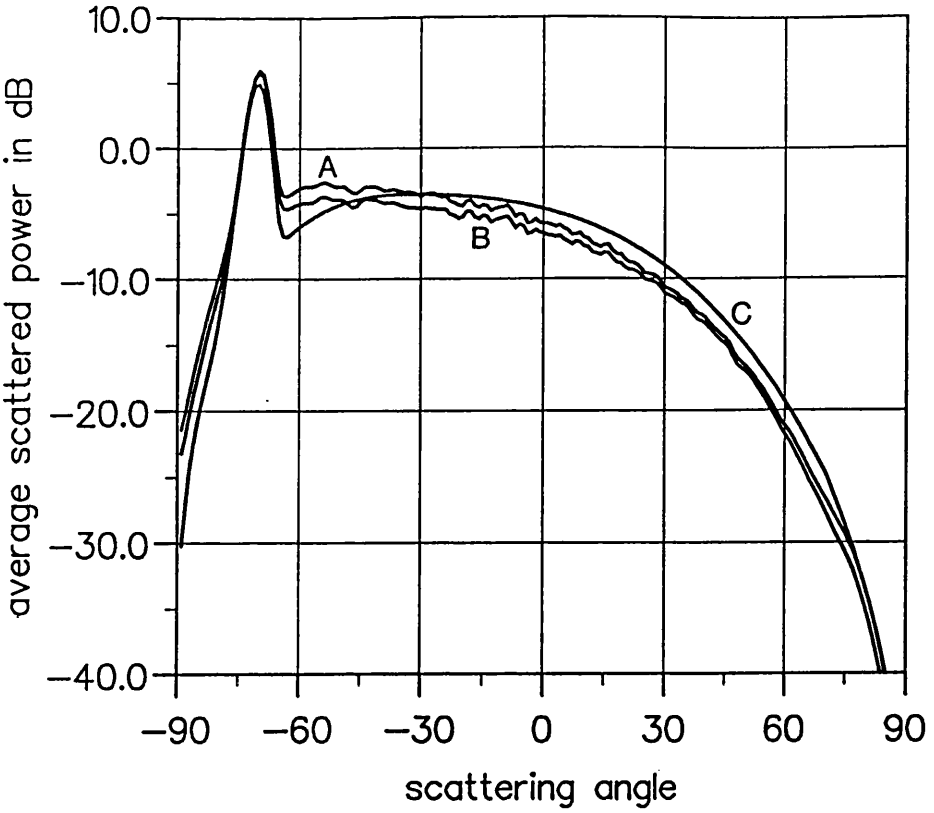

Fig. 6·12. The scattered powers for a Gaussian surface with a RMS slope of 25° and a correlation-length of 0·8λ illuminated by a horizontally polarized wave incident at 70°. Curve (A) is the average scattered power; (B) is σ_{sK}; and (C) is obtained with the shadow-corrected Kirchhoff method.

We have found this interpretation of the results for vertical polarization would lead to the opposite conclusion. In figs. 6·13 and 6·14 we present the scattered powers for a vertically polarized wave incident on a Gaussian rough surface with a RMS slope of 25° and a correlation-length of 0·8λ. In the figures curve (A) is the average scattered power σ_s; (B) is σ_{sK}; and (C) is obtained with the shadow-corrected Kirchhoff method. In fig. 6·13 the wave is incident at an angle of 60°, and in fig. 6·14 the wave is incident at an angle of 70°. It can be easily verified from figs. 6·13 and 6·14, that the shadow-corrected Kirchhoff method underestimates the value of σ_{sK} at scattering angles between -40° and 40°. Numerically, the correction for shadowing is to large. In fact, we have found for the cases in figs 6·13 and fig. 6·14, that a better estimate for the backward scattered power is obtained by using the Kirchhoff method without a correction for shadowing.

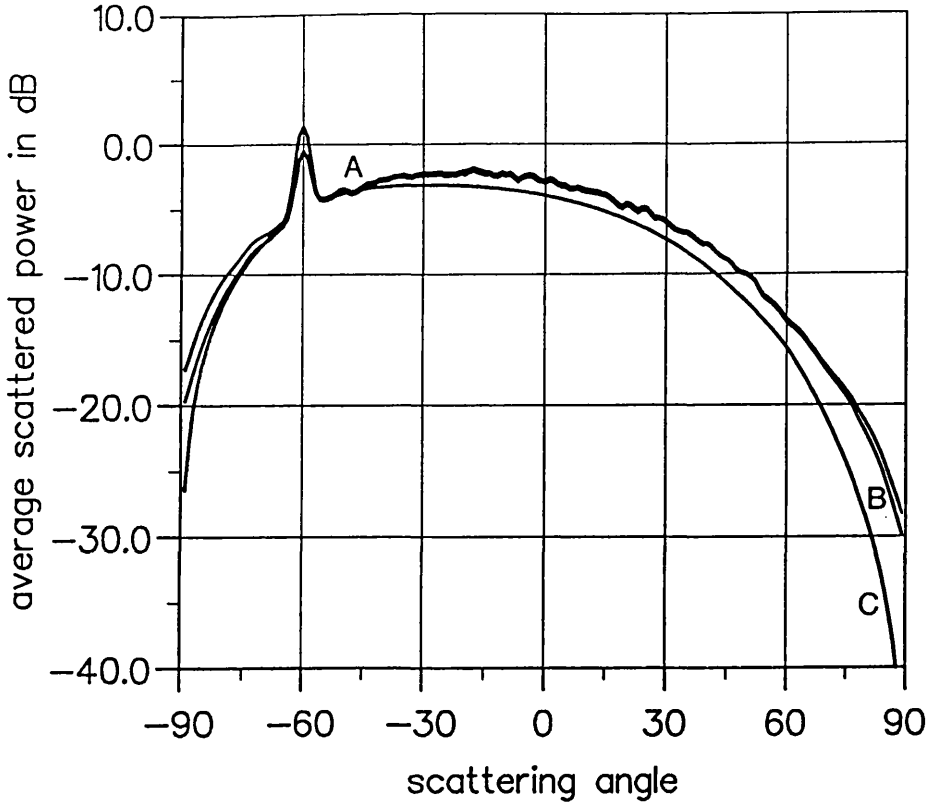

Fig. 6·13. The scattered powers for a Gaussian surface with a RMS slope of 25° and a correlation-length of 0·8λ illuminated by a vertically polarized wave incident at 60°. Curve (A) is the average scattered power; (B) is σ_{sK}; and (C) is obtained with the shadow-corrected Kirchhoff method.

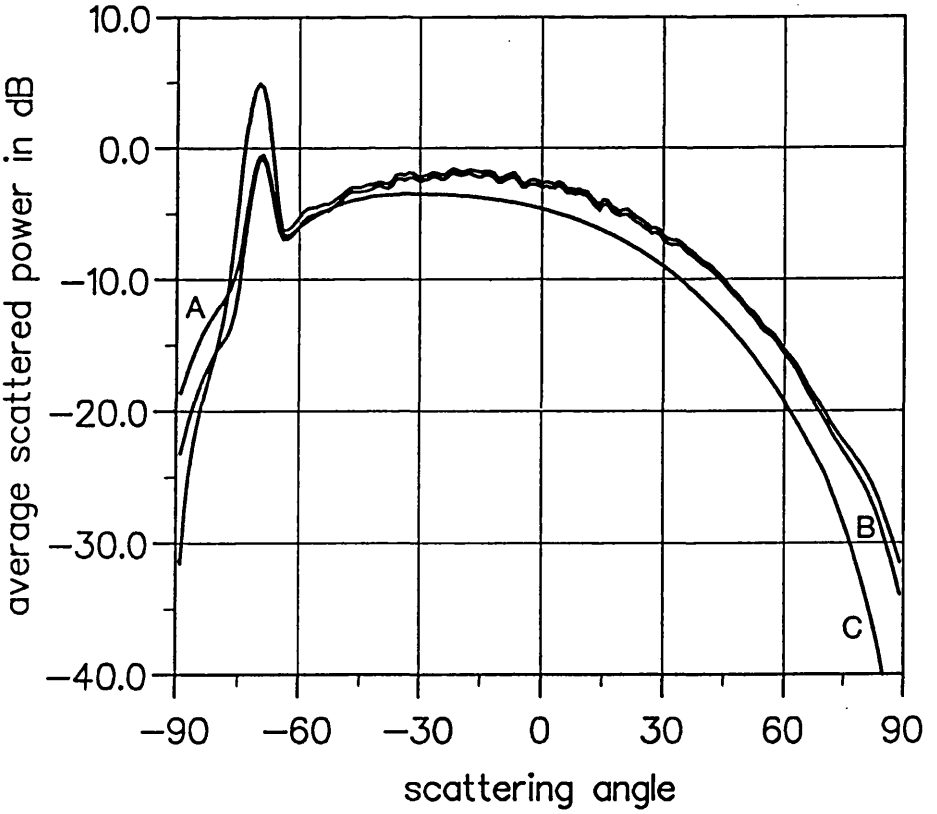

Fig. 6·14. The scattered powers for a Gaussian surface with a RMS slope of 25° and a correlation-length of 0·8λ illuminated by a vertically polarized wave incident at 70°. Curve (A) is the average scattered power; (B) is σ_{sK}; and (C) is obtained with the shadow-corrected Kirchhoff method.

This point is illustrated in fig. 6·15 where we present the scattered powers for a vertically polarized wave incident at an angle of 60°; curve (A) is σ_{sK}; curve (B) is the scattered power obtained with the Kirchhoff approximation; and curve (C) is obtained with shadow-corrected Kirchhoff method. At a scattering angle of 80°, for example, the shadow-corrected Kirchhoff method underestimates σ_{sK} by 8dB. The Kirchhoff approximation on the other hand, underestimates σ_{sK} by only 1dB. Nevertheless, a better description of σ_{sK} at large forward scattering angles is obtained with the shadowing correction.

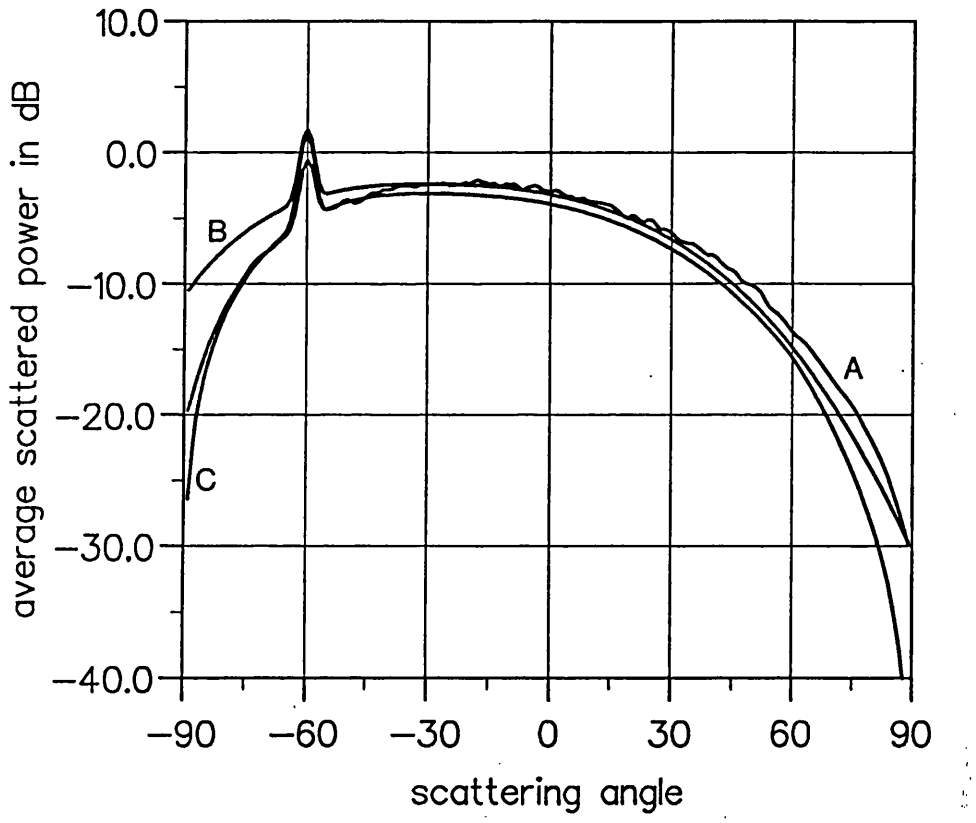

Fig. 6·15. The scattered powers for a Gaussian rough surface with a RMS slope of 25° and a correlation-length of 0·8λ illuminated by a vertically polarized wave incident at 60°. Curve (A) is σ_{sK}; (B) is obtained with the Kirchhoff approximation; and (C) with the shadow-corrected Kirchhoff method.

The results for rough surfaces with a correlation-length of 0·8λ presented in this and the previous section show how the Kirchhoff method can provide a qualitative description of the angular distribution of scattered

power, even when the surface correlation-length is of the same order as the electromagnetic wavelength. In the horizontal polarization case the shadowing correction in (Wagner, 1967) is required to describe the angular distribution of the scattered power. In the vertical polarization case, however, the Kirchhoff method gives a better estimate to the backward scattered power when the shadowing correction is not used.

So far we have discussed the behaviour of the incoherent scattering component. The coherent scattering component can be recognized in the figures as the narrow angular distribution of scattered power centred on the specular angle. We have found that the coherent scattered power is dependent upon the polarization of the incident wave. In figs. 6·11 and 6·12, for example, the Kirchhoff method underestimates the coherent scattered power. In fig. 6·13 and fig. 6·14 the opposite is true. Furthermore, it can be easily verified by comparing fig. 6·11 with fig. 6·13 , and fig. 6·12 with fig. 6·14, that the coherent scattered power is 6dB larger for horizontal polarization than for vertical polarization.

At finite frequencies shadowing cannot occur without diffraction. For simple structures such as cylinders (Poggio and Miller, 1973), and wedges (Ruck *et al*, 1970), it is well known that a vertically polarized wave is to a greater extent diffracted around the target than a horizontally polarized wave. The contour-plots of the electromagnetic-field in the vicinity of the surface boundary provide some evidence that this is true for rough surfaces too. We present in fig. 6·16 the normalized modulus of the total magnetic field in the vicinity of a Gaussian rough surface with a RMS slope of 25°, and a correlation-length of 0·8λ illuminated by a vertically polarized wave. In the figure the bright areas on the surface boundary coincide with where the surface current is a maximum. It can be easily verified from the figure that the largest surface current occurs at (-1·1, 0·0). The surface current at (2·1, 0·0) is smaller, because this part of the surface is partially shadowed by the surface to its right.

Fig. 6·16. The normalized modulus of the total magnetic field in the vicinity of a rough surface with a RMS slope of 25° and a correlation-length of 0·8λ, when a vertically polarized wave is incident from the right with an incidence angle of 60°.

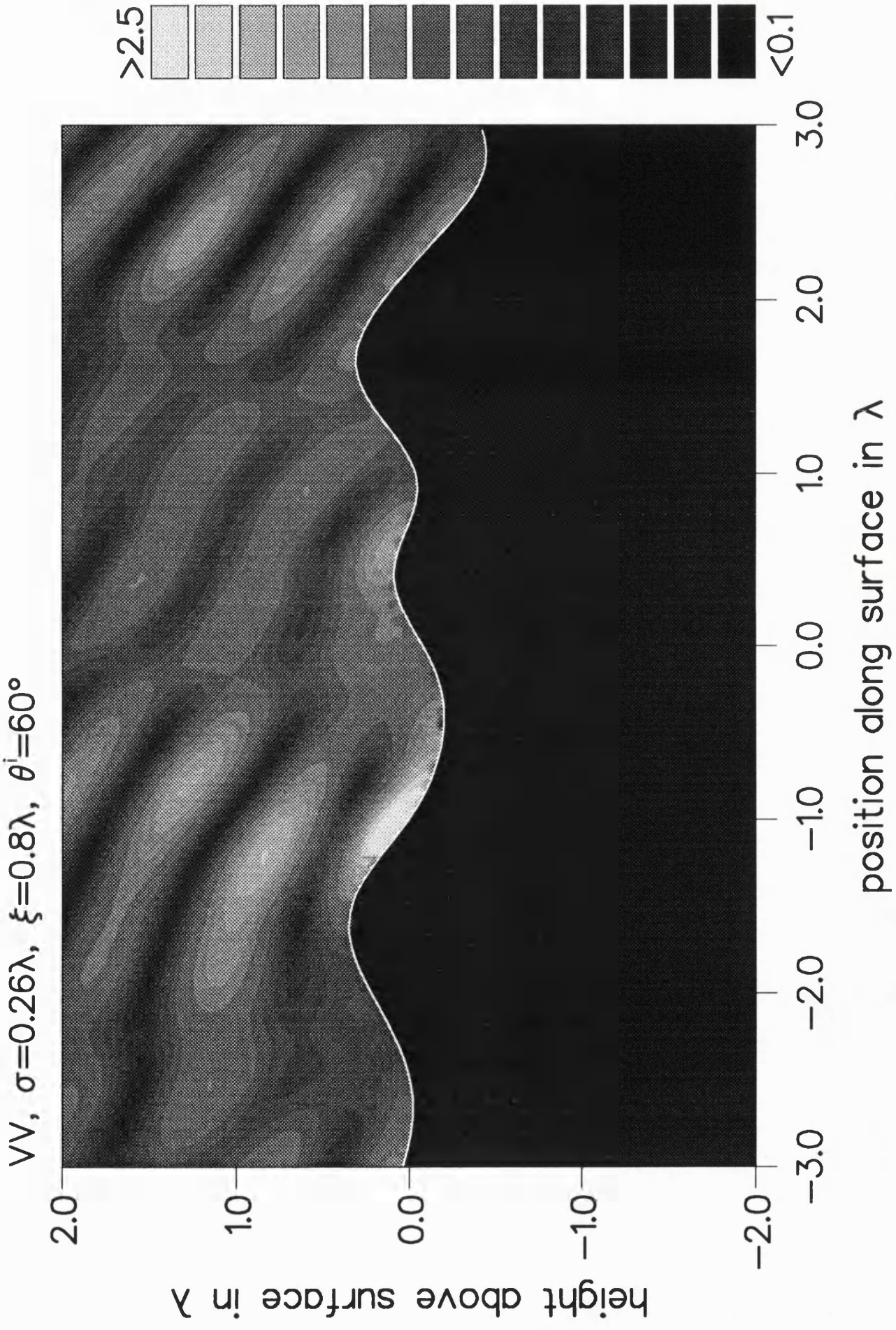

Fig. 6·17. The normalized modulus of the total electric field in the vicinity of a rough surface with a RMS slope of 25° and a correlation-length of 0·8λ, when a horizontally polarized wave is incident from the right with an incidence angle of 60°.

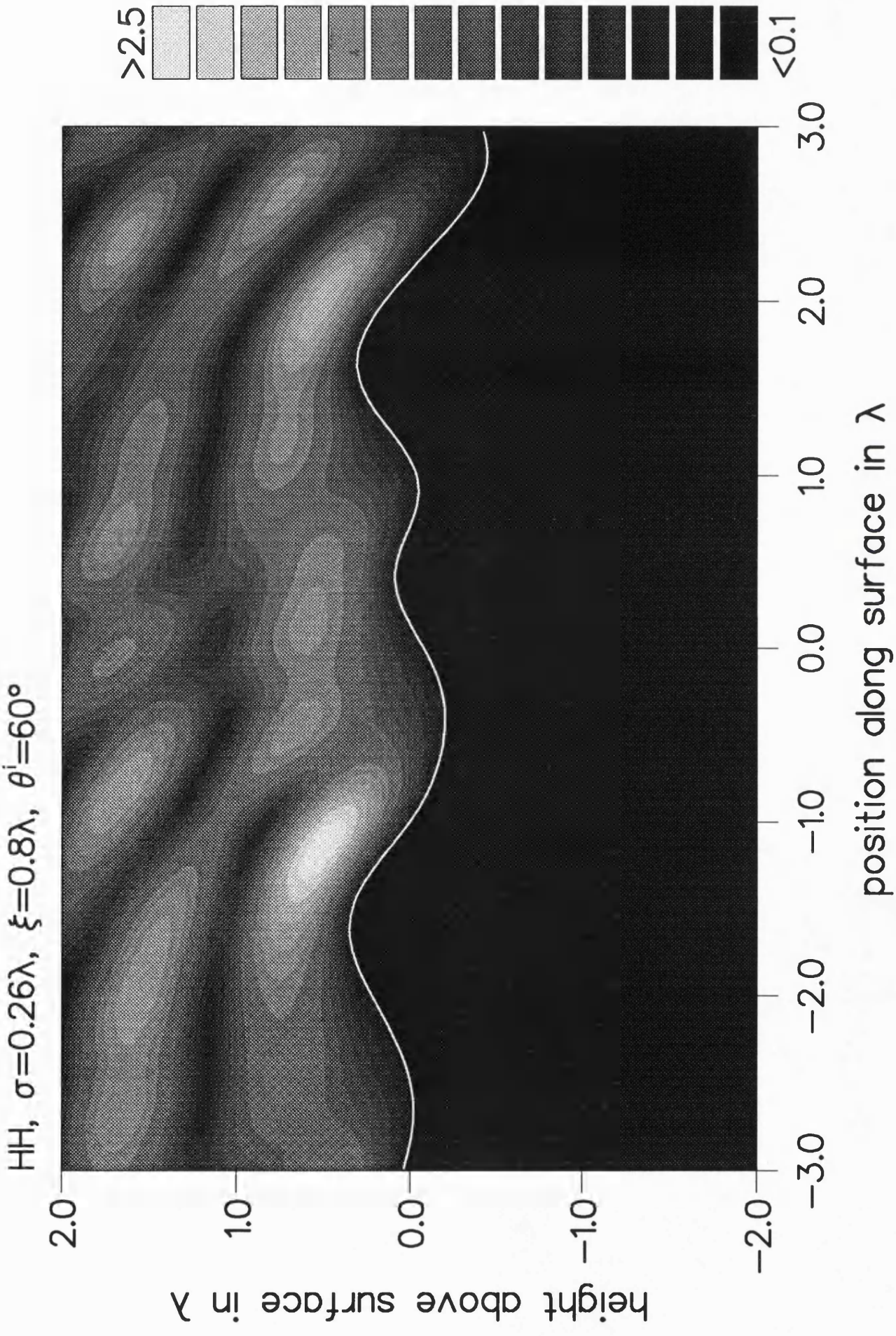

There is evidence in the contour-plot of the diffraction by the surface of the incident wave. The surface current at (-0·5, 0·0), for example, appears to be due to the diffraction of the incident wave around the surface at (-1·5, 0·25).

In fig. 6·17 we present the normalized modulus of the total electric field for a horizontally polarized wave incident at angle of 60° on the same section of surface illustrated in fig. 6·16. In the horizontal polarization case the largest surface currents coincide with where the rate of change of the total electric field along the direction of the vector normal to the surface is largest. It can be verified from the figures that in fig. 6·17 the scattering sites have there centres at (-1·5, 0·25) and (1·75, 0·75), near to the surface peaks. This is in contrast to fig. 6·16 where the scattering sites are distributed along the slopes of the surface. Intuitively, we would expect such a difference between the location of the scattering sites if the degree of shadowing of the surface was greater for horizontal polarization than for vertical polarization.

6·4 A summary of the results for rough surfaces with large slopes.

In the next section, § 6·5, we present the results for a Gaussian rough surface with a RMS slope of 45° and a correlation-length of the same order as the electromagnetic wavelength. In contrast to the results for a RMS slope of 25°, for a RMS slope of 45° the difference between the scattered powers σ_S and σ_{SK} is not small. This difference is the scattered power σ_{mI}. The results presented in § 6·5 illustrate the enhanced backscattering phenomenon reported in the literature (Mendez and O'Donnell, 1987). For the surfaces we have considered, enhanced backscattering occurs for vertically and horizontally polarized waves incident at angles between 0° and 30°. We have found this is true, even when the surface correlation-length is as small as 0·4λ. We have found that near to normal incidence

the angular distribution of the enhanced backward scattered power is described with σ_{mI}, and to a good approximation the shadow-corrected Kirchhoff method describes the scattered power σ_{sK}. According to the ray picture of scattering, the single-scatter of the incident wave from the surface is described with the Kirchhoff method. The intuitive picture of scattering has also provided an explanation of enhanced backscattering as a multiple-scatter phenomenon (O'Donnell and Mendez, 1987). Here, the term "multiple-scatter" describes the scattering due to the illumination of the surface by waves scattered from other parts of the surface. In as far as the intuitive picture of scattering can be applied to our surfaces, the results for rough surfaces with large slopes provide evidence that the scattered powers σ_{sK} and σ_{mI} describe the single and multiple-scatter from the surface, respectively.

6·5 Results for large slopes.

In this section we present the scattered powers for a Gaussian rough surface with a RMS slope of 45° and a correlation-length of the same order as the electromagnetic wavelength. The striking feature of the results for these surfaces is the large difference between the average scattered power σ_s and the scattered power σ_{sK}. For waves incident at angles of less than 30°, we have found that the average scattered power is largest in the backward scattering direction. Moreover, the angular distribution of backward scattered power is relatively narrow. We have found that this enhanced backscattering occurs even when the surface correlation-length is as small as 0·4λ. The results for waves incident at angles of 0° and 15° show how the angular distribution of the backward scattered power is described by the angular distribution of σ_{mI}, and the angular distribution of σ_{sK} is to a good approximation described with the Kirchhoff method. At the end of this

section we present contour-plots of the total field in the vicinity of the surface boundary. The plots illustrate how multiple-scattering enhances the surface current density in the valleys of the rough surface.

We present in figs. 6·18 - 6·20 the scattered powers for a horizontally polarized wave incident at angles of 0°, 15° and 45° on a Gaussian rough surface with a RMS slope of 45° and a correlation-length of 0·8λ. In the figures curve (A) is the average scattered power, and curve (B) is σ_{sK}, The smooth curve, curve (C), is the scattered power obtained with the shadow-corrected Kirchhoff method. In all three figures, the angular distribution of σ_{sK} is described to good approximation with the shadow-corrected Kirchhoff method. However, the fluctuations in the numerical results are large, and we suppose that considerably more averaging would have to be done to obtain a good estimate of their respective expected values.

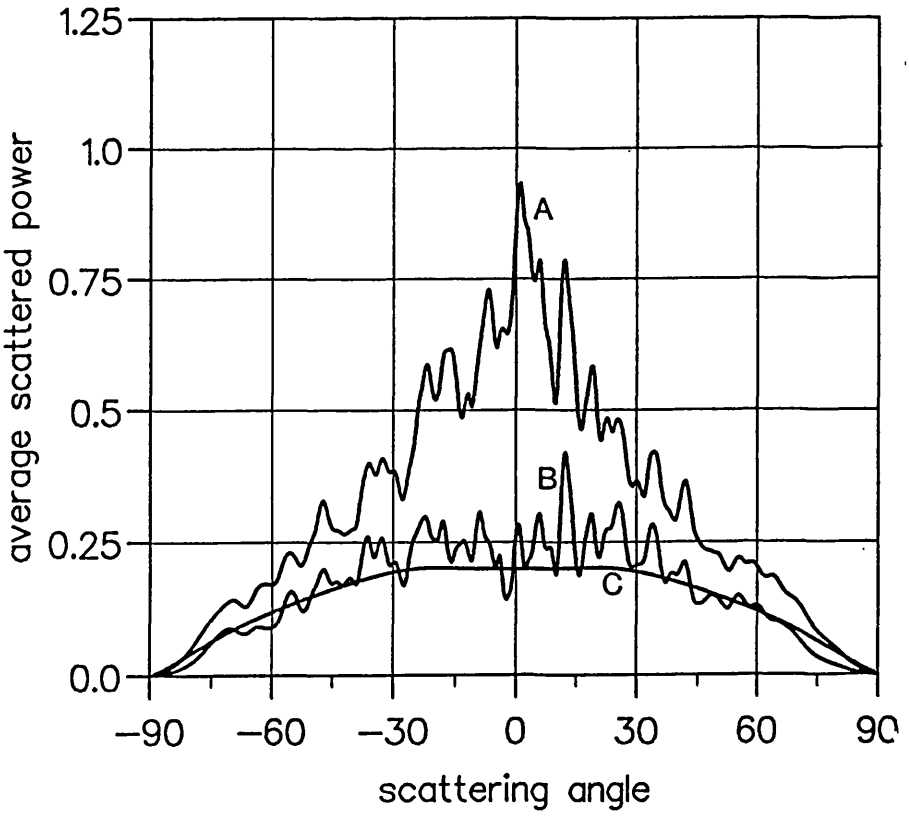

Fig. 6·18. The scattered powers for a Gaussian rough surface with a RMS slope of 45° and a correlation length of 0·8λ illuminated by a horizontally polarized wave incident at 0°. Curve (A) is the average scattered power; (B) is σ_{sK}; and (C) is obtained with the shadow-corrected Kirchhoff method.

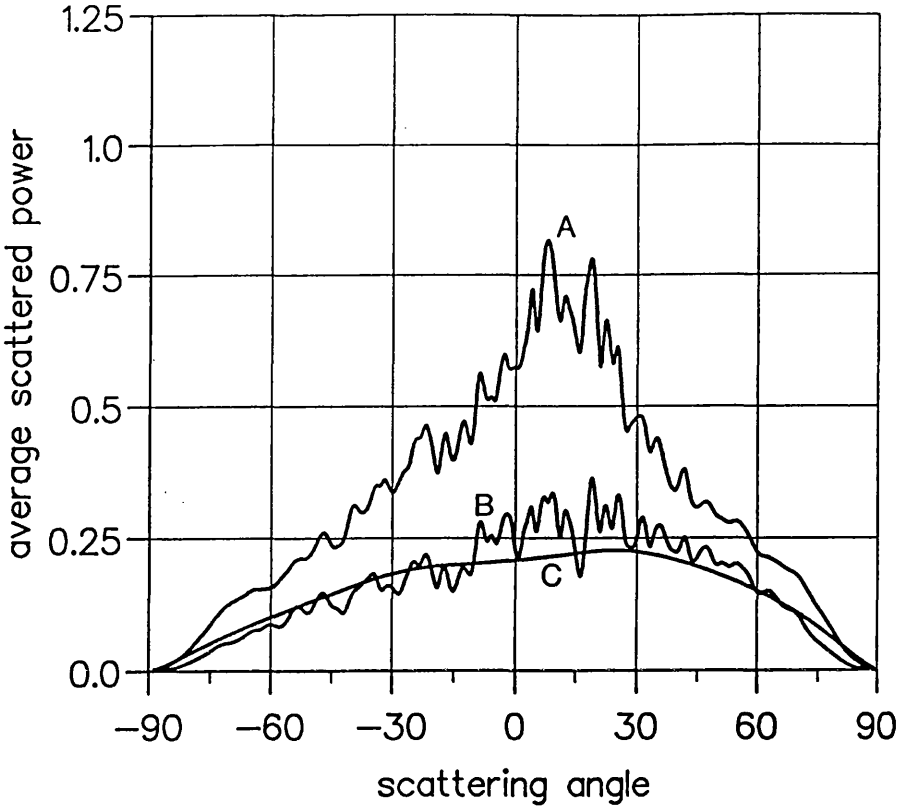

Fig. 6·19. The scattered powers for a Gaussian rough surface with a RMS slope of 45° and a correlation length of 0·8λ illuminated by a horizontally polarized wave incident at 15°. Curve (A) is the average scattered power; (B) is σ_{SK}; and (C) is obtained with the shadow-corrected Kirchhoff method.

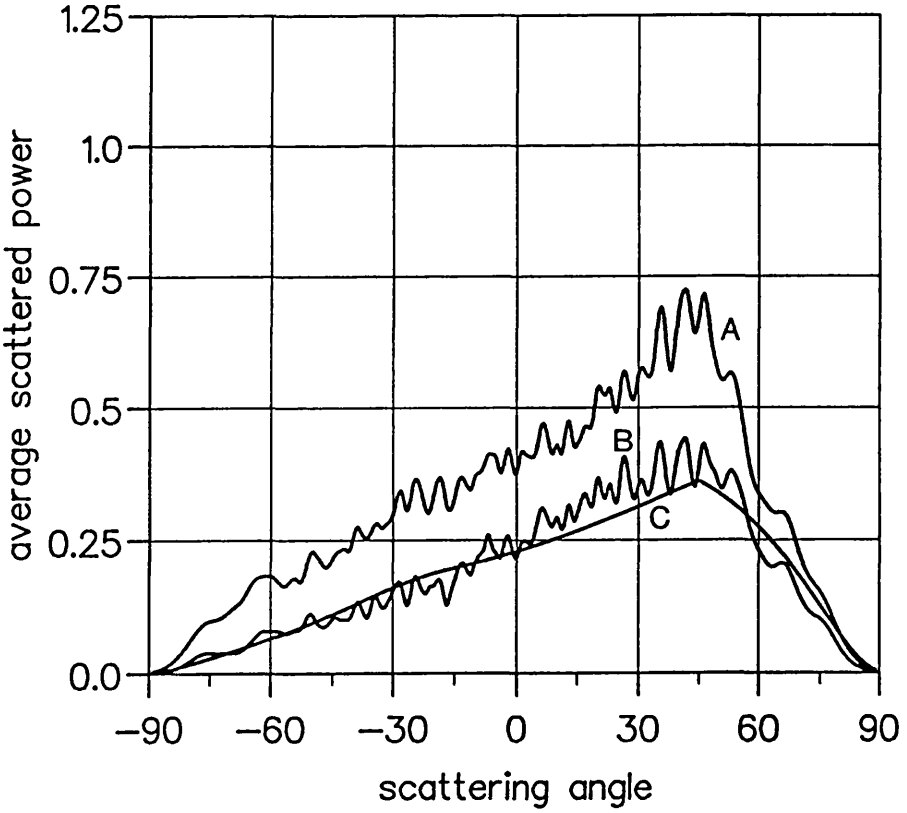

Fig. 6·20. The scattered powers for a Gaussian rough surface with a RMS slope of 45° and a correlation length of 0·8λ illuminated by a horizontally polarized wave incident at 45°. Curve (A) is the average scattered power; (B) is σ_{SK}; and (C) is obtained with the shadow-corrected Kirchhoff method.

The striking feature of the figures is the large difference between the average scattered power and σ_{sK}. In all three figures the average scattered power is largest in the backward scattering direction. In two of the figures, figs. 6·18 and 6·19, this is due to the σ_{mI} contribution. In fig. 6·20 the tilt in the angular distribution of σ_{sK} towards the backward scattering direction is equally responsible for the large backward scattered power.

We present in figs. 6·21 - 6·23 the scattered powers for a vertically polarized wave for the same cases in fig. 6·18 - 6·20. Figs. 6·21 and 6·22 also show how the angular distribution of the average backward scattered power is described by the angular distribution of σ_{mI}. We have found that the angular width of the enhanced backward scattered power is narrower for vertical polarization than for horizontal polarization.

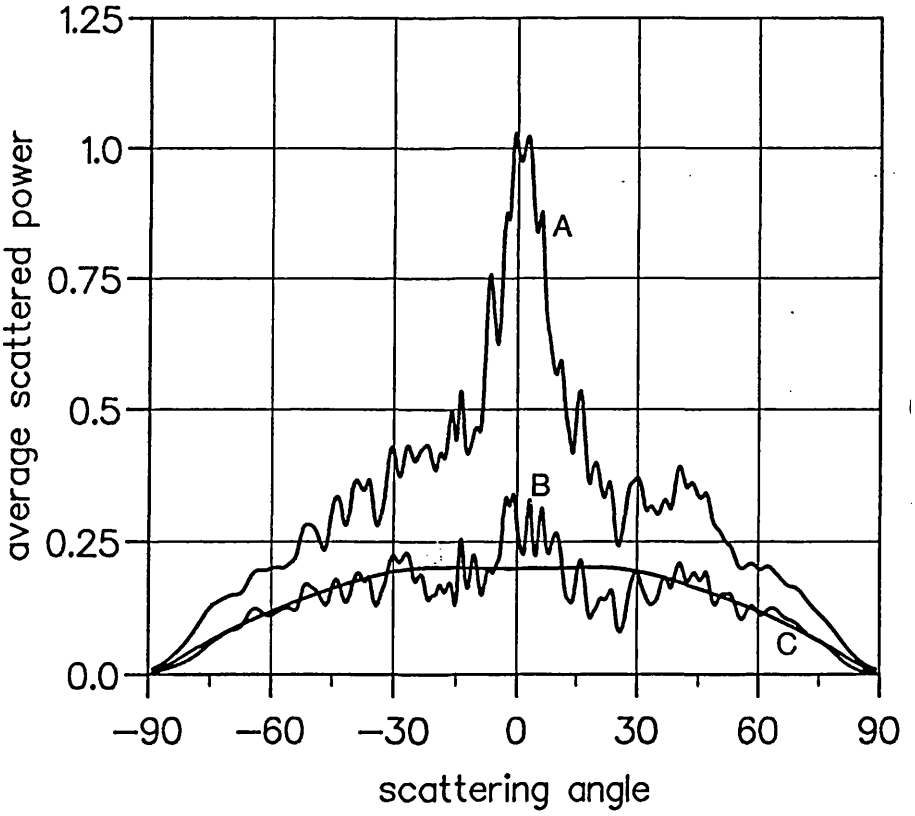

Fig. 6·21. The scattered powers for a Gaussian rough surface with a RMS slope of 45° and a correlation-length of 0·8λ illuminated by a vertically polarized wave incident at 0°. Curve (A) is the average scattered power; (B) is σ_{sK}; and (C) is obtained with the shadow-corrected Kirchhoff method.

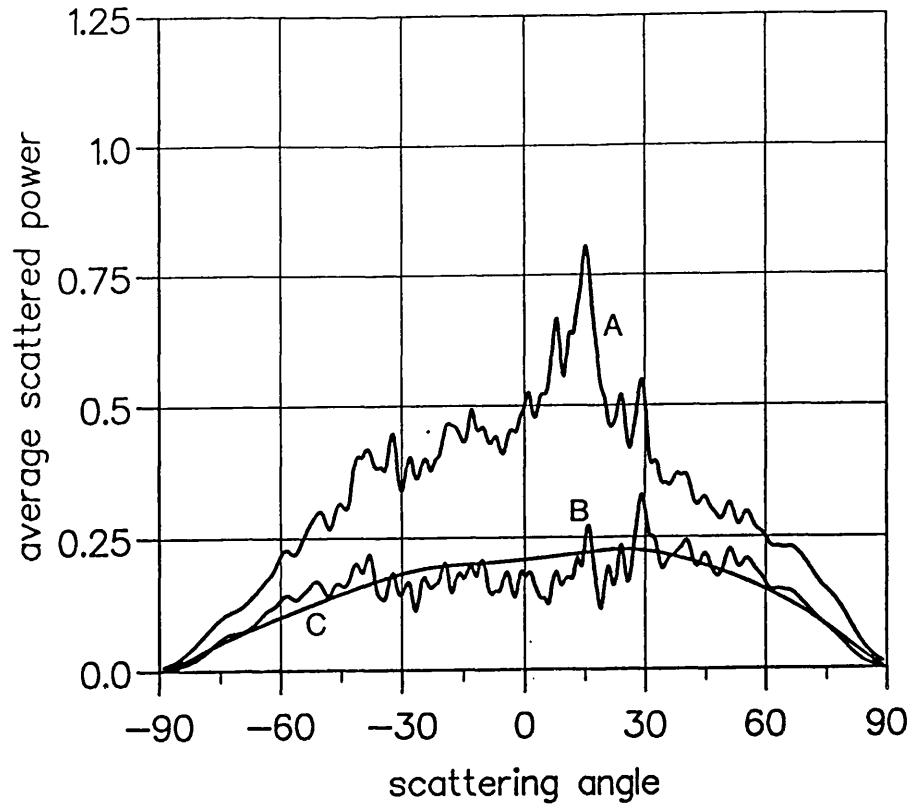

Fig. 6·22. The scattered powers for a Gaussian rough surface with a RMS slope of 45° and a correlation-length of 0·8λ illuminated by a vertically polarized wave incident at 15°. Curve (A) is the average scattered power; (B) is σ_{sK}; and (C) is obtained with the shadow-corrected Kirchhoff method.

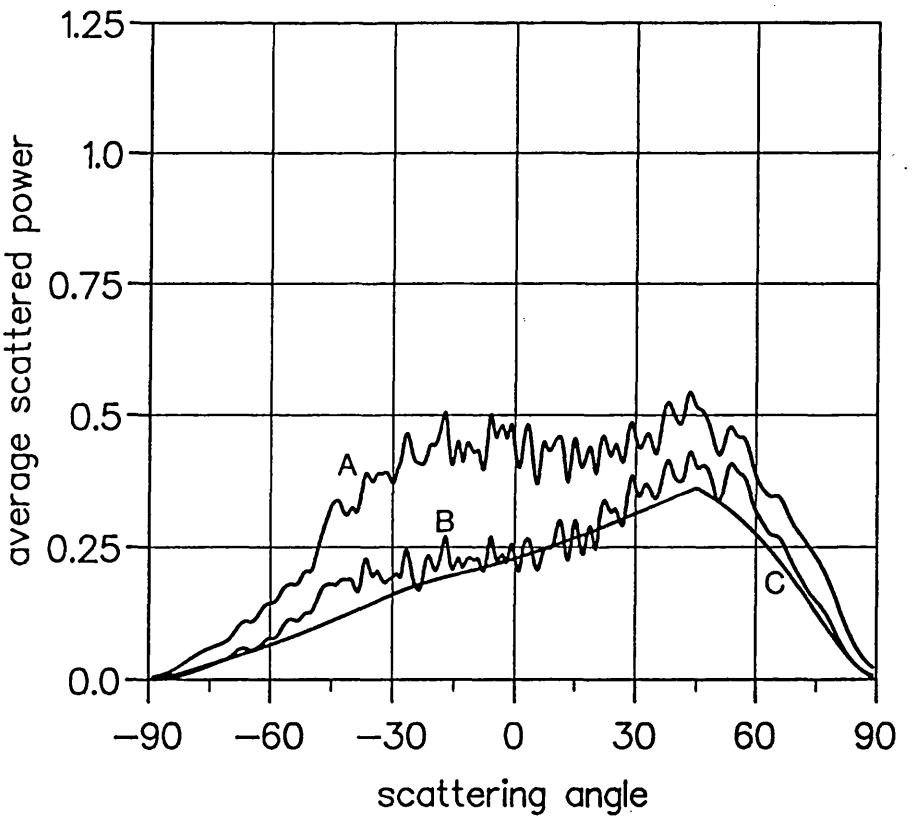

Fig. 6·23. The scattered powers for a Gaussian rough surface with a RMS slope of 45° and a correlation-length of 0·8λ illuminated by a vertically polarized wave incident at 45°. Curve (A) is the average scattered power; (B) is σ_{sK}; and (C) is obtained with the shadow-corrected Kirchhoff method.

In fig. 6·21 the 3dB angular width is ~15°, and in fig. 6·22 the 3dB angular width is ~30°. In the two corresponding figures for horizontal polarization, figs. 6·18 and 6·19, the 3dB angular width is ~30°, and ~45°, respectively. In fig. 6·23 the average scattered power is also largest in the backward scattering direction, but this is due in part to the tilt of σ_{sK} towards the backward scattering direction. However, the striking feature of fig. 6·23 is the large difference between curves (A) and (B) in the forward scattering direction. This feature is not present in the result for the same surface illuminated by horizontally polarized wave. We suspect that this difference between the vertical and horizontal polarization results is related to a difference in the degree of shadowing that takes place. We suspect that the large forward scattering contribution from σ_{mI}, which is present in fig. 6·23 but not in fig. 6·20, is because a vertically polarized wave is to greater extent diffracted around the surface, thereby illuminating more of the surface parallel to the incident wavefront. In this manner, more of the surface acts to source a secondary illumination of slopes capable of scattering in the forward direction. This feature is also present in figs. 6·13 and fig. 6·14.

We have found that enhanced backscattering occurs for a Gaussian-rough surface with a RMS surface slope of 45° and a correlation-length as small as 0·4λ. We present in figs. 6·24 and 6·25 the scattered powers for a wave incident at an angle of 15° on a Gaussian rough surface with a RMS slope of 45° and a correlation-length of 0·4λ. In fig. 6·24 the incident wave is horizontally polarized, and in fig. 6·25 the incident wave is vertically polarized. The two corresponding figures for a surface correlation-length of 0·8λ are figs. 6·19 and figs. 6·22. It can be easily verified by comparing fig. 6·24 with fig. 6·19, and fig. 6·25 with fig. 6·22, that the angular distribution of σ_{sK} is broader in the two figures for a surface correlation-length of 0·4λ.

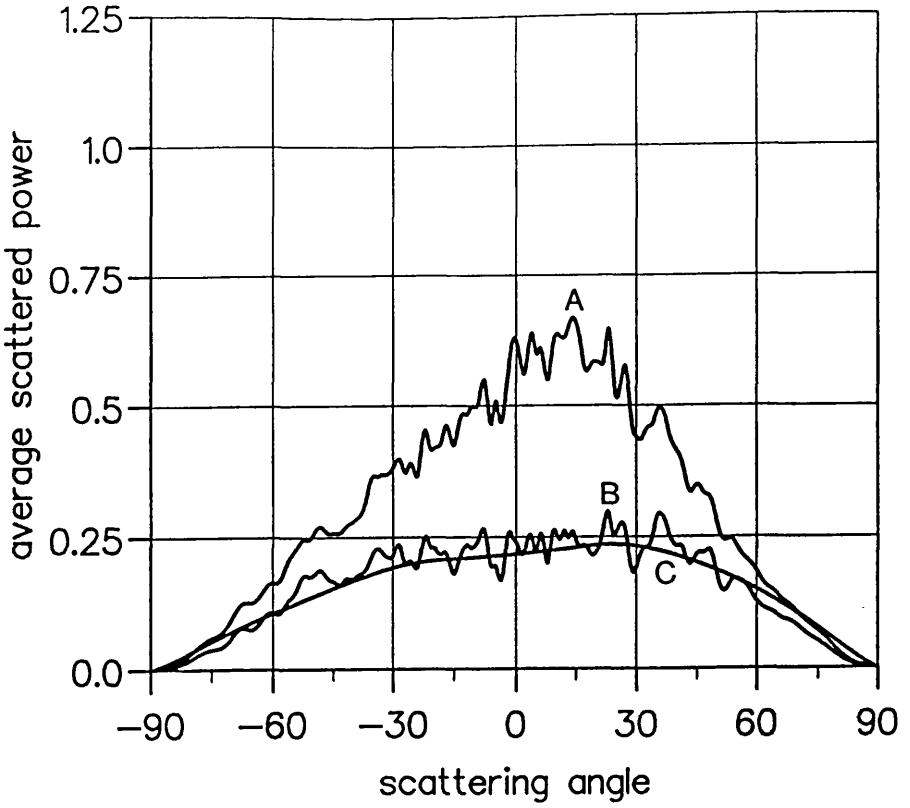

Fig. 6·24. The scattered powers for a Gaussian rough surface with a RMS slope of 45° and a correlation length of 0·4λ illuminated by a horizontally polarized wave incident at 15°. Curve (A) is the average scattered power; (B) is σ_{sK}; and (C) is obtained with the shadow-corrected Kirchhoff method.

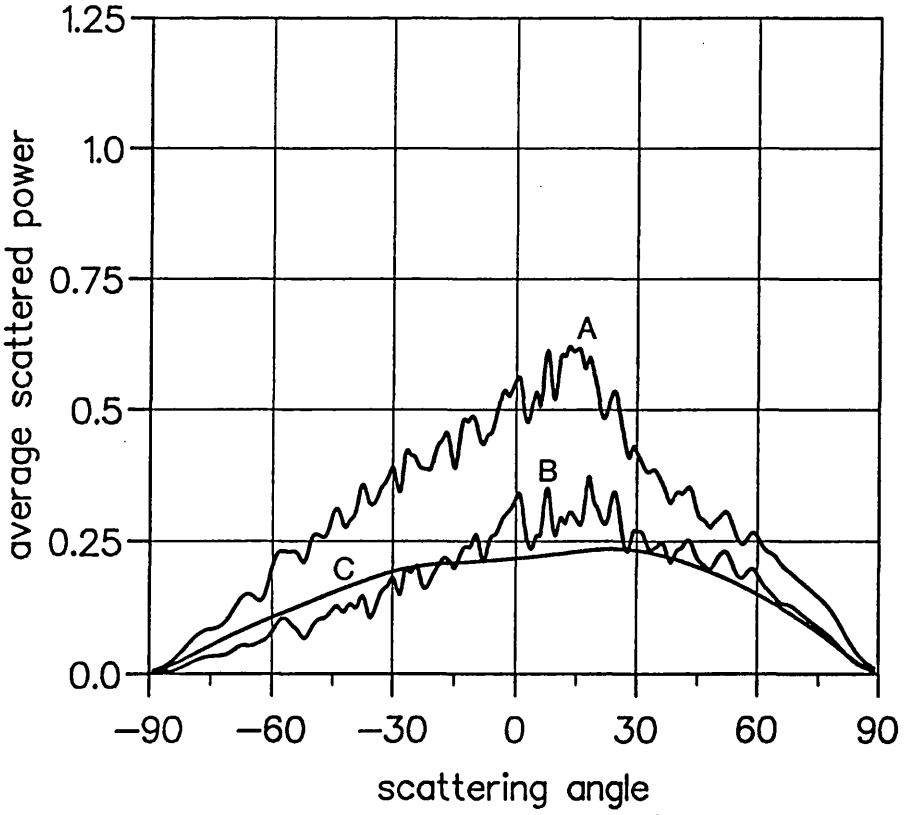

Fig. 6·25. The scattered powers for a Gaussian rough surface with a RMS slope of 45° and a correlation-length of 0·4λ illuminated by a vertically polarized wave incident at 15°. Curve (A) is the average scattered power; (B) is σ_{sK}; and (C) is obtained with the shadow-corrected Kirchhoff method.

The intuitive explanation of enhanced backscattering leads to an inverse relationship between the angular width of the enhanced backward scattered power and the mean free-path of the double-scatter at the surface; the path CD in fig. 1·3, for example. (O'Donnell and Mendez, 1987). The fact that the angular width of the enhanced backward scattered power is smaller for a correlation-length of 0·8λ than for a correlation-length of 0·4λ is consistent with the intuitive explanation of enhanced backscattering. Also, our observation that the angular distribution of the enhanced backward scattered power is narrower in the vertical polarization case than in the horizontal polarization case, would suggest that the mean free-path of the double-scatter is larger for vertical polarization than for horizontal polarization. It is our suspicion that a vertically polarized wave is diffracted around the surface to a greater extent than a horizontally polarized wave. Intuitively, the diffraction of the scattered wave around the surface would indeed act to increase the mean free-path of the double-scatter.

The contour-plots of the electromagnetic field in the vicinity of the surface boundary illustrate how the surface current density is enhanced by multiple-scattering. We present in fig. 6·26 the normalized modulus of the total magnetic field for a vertically polarized wave normally incident on a Gaussian rough surface with a RMS slope of 45° and a correlation-length of 0·8λ. We suspect that the pattern of interference centred at (-0·5, 0·5) is due to the interference between the incident wave, a wave scattered towards the upper-left hand corner of the plot, and a wave scattered towards the upper-right hand corner of the plot. It can be easily verified from the figure that the magnitude of the total magnetic field at (-1·0, 0·0) and (0·0, 0·0) is large compared to its value at (1·25, 0·5), where the surface is not directly confronted by another part of the surface. We suspect that the enhancement of the magnetic-field in the region of (-0·5, 0·5), is due to the illumination of the surface by scattered waves.

Fig. 6·26. The normalized modulus of the total magnetic field in the vicinity of a rough surface with a RMS slope of 45° and a correlation-length of 0·8λ, when a vertically polarized wave is normally incident on the surface.

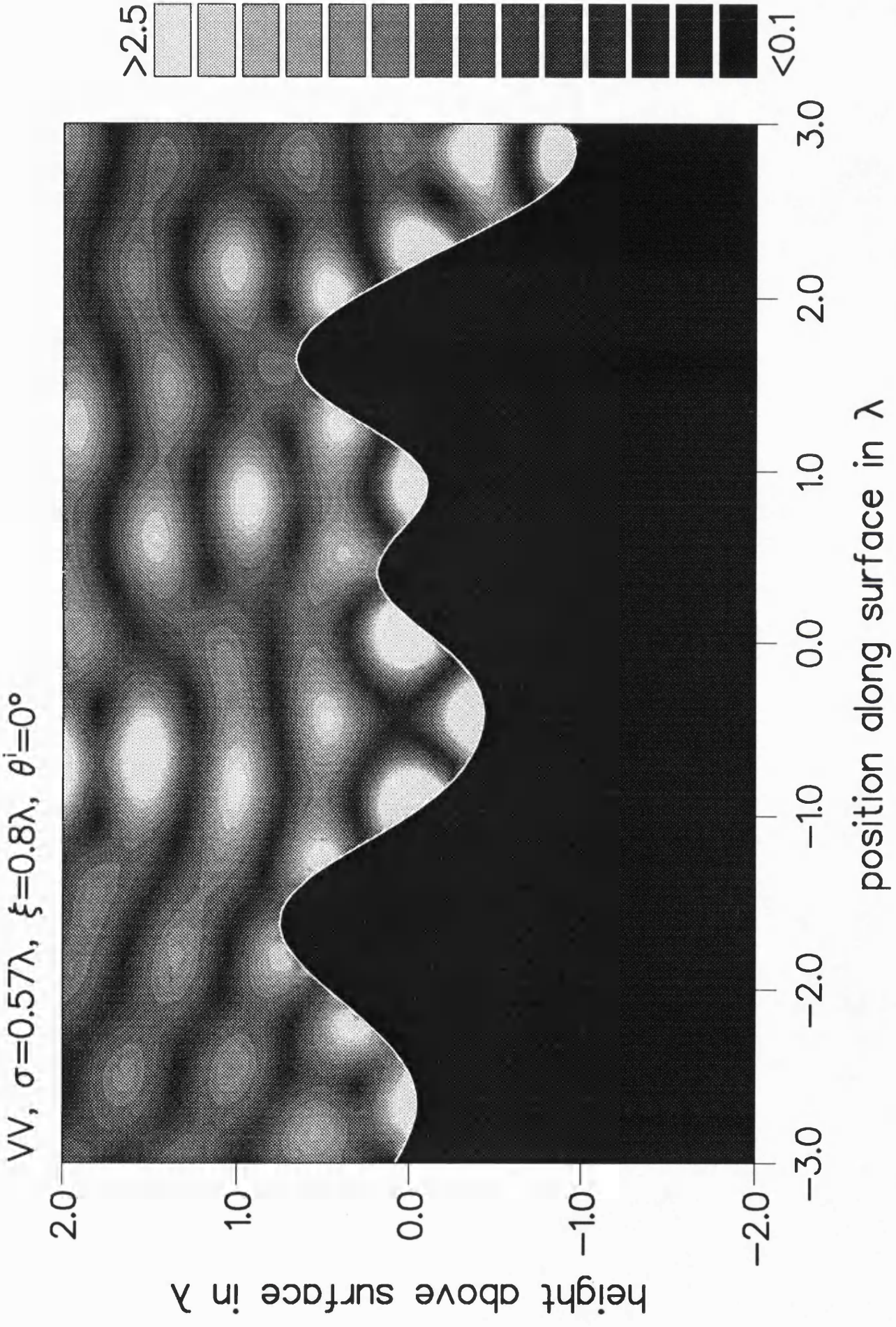

We present in fig. 6·27 the normalized modulus of the total electric field for a horizontally polarized wave for the same section of surface as illustrated in fig. 6·26. The enhancement of the field in the surfaces valleys evident in fig. 6·26, is also evident in fig. 6·27.

Fig. 6·27. The normalized modulus of the total electric field in the vicinity of a rough surface with a RMS slope of 45° and a correlation-length of 0·8λ, when a horizontally polarized wave is normally incident on the surface.

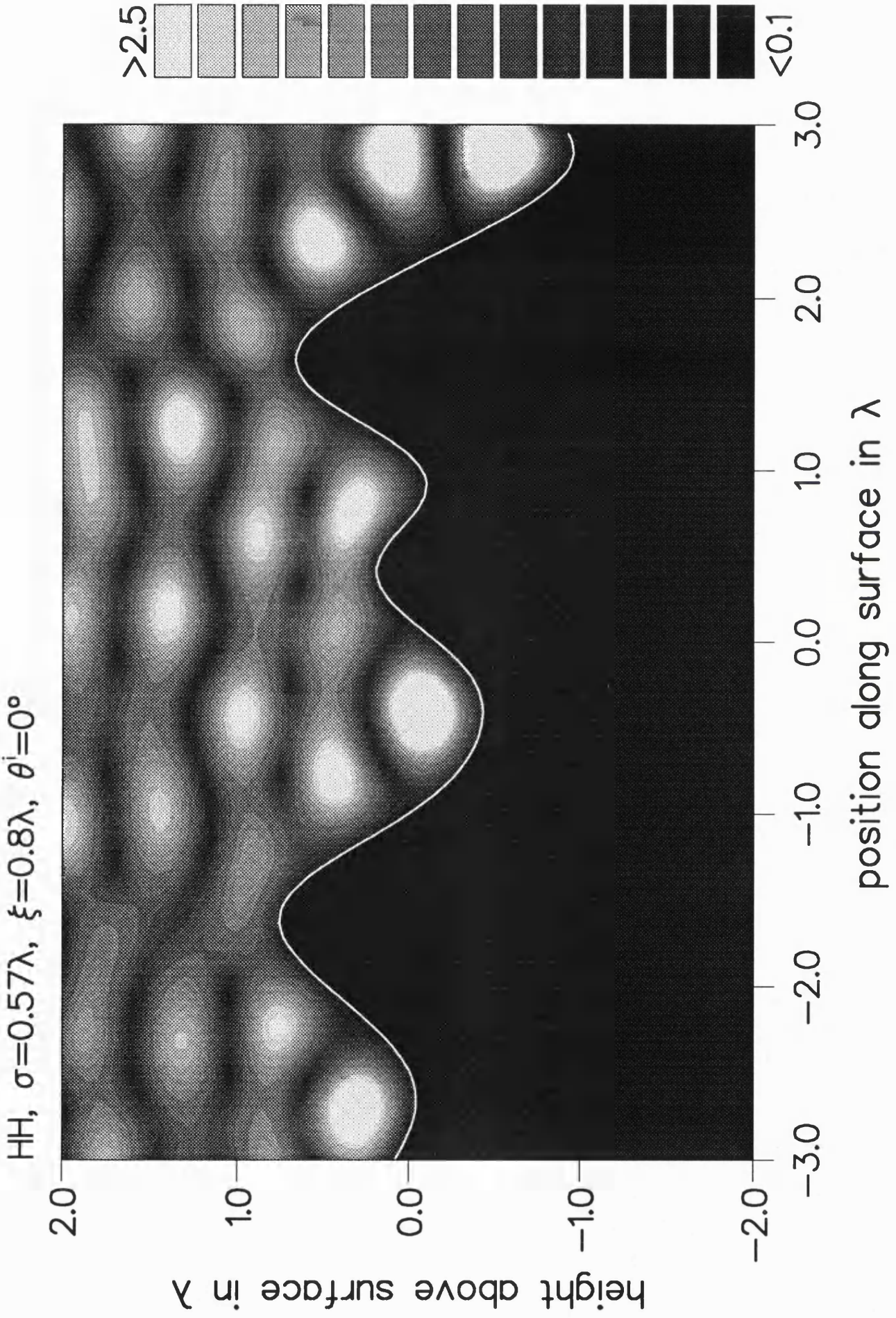

7
Discussion and Conclusions.

In this concluding chapter a review of the main results and conclusions is given, previous work in the field of numerical electromagnetics and rough surface scattering are examined in the light of the present work, and the chapter is completed with some general conclusions.

7·1 Review of the present work.

The aim of this study was to investigate wave scattering from perfectly-conducting, two-dimensional, Gaussian rough surfaces where the RMS height and correlation-length of the surface are of the same order, and of the same order as the electromagnetic wavelength. The investigation started with the two, uncoupled, magnetic-field-integral-equations (MFIEs), and the procedure used to approximate the continuous equation as a discrete equation. For the surfaces we have considered, the matrices generated in the discretization of the continuous equation are not ill-conditioned and can be solved exactly by LU decomposition. We chose to investigate the quality of the numerical solution by examining the degree to which the scattered field beneath the surface boundary cancelled the incident field. This established that the discrete approximation of the MFIE was a good one.

Once confident that the procedure used to discretize the MFIE gave good solutions to the field in the vicinity of the surface boundary, the study progressed onto iterative methods of solving the discrete equation. The convergence and rate of convergence of two iterative methods were examined. The Neumann expansion used by Brown (1982), Holliday (1987),

and Holliday *et al* (1988), appeared to be a natural candidate for an iterative solution of the discrete approximation of the MFIE. However, although the expansion provided a rapid numerical solution for small values of surface height and slope, when the surface structure was of the same order as the electromagnetic wavelength the expansion diverged rapidly. A step-by-step method of identifying divergence was presented (Wingham and Devayya, 1992). This allowed us to identify divergent expansions within a few iterations. To the extent that the numerical simulation is a good one, we also consider that our results provide strong evidence that the Neumann expansion cannot be used without qualification to provide a formal solution to the rough surface MFIE.

The conjugate-gradient methods are iterative methods of solving matrix-equations whose convergence are in theory sure. In spite of the theoretical assurance of convergence, it is not uncommon to find in the literature references to the iteration diverging. We have ourselves found that applied to the discrete approximation of the MFIE, convergence is not sure. The divergence was identified as due to the effect of rounding errors on the theoretical orthogonality properties, which guarantee convergence. To overcome this problem we modified the algorithm to include explicit orthogonalization of the conjugate-vectors at each iteration. We called this algorithm the Gram-Schmidt least-square-conjugate-gradient (GS-LSCG) method. In all the cases we have applied the GS-LSCG method to, we have never experienced a problem with its convergence (Devayya and Wingham, submitted in 1992)

The decision was made to run with the GS-LSCG method and to examine its rate of convergence for various surface parameters and incident waves. We found that the rate of convergence of the GS-LSCG method depends less upon a particular value of the RMS height and correlation-length, but more upon there ratio. This ratio is proportional to the RMS surface slope. We also found that the size of the surface, which

determines the matrix size N, does not affect the rate of convergence. This important, because the advantages of the conjugate-gradient method then grows with N.

The potential advantage of an iterative method is that the iteration can be stopped once a "good solution" has been found. To establish the point at which to truncate the iteration, we examined the difference between the scattered far-field power computed with the iterated solution for the surface current density and the scattered far-field power computed with the solution obtained by LU decomposition. For the surfaces we have considered, small errors in the surface current density are mapped to small errors in the scattered far-field, even when the scattered power is small. The computational issues were investigated in the light of this result, by comparing the CPU-times required by the GS-LSCG method and by LU decomposition. We found that when the RMS surface slope is small, or when N is very large, the GS-LSCG method determines a good solution with an order of magnitude reduction in the computation required by LU decomposition.

From the onset of the investigation our intention was to examine wave scattering for several incident fields. The major disadvantage of the GS-LSCG method is that the method is implemented for one incident field at a time. LU decomposition on the other hand, allows the solution for any incident field to be directly obtained. We have presented in this thesis a numerically robust conjugate-gradient method for scattering problems that require solutions for several incident fields. The method uses the information obtained in previous implementations to determine an initial-guess at the solution of the matrix-equation for each additional incident field. However, for the cases we have considered, the surface currents for different incident fields prove too distinct for the method to provide any significant computational advantage over LU decomposition.

Nevertheless, our work on the numerical solution of the MFIE by the conjugate-gradient method, is relevant to scattering problems that require solutions for a few incident fields, or when the size of the matrix prohibits the use of direct solution methods.

To solve the MFIE numerically the integral must be truncated at some point. The scattering problem described by the truncated integral-equation is that of a wave scattered from a patch of surface. From a computational standpoint a small patch size is preferable. However, since it is hoped that the normalized incoherent scattered power computed for an ensemble of rough surface patches will apply to the infinite rough surface, the patch size must be large enough to accommodate the average scattering properties of the infinite surface. We have placed the point at which to truncate the MFIE into a mathematical context. The incoherent scattered power for an illuminated patch of surface was presented as the integral of the weighted autocorrelation-function of the random component of the field scattered by each point of the surface. By representing the incoherent scattered power in this manner, the factor determining the size of a patch was identified as the separation required for this random process to decorrelate. We presented examples of backscattering-autocorrelation-functions for a perfectly-conducting, Gaussian rough surface. In the horizontal polarization case, the autocorrelation-functions obtain a constant value within a few surface correlation-lengths. This is also true of most of the cases for vertical polarization. The exceptions occur when the RMS surface height is small. For these geometries the autocorrelation-functions have an oscillatory component over the entire length of the footprint. We suspect this phenomenon is due to a surface wave. The presence of a surface wave complicates the issue of where to truncate the MFIE. However, for the surfaces we have considered we suspect that the diffuse scattering of the surface wave is relatively small. The results presented in this study provide evidence that a relatively small patch size can accurately represent the

second-order scattering properties of the infinite surface. This is possible because of the small correlation-length of the random component of the scattering-function. In fact, we consider that the limit on the patch size relates more to the method used to reduce the scattering from the patch edges. The tapered incident wave used in our numerical simulations, for example, is less consistent with the wave equation as the tapering is increased.

Our attention then centred on the scattered far-field and the expected value of the scattered power. The field scattered from a rough surface is the scattered field obtained with the Kirchhoff approximation plus the field due to the integral in the MFIE, which we call the integral-field. In the high frequency limit wave scattering is not complicated by diffraction, and the role of the Kirchhoff and integral-fields are understood. In this limit, the Kirchhoff-field is due to the single-reflection of incoming rays from the surface. The integral-field is required to account for shadowing of the surface, and multiple-reflections at the surface boundary. We presented a procedure for obtaining from the solution of the MFIE two physically distinct corrections to the Kirchhoff approximation. On the assumption that the coherence between the field due to single reflections and the field due to multiple-reflections is negligible, a correction for shadowing is determined from the linear mean-square estimate of the integral-field in terms of the Kirchhoff-field. The error in the estimate, which provides the second correction to the Kirchhoff method, satisfies the coherence properties of the scattered field due to multiple-reflections.

Armed with these procedures we set about applying them to our numerical simulations of wave scattering from Gaussian rough surfaces where the RMS height and correlation-length are of the same order, and of the order as the electromagnetic wavelength. We found that for a RMS slope of 25° there is small difference between the integral-field and the linear, mean-square estimate of the integral-field in terms of the Kirchhoff-

field. Physically, we suspect that because this difference is small, the scattered field due to the illumination of the surface by scattered, wavefronts is small too. We suspect that for these surfaces the correction to the Kirchhoff approximation provided by the integral in the MFIE is for partial-shadowing and the diffraction by the surface of the incident and scattered waves. The discussions for surfaces with moderate slopes centred on the relationship between the polarization of the incident wave, and the degree of shadowing at the surface. We consider that both the near and far-field results provide strong evidence that the degree of shadowing is smaller for vertical polarization than for horizontal polarization. Contour-plots of the electromagnetic field in the vicinity of the surface boundary were used to illustrate this point in the near-field. In the far-field, we have found that the average scattered power in the horizontal polarization case is better described by the Kirchhoff method when the correction for shadowing derived in (Wagner, 1967) is used. The results for vertical polarization on the other hand, show how the Kirchhoff method gives a better estimate of the backward scattered power when the shadowing correction is not used.

The results for Gaussian rough surfaces with very large slopes illustrate the enhanced backscattering reported in the literature (O'Donnell and Mendez, 1987). In contrast to the results for a RMS slope of 25°, for a RMS slope of 45° the difference between the integral-field and the estimate of the integral-field in terms of the Kirchhoff-field is not small. Physically, we suspect this difference is due to the illumination of the surface by waves scattered from other parts of the surface.

7·2 Review of previous work.

Our work on iterative methods of solving the magnetic-field-integral-

equation has a much wider scope of application. There is considerable interest in iterative methods within the electromagnetic scattering community (Sarkar *et al*, 1981), (Umashankar, 1988), (Marks, 1990). The procedures used to identify the divergence of the Neumann expansion, for example, can be applied to Neumann expansion of any Fredholm integral-equation (Baker, 1977) of the second-kind. Also, the work presented on the conjugate-gradient method, and in particular, avoiding rounding errors by using Gram-Schmidt orthogonalization should be of interest to those researchers who have found the initial convergence of the conjugate-gradient method applied to there problem to be rapid, but then diverges due to rounding errors.

In the numerical studies of rough surface scattering the point at which the integral-equations are truncated varies markedly from study to study. Given the problem of choosing a patch size large enough to preserve the second-order scattering properties of the infinite surface, but at the same time small enough to limit the computational requirement, we have placed the point at which to truncate the integral into a mathematical context. Our simulations suggest that a relatively small patch size can describe the second-order scattering properties of the infinite surface. In fact, the limit on the patch size appears to relate more to method used to guard edge effects. The method we have used to guard against these effects is to taper the incident wave to negligible levels at the patch edges. This method has also been used by Thorsos (1988), Thorsos and Jackson (1989), Broschat *et al* (1989) and most recently by Ishimaru and Chen (1991). It would have been useful, if we had had the time, to compare this approach with the method for periodic gratings due to Jordan and Lang (1979). The integral-equation for a periodic grating is described along a closed contour over one period of the grating. The periodic nature of the surface is accommodated into the Greens' function for the scattering problem. Applied to the random, rough surface scattering problem, the random

roughness is defined over one period of the grating. Although the periodicity of the surface roughness modulates the angular distribution of scattered power by a pattern of interference fringes, the method of Jordan and Lang does not suffer from "edge effects", because the integral-equation is bounded.

This thesis has compared wave scattering for both polarizations. The bulk of the literature on wave scattering is on the Dirichlet scattering problem, which in the context of this study is the horizontal polarization case. Our results for horizontal polarization are consistent with the results presented by Thorsos (1988). We have also found that the Kirchhoff approximation when used with the correction for shadowing derived in (Wagner, 1967), gives a better description of the scattered power as the surface correlation-length approaches the electromagnetic wavelength. Our work has also dealt with the vertical polarization case. Here, we have found that the backward scattered power is better described with the Kirchhoff method when the correction for shadowing is not used.

The results for a RMS slope of 25° show that there is small difference between the integral-field and the linear mean-square estimate of the integral-field in terms of the Kirchhoff-field. Analytic theories of wave scattering, with the exception of the second-order Kirchhoff-iteration (Ishimaru and Chen (1990 a, b), are appropriate when the RMS surface slope is less than 25°. We suspect that these theories operate in a region of the parameter space where the scattered field due to the illumination of the surface by scattered, wavefronts is small. The nature of the results for rough surfaces with large slopes bare a striking resemblance to those presented by Ishimaru and Chen (1990 a, b), (1991) and Bruce and Dainty (1991). These authors have used the first two terms of a Kirchhoff iteration to describe wave scattering from very rough surfaces in the region "SKI" of fig. 1·3. The first term of the iteration gives the expected scattered power

obtained with the shadow-corrected Kirchhoff method. The second term is required to account for enhanced backscattering. We have presented a procedure for obtaining from the solution of the MFIE two corrections to the expected scattered power obtained with the Kirchhoff approximation. This procedure has allowed us to gain valuable insight into the scattering mechanisms that operate at the surface boundary. We have found that in many cases the correction for shadowing is close to the correction for shadowing derived in (Wagner, 1967). The second correction, which physically we suspect accounts for the illumination of the surface by waves scattered from other parts of the surface, for very rough surfaces is required to describe the angular distribution of the enhanced backward scattered power.

7·3 Conclusions.

The purpose of this study was primarily to investigate wave scattering from perfectly-conducting, two dimensional Gaussian rough surfaces where the RMS height and correlation-length are of the same order, and of the order of the electromagnetic wavelength. Existing scattering theories do not apply to these geometries and at present there is little alternative but to solve the scattering equations numerically.

A suitable equation to solve is the magnetic-field-integral-equation (MFIE). The principal problem that emerges in the numerical solution of the MFIE is that very large matrices are generated, even for moderately sized two-dimensional surfaces. Iterative methods were used to solve the discrete representation of the MFIE, with the hope that good solutions could be obtained within a few iterations, thereby reducing the computational requirement. Two iterative methods were investigated; the Neumann expansion, a method that had been used to formally represent the solution of the rough surface scattering problem; and the conjugate-

gradient method, an iterative of solving matrix equations whose convergence is in theory sure. The convergence of both methods were found to be in question. The Neumann expansion suffers from convergence difficulties in theory, as well as in practice. The divergence of the conjugate-gradient method, however, was identified as due to rounding errors. A conjugate-gradient far less susceptible to rounding errors was presented, and this method has been applied successfully to a number of scattering geometries.

Procedures were presented for determining from the solution of the MFIE, two corrections to the Kirchhoff method. The results presented in this thesis provide evidence that one of the corrections is for partial-shadowing, and the diffraction by the surface of the incident and scattered waves, and the other correction is for the illumination of the surface by scattered, wavefronts. The increase from a RMS slope of 25° to a RMS slope of 45° marks the transition into the region of the parameter space where enhanced backscattering occurs. Moreover, this transition is marked by an increase in the degree of incoherence between the scattered field obtained with the Kirchhoff approximation and the scattered field obtained with the surface current due to the integral in the MFIE. Physically, we suspect that the increase in the degree of incoherence between these two fields, is due to a marked increase in the illumination of the surface by waves scattered from the other parts of the surface. It remains to be seen whether the algorithms and procedures presented in this thesis will be adopted by the rough surface scattering community

Appendix A.
Derivation of the magnetic-field-integral-equation.

The integral formulation of Maxwell's equations are dealt with by, among others, Poggio and Miller (1973). In this appendix, we will derive the magnetic-field-integral-equation (MFIE) for the case of a horizontally polarized wave incident upon a two-dimensional (corrugated), surface. The derivation of this MFIE is not in the literature. For a two dimensional surface, the general form of the MFIE is (Poggio and Miller, 1973)

$$J(x) = 2\hat{n}(x) \times H^i(x) + \frac{1}{2\pi} \hat{n}(x) \times \int_{-\infty}^{\infty} J(x') \times \nabla\Phi(r, r') \left| \hat{z} + \hat{x} \frac{dz'}{dx} \right| dx' \quad (A\cdot1)$$

Here, J is the surface current density, H^i is the incident magnetic field at the surface, Φ is the Greens' function for the scattering problem, **r** and **r'** are position vectors of the surface at x and x', $(\mathbf{r} - \mathbf{r}') = (x - x')\,\hat{x} + (z - z')\,\hat{z}$, and $\hat{n}$ is the unit vector normal to the surface boundary at x',

$$\hat{n}(x) = \frac{\hat{z} - \hat{x}\, dz/dx}{\sqrt{1 + (dz/dx)^2}} \quad (A\cdot2)$$

Here, the bold type face is used to indicate a vector, and the hat symbol denotes a unit vector. A suitable Greens function for the two-dimensional, scattering problem is (Poggio and Miller, 1973),

$$\Phi(\mathbf{r}, \mathbf{r}') = -i\pi H_0^{(2)}[k\,|\mathbf{r} - \mathbf{r}'|], \quad (A\cdot3)$$

and taking the partial derivatives of the zero-order Hankel function (Abramowitz and Stegun, 1970),

$$\nabla\Phi(r, r') = -i\pi k \ (r - r') \frac{H_1^{(2)}[k\,|r - r'|]}{|r - r'|} \qquad (A\cdot4)$$

In the horizontal polarization case, the surface current induced by the incident wave

$$H^i(x) = H^i(x)\,(\hat{z}\cos\theta^i - \hat{x}\sin\theta^i), \qquad (A\cdot5)$$

is the vector

$$J(x) = -J(x)\,\hat{y}. \qquad (A\cdot6)$$

With (A·2) and (A·5), the first term on the right-hand-side (RHS) of (A·1)

$$\hat{n}(x) \times H^i(x) = H^i(x) \frac{(\cos\theta^i\, dz/dx - \sin\theta^i)}{\sqrt{1 + (dz/dx)^2}}\hat{y}. \qquad (A\cdot7)$$

While the vector cross-product in the second term on the RHS of (A·1) is

$$\hat{n}(x) \times (-\hat{y} \times (r - r')) = \frac{(x - x')\, dz/dx - (z - z')}{\sqrt{1 + (dz/dx)^2}}\hat{y}. \qquad (A\cdot8)$$

Finally, substituting (A·6), (A·7) and (A·8) into the RHS of (A·1), we obtain the MFIE for the horizontal polarization case as

$$J(x)\,\hat{y} = 2H^i(x) \frac{(\sin\theta^i - \cos\theta^i\, dz/dx)}{\sqrt{1 + (dz/dx)^2}}\hat{y} -$$

$$-\frac{ik}{2}\hat{y}\int_{-\infty}^{\infty} J(x') \frac{H_1^{(2)}[k\,|r - r'|]}{|r - r'|} ((z - z') - (x - x')\, dz/dx) \sqrt{\frac{1 + (dz'/dx)^2}{1 + (dz/dx)^2}}\, dx'. \qquad (A\cdot9)$$

The MFIE for a vertically polarized wave is derived in a similar fashion. For the incident wave

$$H^i(x) = -H^i(x)\hat{y}. \tag{A·10}$$

the surface current density is the vector

$$J(x) = J(x)\hat{p}, \tag{A·11}$$

where,

$$\hat{p} = \frac{\hat{x} + \hat{z}\, dz/dx}{\sqrt{1 + (dz/dx)^2}}. \tag{A·12}$$

Using (A·2) and (A·10), the first term on the RHS of (A·1) is

$$\hat{n}(x) \times H^i(x) = H^i(x)\, \hat{p}. \tag{A·13}$$

While the vector cross-product in the second term on the RHS of (A·1) is

$$\hat{n}(x) \times (\hat{p'} \times (r - r')) = \frac{\hat{p}}{\sqrt{1 + (dz'/dx)^2}} ((z - z') - (x - x')\, dz'/dx'). \tag{A·14}$$

Then, substituting (A·11), (A·13) and (A·14) into the RHS of (A·1), we obtain the MFIE for a vertically polarized wave as

$$J(x)\,\hat{p} = 2H^i(x)\,\hat{p} - \frac{ik}{2}\hat{p} \int_{-\infty}^{\infty} J(x') \frac{H_1^{(2)}[k|r - r'|]}{|r - r'|} ((z - z') - (x - x')\, dz'/dx)\, dx' \tag{A·15}$$

Appendix B.

The variance in the estimate of the autocorrelation function of a Gaussian, rough surface.

To test whether the autocorrelation function of a sample of the generated surface is consistent with that of a sample of a Gaussian rough surface, we need to have some idea of the error in the estimate of the theoretical autocorrelation function made from a sample of a Gaussian rough surface. The variance in the estimate of the autocorrelation function of a Gaussian, random process made from a sample of length L is (Priestley, 1987)

$$\text{var}\,(\hat{r}(\tau)) = \frac{1}{L}\int_{-\infty}^{\infty} r^2(m) + r(m+\tau)\,r(m-t) + 2r^2(m)\,r^2(\tau) + 4r(\tau)\,r(m)\,r(m-\tau)\,dm \quad \text{(B·1)}$$

Here, $\hat{r}(\tau)$ is the estimate of the normalized autocorrelation made from a sample of length L and $r(\tau)$ is the theoretical nomalized autocorrelation function of the Gaussian, random process.

The autocorrelation function of a Gaussian rough surface is the Gaussian

$$R(\tau) = \sigma^2 \exp\left[-\frac{\tau^2}{\xi^2}\right] \quad \text{(B·2)}$$

and the normalized autocorrelation function

$$r(\tau) = R(\tau) \,/\, R(0). \quad \text{(B·3)}$$

With (B·3) substituted into the integral (B·1), the two following identities are then used to evaluate (B·1), (Gradshteyn and Ryzhik, 1980),

$$\int_{-\infty}^{\infty} e^{-q^2m^2}\, dm = \frac{\sqrt{\pi}}{q} \tag{B·4}$$

$$\int_{-\infty}^{\infty} e^{-p^2m^2 \pm qm}\, dm = \frac{\sqrt{\pi}}{p} e^{\,q^2/4p^2} \quad p > 0 \tag{B·5}$$

The integral is easily evaluated with knowledge of the identities (B·4) and (B·5);

$$\text{var}\,(\hat{r}(\tau)) = \frac{\xi}{L}\sqrt{\frac{\pi}{2}}\left(1 + 3\exp\left[-\frac{2\tau^2}{\xi^2}\right] - 4\exp\left[-\frac{3\tau^2}{2\xi^2}\right]\right) \tag{B·6}$$

For $\tau = 0$, $\hat{r}(0)$ always equals 1. It can be easily verified from (B·6) that the variance in the estimate at $\tau = 0$ is correctly zero. The asymptotic value of (B·6) is

$$\text{var}\,(\hat{r}(\infty)) = \frac{\xi}{L}\sqrt{\frac{\pi}{2}} \tag{B·7}$$

For most Gaussian, random processes the error in the estimate is a Gaussian, random process too (Priestley, 1981). With the errors normally distributed, the 5% significance level for the estimate is twice the square-root of the variance; *i.e.* in 95% of the autocorrelation functions made from a sample of a Gaussian rough surface with length L, the error in the estimate will lie between plus and minus twice the square-root of the variance (B·6). This significance level is illustrated in fig. 2·2(B) for a 3000 correlation-length sample of a Gaussian rough surface with a correlation-length of 0·4λ.

Appendix C·
Derivation of the scattered field integrals.

In this appendix we will derive the scattered field integrals. We begin with the following integral equations for the scattered magnetic field, and the scattered electric field;

$$H^S(R) = \frac{1}{4\pi}\int_{-\infty}^{\infty} J(x') \times \nabla\Phi(R, r') \left|\hat{z} + \hat{x}\frac{dz'}{dx}\right| dx' \qquad (C\cdot1)$$

$$E^S(R) = -\frac{ik Z_0}{4\pi}\int_{-\infty}^{\infty} J(x')\, \Phi(R, r') \left|\hat{z} + \hat{x}\frac{dz'}{dx}\right| dx'. \qquad (C\cdot2)$$

Here, J is the surface current density, H^S is the scattered magnetic field, E^S is the scattered electric field, Φ is the Greens' function for the scattering problem, r' is a position vector of the surface a x', and R is a position vector for a point off the surface boundary at (X , Z). A suitable Greens function for the two-dimensional scattering problem is (Poggio and Miller, 1973),

$$\Phi(R , r') = -i\pi H_0^{(2)}[k\,|R - r'|], \qquad (C\cdot3)$$

and

$$\nabla\Phi(R , r') = -i\pi k\ (R - r')\frac{H_1^{(2)}[k\,|R - r'|]}{|R - r'|}. \qquad (C\cdot4)$$

In the horizontal polarization case, the surface current induced by the incident wave is

$$J(x) = -J(x)\,\hat{y}. \qquad (C\cdot5)$$

Substituting (C·3) and (C·5) into the RHS of (C·2), the scattered electric field is then obtained from the integral

$$E^S(X, Z)\,\hat{y} = \frac{kZ_0}{4}\hat{y}\int_{-\infty}^{\infty} J(x')\; H_0^{(2)}[k\,|R - r'|]\sqrt{1 + (dz'/dx)^2}\; dx'. \quad (C\cdot6)$$

For a vertically polarized wave the surface current density is

$$J(x) = J(x)\hat{p}, \quad (C\cdot7)$$

where,

$$\hat{p} = \frac{\hat{x} + \hat{z}\,dz/dx}{\sqrt{1 + (dz/dx)^2}}. \quad (C\cdot8)$$

In this case, the scattered magnetic field is perpendicular to the x-z plane. With (C·4), (C·7), and (C·8) substituted into the RHS of (C·1), the scattered magnetic field is obatined from the intgral

$$H^S(X, Z)\,\hat{y} = \frac{ik}{4}\hat{y}\int_{-\infty}^{\infty} J(x')\;\frac{H_1^{(2)}[k\,|R - r'|]}{|R - r'|}\;((Z - z') - (X - x')\,dz'/dx)\;dx'. \quad (C\cdot9)$$

When the observation point is distant form the surface boundary,

$$|R - r'| = \sqrt{(R\cos\theta^S - z)^2\,(R\sin\theta^S - x)^2}$$

$$\approx R\left(1 - \frac{1}{R}(z\cos\theta^S + x\sin\theta^S)\right), \quad (C\cdot10)$$

the Green's function (C·3) can be replaced with its asymptotic value, (Abramowitz and Stegun, 1970)

$$\Phi(R , r') = \sqrt{\frac{1}{R}} \exp\left(-\frac{i\pi}{4}\right) \exp\ (-ikR) \exp\ (ik\ (z \cos\theta^S + x \sin\theta^S)), \quad (C{\cdot}11)$$

and

$$\nabla\Phi(R , r') = \sqrt{\frac{2\pi k}{R}} \exp\left(\frac{i\pi}{4}\right) \exp\ (-ikR) \exp\ (ik\ (z \cos\theta^S + x \sin\theta^S)). \quad (C{\cdot}12)$$

Using the Greens function (C·11) in (C·2),

$$E^S(\theta^S) = Z_0 \sqrt{\frac{k}{8\pi R}} \exp\left(-\frac{i\pi}{4}\right) \exp\ (-ikR)$$

$$\int_{-\infty}^{\infty} J(x') \exp\ (ik\ (z' \cos\theta^S + x' \sin\theta^S)) \sqrt{1 + (dz'/dx)^2}\ dx', \quad (C{\cdot}13)$$

and with (C·12) used in (C·1),

$$H^S(\theta^S) = Z_0 \sqrt{\frac{k}{8\pi R}} \exp\left(-\frac{i\pi}{4}\right) \exp\ (-ikR)$$

$$\int_{-\infty}^{\infty} J(x') \exp\ (ik\ (z' \cos\theta^S - x' \sin\theta^S))\ (\cos\theta^S - dz'/dx \sin\theta^S) \sqrt{1 + (dz'/dx)^2}\ dx'$$

(C·14)

Appendix D
The Wagner shadow-function.

The Kirchhoff method neglects the shadowing by the surface of the incoming and outgoing waves. The correction for shadowing derived in (Wagner, 1967) assumes that the incoming and outgoing waves can be represented as rays. Physically the correction describes the area of surface geometrically visible to both source and observation points. The shadowing correction is applied to the Kirchhoff result for the expected value of the scattered power, by multiplying the incoherent scattered power (D·1) by the shadow-function $S(\theta^i,\theta^i)$. Where

$$S(\theta^i,\theta^s) = S(\theta^s) \quad 90° \le \theta^s \le \theta^i, \tag{D·1}$$

$$S(\theta^i,\theta^s) = S(\theta^i) \quad \theta^i \le \theta^s \le 0°, \tag{D·2}$$

$$S(\theta^i,\theta^s) = S(\theta^i,\theta^s) \quad -90° \le \theta^s \le 0°, \tag{D·3}$$

where

$$S(\theta^s) = \frac{[\,1 + \mathrm{erf}\,(v_s)\,]\,(\,1 - e^{-2B_s})}{4B_s}, \tag{D·4}$$

$$B_s = \frac{e^{-9v_s^2/8}}{(48\pi v_s^2)^{\frac{1}{2}}} + \frac{e^{-v_s^2}}{(16\pi v_s^2)^{\frac{1}{2}}} - \frac{[\,1 + \mathrm{erf}(v_s)\,]}{4}, \tag{D·5}$$

$$v_s = \frac{|\cot\theta^s|}{2\sigma/\xi}, \tag{D·6}$$

$$S(\theta^i,\theta^s) = \frac{[\,\mathrm{erf}\,(v_i) + \mathrm{erf}\,(v_s)]\,(\,1 - e^{-2(B_s + B_i)})}{4\,(B_s + B_i)}, \tag{D·7}$$

The quantities $S(\theta^i)$, B_i and v_i are obtained by substituting the angle of incidence θ^i and the scattering angle θ^s in (D·4) - (D·7). The geometric factor in the shadow-function occurs in the denominator of (D·7). The ratio of the RMS surface height σ and the surface correlation-length ξ is proportional to the RMS surface slope.

References.

Abramowitz, A. and Stegun, I. A., 1970, "Handbook of Mathematical functions", Dover Publications, New York.

Axline, R. M. and Fung, A. K., 1978, "Numerical computation of the scattering from a perfectly conducting random surface", IEEE. Trans. Antennas Propagat., AP-26, pp. 482 - 488; corrections to "Numerical computation of the scattering from a perfectly conducting random surface",IEEE. Trans. Antennas Propagat., AP-28, p. 949.

Bahar, E., 1981, "Scattering cross sections of randomly rough surfaces: Full wave analysis.", Radio. Sci., vol. 16, pp. 331- 334.

Baker, C. T. H., 1977, "The numerical treatment of integral equations", Clarendon-Press, Oxford.

Beckmann, P. and Spizzichino, A., 1963, "The scattering of electromagnetic waves from rough surfaces", Pergammon-Press, New York.

Beckmann, P., 1965, "Shadowing of random rough surfaces.", IEEE. Trans. Antennas and Propagat., AP-13, pp. 384-388.

Bendat, J. S., and Piersol, A. G., 1986, "Random data", 2nd edition. John Wiley & Sons, New York.

Brockelmann R. A., and Hagfors. T., 1966, "Note on the effect of shadowing on the Backscattering of waves from random rough surfaces.", IEEE. Trans. Antennas Propagat., AP-14, pp. 621 - 629.

Broschat, S. L., Thorsos, E. I. and Ishimaru. A., 1989, "The phase perturbation method versus an exact numerical method for random rough surface scattering", J. Electro. Waves Applic., 3, pp. 237 - 256.

Brown, G. S., 1982, "A stochastic Fourier transform approach to scattering from perfectly conducting random rough surfaces", IEEE. Trans. Antennas Propagat., AP-30, pp. 1135 - 1144.

Bruce, N. C., and Dainty, J. C., 1991, "Multiple-scattering from random

rough surfaces using the Kirchhoff approximation.", J. Mod. Opt., 38, pp. 579 - 590.

Chan, H. L. and Fung, A. K., 1978, "A numerical study of the Kirchhoff approximation in horizontally polarized backscattering from a random rough surface", Radio Sci., 13, pp. 811 - 818.

Celli, V., Maradudin, A. A., Marvin A. M., and McGurn, A. R., 1985, "Some aspects of light scattering from a randomly rough metal surface.", J. Opt. Soc. Am., A 2, pp. 2225 - 2239.

Devayya, R. H., and Wingham, D. J., 1992, "The numerical calculation of rough surface scattering by the conjugate-gradient method.", accepted for publication in IEEE. Trans. Geosci. Remote Sensing.

Devayya, R. H., and Wingham, D. J., "Avoiding rounding errors in the conjugate-gradient method by Gram-Schmidt orthogonalization.", submitted in 1992 to IEEE. Trans. Antennas Propagat.

Fung, A. K., and Chen, M. F., 1985, "Numerical simulation of scattering from simple and composite random surfaces.", J. Opt. Soc. Am., vol. 2, pp. 2275 - 2283.

Fung, A. K., and Pan. G. W., 1987, "A scattering model for perfectly conducting random surfaces: I. Model development", Int. J. Remote. Sensing., 8, pp. 1579 - 1593.

Gradshteyn, I. S., and Ryzhik, M., 1980, "Table of integral, series and products.", 4th edition, Academic Press, London.

Hestenes, M., 1980, "Conjugate direction methods in optimization", Springer Verlag, New York.

Holliday, D., 1985, "Resolution of a controversy surrounding the Kirchhoff approximation and the small perturbation method in rough surface scattering theory", IEEE. Trans. Antennas Propagat., AP-30, pp. 1135 - 1144.

Holliday, D., St-Cyr, G., and Woods, N. E., 1987, "A radar ocean imaging model for small to moderate angles of incidence", Int. J. Remote

Sensing, 8, pp. 1809 - 1834.

Ishimaru, A., 1978, "Wave propagation and scattering in random media", Academic Press, New York, Ch. 17, Ch. 21.

Ishimaru, A., and Chen, J. S., 1990 a, "Numerical simulation of the second-order Kirchhoff approximation for very rough surfaces and a study of backscattering enhancement.", J. Acoust. Soc. Am., 88, pp. 1846 -1850.

Ishimaru, A., and Chen, J. S., 1990 b, "Scattering from very rough surfaces based on the modified second-order Kirchhoff approximation with angular propagation shadowing", J. Acoust. Soc. Am., 88, pp. 1877 - 1883.

Ishimaru, A., and Chen, J. S., 1991, "Scattering from very rough metallic and dielectric surfaces: a theory based on the modified Kirchhoff approximation", Waves in Random Media, 1, pp. 21-33.

Jones, D. S., 1979, "Methods in electromagnetic wave propagation", Clarendon-Press, Oxford.

Jordan, A. K. , and Lang., R. H., 1979, "Electromagnetic scattering patterns for sinusoidal surfaces.", Radio Sci., 14, pp. 1077 - 1088.

Kachoyan, B. J., and Macaskill, C., 1987, "Acoustic scattering from an arbitrarily rough surface.", J. Acoust. Soc. Am., 82, pp. 1720 - 1726.

Kim, M. J., Dainty, J. C., Friberg, A. T., and Sant, A. J., 1990, "Experimental study of enhanced backscattering from one- and two-dimensional random, rough surfaces.", J. Opt. Soc. Am. A 7, pp. 569 - 577.

Kim, Y. K., Rodriguez. E. and Durden, S. L., 1990, "A numerical assessment of rough surface scattering theories: Vertical polarization", submitted to Radio. Sci.

Kodis, R. O., 1966, "A note on the theory of scattering from an irregular surface", IEEE Trans. Antennas Propagat., AP-14, pp. 77 - 82.

Kong, J. A., 1986, "Electromagnetic wave theory.", John Wiley & Sons.

Kreysig, E., 1978, "Introductory functional analysis with applications", John Wiley & Sons.

Liszka, E. G., and McCoy, J. J, 1982, "Scattering at a rough surface boundary - extension of the Kirchhoff approximation.", J. Acoust. Soc. Am., 71, pp. 1093 - 1100.

Macaskill, C., and Kachoyan, B. J., 1988, "Numerical evaluation of the statistic of acoustic scattering from an arbitrarily rough surface.", J. Acoust. Soc. Am., 84, pp. 1826 - 1835.

Marcuse, D., 1982, "Light transmission optics", 2nd ed., Van Nostrand Reinhold, New York.

Marks, R. B., 1990, "An iterative method for high frequency scattering.", Wave Motion, Vol. 12, pp. 461 - 474.

Nieto-Vesperinas, M., and Soto-Crespo, J. M., 1987, "Monte -Carlo simulations for scattering of electromagnetic waves from perfectly conductive random rough surface.", Optics Letters, Vol. 12, pp. 979 - 981.

O'Donnell, K. A. and Mendez, E. R., 1987, "Experimental study of scattering from characterized random surface", J. Opt. Soc. Am. , A 2, pp. 2225 - 2239.

Papoulis, A, 1984, "Probability, random variables and stochastic processes.", McGraw-Hill, Singapore, 2nd. edition.

Peterson, A. F. and Mittra, R., 1984, "Method of conjugate gradient for the numerical solution of large body electromagnetic scattering problems", J. Opt. Soc. Am., 2, pp. 971 - 977.

Peterson, A. F. and Mittra, R., 1985, "The convergence of the conjugate gradient method when applied to matrix equations representing electromagnetic scattering problems", IEEE. Trans. Antennas Propagat., AP-34, pp. 1447 - 1454.

Poggio, A. J. and Miller, E. K., 1984, "Integral equation solution of three dimensional scattering problems", in "Computer techniques for electromagnetics", ed. R. Mittra, Pergammon-Press, Oxford.

Priestley, M. B., 1987, "Spectral analysis and time series.", 6th edition, Academic Press.

Rice, S. O., 1951, "Reflection of electromagnetic waves from slightly rough surfaces", Commun. Pure Appl, Math., pp. 351-378.

Rodriguez, E., 1989, "Beyond the Kirchhoff approximation.", Radio Sci., Vol. 24, pp. 681 - 693.

Rodriguez. E. and Kim, Y. K., 1990, "A unified perturbation expansion for surface scattering.", submitted to Radio. Sci..

Rodriguez. E., Kim, Y. K. and Durden, S. L., 1990, "A numerical assessment of rough surface scattering theories: Horizontal polarization", submitted to Radio. Sci..

Ruck, G. T., Barrick, D. E., Stuart, W. D. and Krichbaum, C. K., 1970, "Radar Cross section handbook.", Plenum Press, New York.

Saillard, M. and Maystre, D., 1990, "Scattering from metallic and dielectric rough surface.", J. Opt. Soc., A 7, pp. 982 - 990.

Schilling, R. J. and Lee. H., 1988, " Engineering analysis: A vector space approach", John Wiley & Sons, London.

Shen, J. and Maradudin, A. A., 1980, "Multiple scattering of waves from random rough surfaces", Phys. Rev. B., 22, pp. 4234 - 4240.

Sarkar, T. K., Siarkiewicz, K. R. and Stratton, R. F., 1981, "A survey of numerical methods applied to large system of linear equations for field problems", IEEE. Trans. Antennas Propagat., AP-29, pp. 847 - 856.

Sarkar, T. K., 1983, "A note on the variational method (Rayleigh-Ritz), Galerkins' method and the method of least-squares.", Radio Sci., Vol. 18, pp. 1207 - 1224.

Sarkar, T. K. and Rao, S. M., 1984, "The application of the conjugate gradient method for the solution of electromagnetic scattering from arbitrarily oriented antennas", IEEE. Trans. Antennas Propagat., AP-32, pp. 398 - 403.

Sarkar, T. K. and Arvas, E., 1985, "On a class of finite step iterative methods

(conjugate directions) for the solution of an operator equation arising in electromagnetics", IEEE. Trans. Antennas Propagat., AP-33, pp. 1058 - 1065.

Sarkar, T. K., Yang, X., and Arvas, E., 1988, "A limited survey of various conjugate-gradient methods for solving complex-matrix equations arising in electromagnetic wave interactions", Wave Motion, 10, pp. 527 - 546.

Scott, L. and Peterson, A. F., 1988, "Error and convergence in the numerical implementation of the conjugate-gradient method", IEEE. Trans. Antennas Propagat., AP-36, pp. 1824 - 1827.

Soto-Crespo, J. M., and Nieto-Vesperinas, M., 1989, "Electromagnetic scattering from very rough random surfaces and deep reflection gratings.", J. Opt. Soc. Am. A, 6, pp. 367 - 384.

Smith, C. F., Peterson, A. F. and Mittra, R., 1989, "A conjugate-gradient algorithm for the treatment of multiple incident electromagnetic fields.", IEEE. Trans. Antennas Propagat., AP-37, pp. 1491 - 1493.

Stratton, J. A. and Chu, L. J., 1939, "Diffraction theory of electromagnetic waves", Phys. Review, 56, pp. 99 - 107.

Stoddart, A. J., 1992, "An iterative method for scattering from randomly rough dielectric or conducting interfaces.", accepted for publication in Waves and random media.

Thorsos, E. I., 1988, "The validity of the Kirchhoff approximation for rough surface scattering using a Gaussian Roughness spectrum", J. Acoust. Soc. Am., 83, pp. 78 - 92.

Thorsos, E. I., and Jackson, D. R. 1989, "The validity of the perturbation approximation for rough surface scattering using a Gaussian Roughness spectrum", J. Acoust. Soc. Am., 86, pp. 261 - 277.

Ulaby, F. T., Moore, R. K. and Fung, A. K., 1982, "Microwave remote sensing: Active and Passive", Addison-Wesley, Reading, Vol. II.

Umashankar, K. R., 1988, "Numerical analysis of electromagnetic wave

scattering and interaction based on frequency-domain integral equation and moment techniques", Wave Motion, 12, pp. 493 - 525.

Valenzuela, G. R., 1967, "Depolarization of EM waves by slightly rough surfaces", IEEE. Trans. Antennas Propagat., AP-15, pp. 552 - 557.

Wagner, R. J., 1967, "Shadowing of randomly rough surfaces.", J. Acoust. Soc. Am. 41, pp. 138 - 147.

Wingham D. J., and Devayya, R. H., 1992, "A note on the use of the Neumann expansion in calculating the scatter from rough surfaces.", accepted for publication in IEEE. Trans. Antennas Propagat.

Wilkinson, J. H. and Rheinsch, C., 1963, "Notes on Applied Science No. 32; Rounding errors in algebraic processes", HMSO, London.

Wilkinson, J. H. and Rheinsch, C., 1971, "Handbook for automatic computation", Springer-Verlag.

Wilkinson, J. H., 1978, "Singular value decomposition: Basic aspects", in, "Numerical Software: Needs and Availability", ed. D. A. H. Jacobs, Academic Press, London.

Winebrenner, D. P. and Ishimaru, A., 1985 a, "Investigation of a surface field phase perturbation technique for scattering from rough surfaces", Radio Sci., 20, pp. 161 - 170.

Winebrenner, D. P. and Ishimaru, A., 1985 b, "Application of the phase-perturbation technique to randomly rough surfaces", J. Opt. Soc. Am. A, 2, pp. 2285 - 2293.